A CONSTITUTIVE MODEL FOR FRICTION IN METAL-WORKING

by

ATTILIO C. PISONI

Laurea in Mechanical Engineering, University of Ancona
(Ancona, Italy, 1989)

Submitted to the Department of
Mechanical Engineering
in Partial Fulfillment of
the Requirements for the Degree of

Master of Science in Mechanical Engineering

at the

MASSACHUSETTS INSTITUTE OF TECHNOLOGY

October, 1992

© Massachusetts Institute of Technology 1992

Signature of Author_____
Department of Mechanical Engineering
October, 1992

Certified by_____
Lallit Anand
Professor of Mechanical Engineering
Thesis Supervisor

Certified by_____
David M. Parks
Professor of Mechanical Engineering
Thesis Supervisor

Accepted by_____
Ain A. Sonin, Chairman
Departmental Committee on Graduate Studies

MASSACHUSETTS INSTITUTE
OF TECHNOLOGY

MAR 24 1993

LIBRARIES

A Constitutive Model for Friction in Metal-Working

by

Attilio C. Pisoni

Submitted to the Department of Mechanical Engineering
on October 28, 1992, in partial fulfillment of the requirements for the
Degree of Master of Science in Mechanical Engineering

Abstract

The formulation of accurate and robust friction models has been recognized to be a key for successful numerical simulations of forming operations. Based on a recent proposal by ANAND (1992), an interface constitutive model for dry metallic surfaces in contact is formulated, and a fully-implicit, objective time-integration procedure is developed. The notion of an evolving "slip resistance" is used to account for the dependence of the frictional stress upon the relative sliding and the contact pressure.

The model and the time-integration procedure have been implemented in a finite element program and example calculations are presented for: (a) Simple sliding with superposed rigid body rotation. This calculation is performed to verify the objectivity of the constitutive model and the time-integration procedure. (b) The ring compression test. This test is the most widely used experiment to indirectly assess the frictional properties of interfaces in metalworking. Predictions from the computational procedures show excellent agreement with experimental results. (c) Extrusion of a cylindrical billet. This calculation illustrates the effect of extensive sliding on the frictional properties of the interface. (d) Formation of central damage in the form of central bursts during drawing of a rod. This calculation extends the work of ZAVALIANGOS & ANAND (1992) by including the effect of heat generated at the sliding interfaces between the die and the workpiece. These examples show the versatility of the constitutive model and the robustness of the time-integration procedure.

A very important feature of the constitutive model used in the present work to describe interface friction of dry metallic surfaces, is the direct extendability of the model to other regimes of frictional behavior.

Thesis supervisors:
Dr. Lallit Anand, Associate Professor of Mechanical Engineering;
Dr. David M. Parks, Professor of Mechanical Engineering.

Acknowledgements

I would like to thank my thesis supervisors Prof. L. Anand and Prof. D. M. Parks. Working for them has been a great learning experience. My thanks also go to my friends and collegues in the Mechanics of Materials Research Group.

I would like to thank my family, from my mother and father, whose advice made my experience in the USA possible, down to my niece Erica, all of whom have always provided me with strength and security. Finally, my gratitude goes to Dagmar, who shared with me these years at MIT, for giving me invaluable help and joy.

Support for this work was provided by the Design and Manufacturing Division of NSF (Grant No. DDM-8914161).

Contents

List of Figures

Chapter 1

Introduction

Successful numerical simulations of forming operations require not only an accurate constitutive description of the workpiece material, but also a realistic representation of the contacting interface between the workpiece and the tool. The displacement and traction boundary conditions, together with heat generation and transfer at the interface, define a complete set of boundary conditions for such simulations. However, while there has been substantial progress in the modeling of bulk material for a wide variety of materials and different temperature and deformation regimes, the development of truly predictive numerical simulations has been hampered by the lack of accurate and robust friction models.

It is the complexity of the phenomena taking place at an interface and the influence of many and diverse physical variables which have hampered the development of friction models suitable for metal-working. The interface between contacting bodies constitutes a very complicated region with properties different from that of the bulk materials. In the case of metals, with reference to fig. (1.1) taken from the book by RABINOWICZ (1965), different layers can be identified at the vicinity of the surface. First, there is a layer which is usually very heavily plastically deformed. Next, an oxide layer is observed over the heavily deformed layer. Under normal conditions

the oxide layers are covered with absorbed layers of gas and moisture, and finally the outermost layer may be covered with lubricants and contaminants such as dust. Based on the amount of lubricant at the interface, frictional conditions in metalforming have been classified in four different regimes (SCHEY, 1983), ranging from dry frictional conditions, boundary lubrication, mixed lubrication to hydrodynamic lubrication, each one with its own distinctive characteristics. Even within each one of these categories other distinctions can be made. For dry metallic surfaces with engineering finishes, ODEN & MARTIN (1985) suggest the classification into three general categories, namely quasi-static friction; dynamic, sliding friction; wear and plowing. In light of this complexity, as also pointed out by ODEN & MARTIN, just as different constitutive models describe the behavior of the bulk material for different regimes of strain, strain rate and temperature, it is not reasonable to expect a single theory to describe all frictional phenomena.

In the present work we focus on a simple constitutive model and computational procedure for interface friction of dry metallic surfaces with engineering finishes. While both a rate-independent and a rate-dependent model are presented, only the rate-independent model is experimentally tested, implemented into a finite element code, and used to perform several numerical simulations. Following the work of ANAND (1992), which is based on the papers by FREDRIKSSON (1976), MICHALOWSKI & MROZ (1978) and CHENG & KIKUCHI (1985), the proposed model is based on the decomposition of the relative tangential velocity into adhering and slipping components, and on the definition of a slip condition[1] and a slip rule. The concept of a scalar slip resistance is introduced. This quantity, which has the dimension of stress, represents an isotropic resistance to tangential relative sliding across the interface.

[1]Such a slip condition is absent in the rate-dependent model.

The currently accepted theories concerning the mechanisms of the origin and evolution of the slip resistance for dry metallic surfaces (see SUH & SIN, 1981, SUH, 1986, BOWDEN & TABOR, 1964) stress the combined contribution of different phenomena such as asperity interlocking, deformation and fracture of asperities, adhesion of newly created surfaces, surface damage and particle formation caused by plowing, and plastic deformation in the near-surface layers.

The classical law of friction states that the shear stress τ at the interface of sliding bodies is proportional to the pressure p, that is $\tau = \mu\, p$. This law has proven to be very accurate at low levels of contact pressure. For higher levels of pressure, the shear stress is seen to reach a saturation value such that the shear stress at the interface becomes independent of p and equal to a fraction of the shear yield strength k of the deformable surface, namely $\tau = m\, k$, where m is the "friction factor" in the range $0 \leq m \leq 1$.

Based on a micro-mechanical model, BAY, WANHEIM & AVITZUR (1987) proposed a relation between the shear stress τ and the pressure p, according to which the slip resistance deviates from proportionality at increasing values of pressure, and its rate of change gradually decreases with increasing contact pressure until a saturation value is reached, fig. (1.2). Using the notion of the contact area ratio, $\zeta \equiv A_r/A$, of a true or real area of contact, A_r, to an apparent area of contact, A, these authors propose that

$$\tau = \tau_{lim}\zeta\,, \qquad \text{with} \qquad \zeta = \hat{\zeta}(p)\,.$$

They argue that the real area of contact A_r increases linearly with p in the low pressure range and that $\zeta \to 1$ as $p \to \infty$.

Although the micro-mechanical model of BAY, WANHEIM & AVITZUR offers an ex-

planation for the effect of the pressure on the frictional resistance, they do not take into account the effect of the evolution of the interface during sliding due to substrate deformation, evolution of the surface roughness and wear particle formation. Experimental work to document the evolution of the slip resistance with sliding has been carried out at MIT in the context of the present research project. This work shows that the slip resistance evolves from an initial value to a higher steady state value after an initial transient of the order of a few millimeters. This feature of the frictional behavior of dry metallic surfaces can be very important in those metalforming operations where each point of the tool-workpiece interface experiences a moderate amount of sliding. Acknowledging the evolution of the slip resistance with sliding is also important when the frictional properties of an interface are determined by means of indirect test procedures, like the ring compression test, where the distance slid is relatively small.

In the present work an attempt to model the evolution of the slip resistance is made by adopting an internal state-variable approach. This type of approach has been explored by RUINA (1985) and PELSHA, BALLARINI & PARULEKAR (1989) in the context of modeling friction in rocks. According to this approach the state of the interface is denoted by[2] $\boldsymbol{\alpha}$. This parameter symbolically represents all the surface roughness and microstructural details of the interface. Then the slip resistance s is given as a function of the pressure p and the state $\boldsymbol{\alpha}$ of the interface, namely $s = \hat{s}(p, \boldsymbol{\alpha})$. An advantage of this formulation is that the model can be directly extended to other frictional regimes by choosing appropriate internal state variables α_i, and appropriate functional forms describing their evolution and the evolution of

[2]In general $\boldsymbol{\alpha}$ should represent the combination of the state of the workpiece ($\boldsymbol{\alpha}^+$) and that of the tool ($\boldsymbol{\alpha}^-$). However, in this work we will assume $\boldsymbol{\alpha}=\boldsymbol{\alpha}^+$, and assume the state of the "rigid" tool to be fixed.

s. For the same reason the proposed model, used in this work to describe interface friction of dry metallic surfaces, also constitutes a general framework within which other regimes of frictional behavior may be modeled.

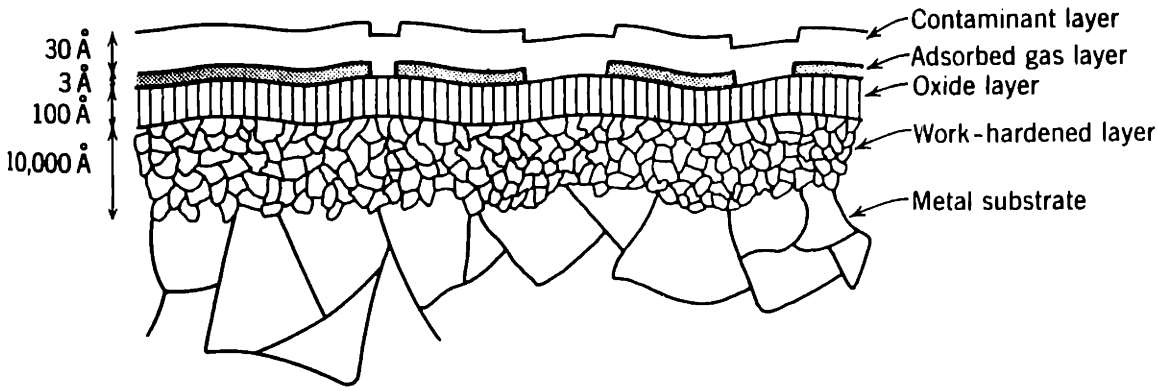

Figure 1.1: Schematic illustration of surface layers on a workpiece. Not to scale. Reproduced from Rabinowicz (1965). The total thickness of the "surface layer", including the surface roughness which is not shown here, is usually $1 - 10\mu$m.

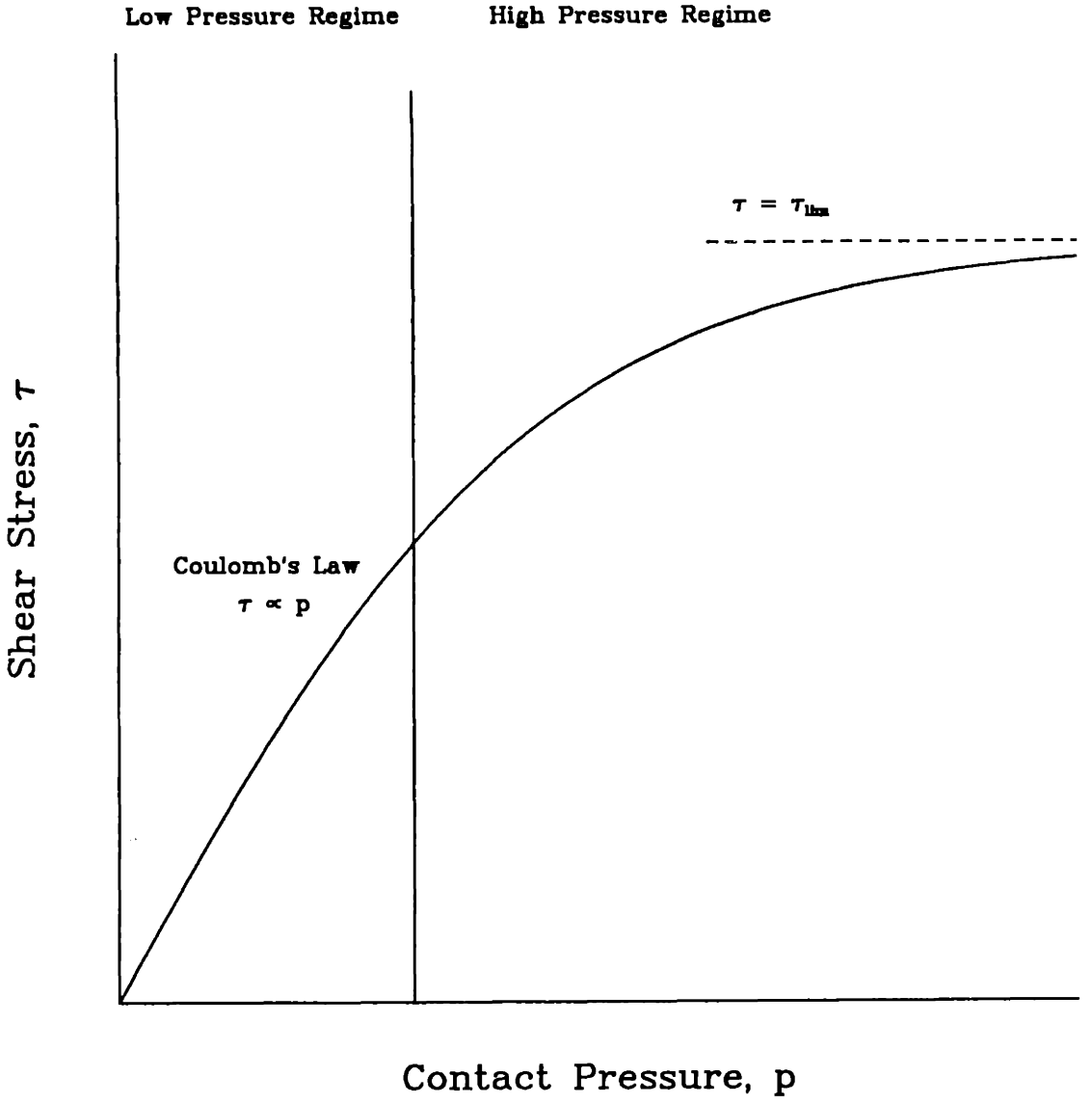

Figure 1.2: Schematic of interface shear stress *vs.* contact pressure as proposed by Bay, Wanheim & Avitzur (1987).

Chapter 2

Interface Constitutive Model

2.1 Introduction

In this chapter a constitutive model for the interface of contacting and sliding bodies, formulated by ANAND (1992), is presented. Only dry metallic surfaces at low sliding speed are taken into consideration, and therefore the model is formulated to be rate-independent[1]. While all friction problems involve thermal effects, only the isothermal approximation is considered. The assumption of isotropy of the frictional properties is used. Furthermore, based on the paper by ANAND (1992), a consistent, objective and stable time-integration algorithm for this interface constitutive model is presented.

The theory has the following main ingredients:

1. The state of a material point at the interface at any given time is characterized by the applied traction $\mathbf{t}$, and a scalar internal variable called the isotropic slip resistance s. The constitutive model consists essentially of a coupled set of differential equations which describe the evolution of the pair $(\mathbf{t}, s)$.

2. The tangential component of the relative velocity at the interface is divided into

[1]Nevertheless, in light of possible future extensions of the present model into regimes of frictional behavior (such as lubricated conditions or higher values of sliding velocities) where slip-rate effects could be important, a rate-dependent version is discussed in Appendix A.

an adhering (recoverable) part and a slipping part. The rate of the tangential traction component is then given by a linear isotropic function of the adhering part of the tangential component of the relative velocity, while the rate of the normal traction component is given by a linear isotropic function of the normal component of the relative velocity at the interface.

3. The relative tangential slipping velocity is given by a slip rule. No slipping takes place as long as a slipping condition (in stress space) is not met. According to this condition, slipping takes place when the magnitude of the applied shear stress equals the isotropic slip resistance and a loading/unloading criterion is satisfied. When slipping occurs, the slipping velocity is parallel (but directed opposite) to the tangential component of the traction vector.

4. The value of the slip resistance is related to the pressure p and the state of the interface $\boldsymbol{\alpha}$ by means of a constitutive equation.

5. The magnitude of the tangential slipping velocity is defined by a consistency condition which ensures that during a slipping process the values of the shear stress and the slip resistance are consistent with each other.

2.2 Notation and Definitions

We consider two bodies in contact, which we identify with the workpiece and the tool, and denote them by $\mathcal{B}^+$ and $\mathcal{B}^-$, respectively. The motion of these two bodies with respect to the reference configurations $\mathcal{B}_o^+$ and $\mathcal{B}_o^-$ is given by

$$\mathbf{x}^+ = \hat{\mathbf{x}}^+(\mathbf{p}^+, t) \quad \text{and} \quad \mathbf{x}^- = \hat{\mathbf{x}}^-(\mathbf{p}^-, t), \tag{2.1}$$

where $\mathbf{p}$ indicates the position of the a material point at time $t = 0$. If we consider the time $\tau = t + \Delta t$, the motion of the bodies with respect to their current configurations $\mathcal{B}_t^+$ and $\mathcal{B}_t^-$ are given by

$$\boldsymbol{\xi}^+ = \hat{\mathbf{x}}_t^+(\mathbf{x}^+, \tau) \quad \text{and} \quad \boldsymbol{\xi}^- = \hat{\mathbf{x}}_t^-(\mathbf{x}^-, \tau), \tag{2.2}$$

so that the incremental displacements are given by

$$\mathbf{u}_t^+(\mathbf{x}^+, \tau) = \boldsymbol{\xi}^+ - \mathbf{x}^+ \quad \text{and} \quad \mathbf{u}_t^-(\mathbf{x}^-, \tau) = \boldsymbol{\xi}^- - \mathbf{x}^-, \tag{2.3}$$

and the spatial velocities by

$$\mathbf{v}^+(\mathbf{x}^+, t) = \frac{\partial}{\partial \tau}\{\mathbf{u}_t^+(\mathbf{x}^+, \tau)\}\Big|_{\tau=t} \quad \text{and} \quad \mathbf{v}^-(\mathbf{x}^-, t) = \frac{\partial}{\partial \tau}\{\mathbf{u}_t^-(\mathbf{x}^-, \tau)\}\Big|_{\tau=t}. \tag{2.4}$$

The interface region where the two bodies come into contact is assumed to be of zero thickness, and we set $\mathbf{x} \equiv \mathbf{x}^+ = \mathbf{x}^-$. Also, denoting with $\mathbf{n}(\mathbf{x}, t)$ the outward normal to the surface of the workpiece $\mathcal{B}_t^+$ at the point $\mathbf{x}$ under consideration[2] at time t, we define the following quantities:

- the *relative velocity* between the workpiece and the tool:

$$\bar{\mathbf{v}} = \bar{\mathbf{v}}_N + \bar{\mathbf{v}}_T \equiv \mathbf{v}^+ - \mathbf{v}^-, \tag{2.5}$$

where

$$\bar{\mathbf{v}}_N = (\mathbf{n} \otimes \mathbf{n})\bar{\mathbf{v}} = (\bar{\mathbf{v}} \cdot \mathbf{n})\,\mathbf{n} = \bar{v}_N\,\mathbf{n}, \tag{2.6}$$

$$\bar{\mathbf{v}}_T = (\mathbf{1} - (\mathbf{n} \otimes \mathbf{n}))\,\bar{\mathbf{v}} = \bar{\mathbf{v}} - \bar{v}_N\,\mathbf{n}. \tag{2.7}$$

- the *relative displacement increment*:

$$\bar{\mathbf{u}}_t(\tau) = \bar{\mathbf{u}}_t(\tau)_N + \bar{\mathbf{u}}_t(\tau)_T \equiv \mathbf{u}_t^+(\mathbf{x}^+, \tau) - \mathbf{u}_t^-(\mathbf{x}^-, \tau), \tag{2.8}$$

[2]Henceforth, wherever there is no danger of confusion, the arguments $(\mathbf{x}^+, t)$, $(\mathbf{x}^-, t)$ will be suppressed.

where

$$\bar{\mathbf{u}}_t(\tau)_N = (\mathbf{n}(t) \otimes \mathbf{n}(t))\,\bar{\mathbf{u}}_t(\tau) = (\bar{\mathbf{u}}_t(\tau) \cdot \mathbf{n}(t))\,\mathbf{n}(t) \equiv \Delta\bar{u}_N(\tau)\mathbf{n}(t) \quad (2.9)$$

$$\bar{\mathbf{u}}_t(\tau)_T = (\mathbf{1} - \mathbf{n}(t) \otimes \mathbf{n}(t))\,\bar{\mathbf{u}}_t(\tau) \equiv \Delta\bar{\mathbf{u}}_T(\tau)\,. \quad (2.10)$$

- the *instantaneous traction exerted by the tool on the workpiece*:

$$\mathbf{t} = \mathbf{t}_N + \mathbf{t}_T\,, \quad (2.11)$$

where

$$\mathbf{t}_N = (\mathbf{n} \otimes \mathbf{n})\mathbf{t} = (\mathbf{t} \cdot \mathbf{n})\,\mathbf{n} \equiv t_N\,\mathbf{n}\,, \quad (2.12)$$

$$\mathbf{t}_T = (\mathbf{1} - (\mathbf{n} \otimes \mathbf{n}))\mathbf{t} = \mathbf{t} - t_N\,\mathbf{n}\,. \quad (2.13)$$

Also, the quantity $p \equiv -t_N$ represents the *normal pressure* or *contact pressure* and the magnitude of the tangential traction vector, $\mathbf{t}_T$, is denoted by

$$\bar{\tau} \equiv \sqrt{\mathbf{t}_T \cdot \mathbf{t}_T}\,, \quad (2.14)$$

and is called the *effective tangential traction* or simply the *shear stress.*

In order to guarantee the objectivity of the interface constitutive model to be discussed, we need to consider the transformation of the governing parameters under an observer transformation. Under a change in observer, for every material point $\mathbf{p}$ and time t, we have

$$\hat{\mathbf{x}}^*(\mathbf{p},t) = \mathbf{c}(t) + \mathbf{Q}(t)\,\{\mathbf{x}(\mathbf{p},t) - \mathbf{o}\} \quad (2.15)$$

where $\mathbf{c}(t)$ is a point in space and $\mathbf{Q}(t)$ is a rotation matrix. Thus, differentiating eqn (2.15) with respect to time, we obtain the transformation rules for the velocities

$\mathbf{v}^+(\mathbf{x}^+,t)$ and $\mathbf{v}^-(\mathbf{x}^-,t)$ under a change in observer:

$$\mathbf{v}^{+*}(\mathbf{x}^{+*},t) = \dot{\mathbf{c}}(t) + \mathbf{Q}(t)\mathbf{v}^+(\mathbf{x}^+,t) + \dot{\mathbf{Q}}(t)(\mathbf{x}^+ - \mathbf{o}), \tag{2.16}$$

$$\mathbf{v}^{-*}(\mathbf{x}^{-*},t) = \dot{\mathbf{c}}(t) + \mathbf{Q}(t)\mathbf{v}^-(\mathbf{x}^-,t) + \dot{\mathbf{Q}}(t)(\mathbf{x}^- - \mathbf{o}). \tag{2.17}$$

Upon subtraction of (2.17) from (2.16) we obtain the transformation rule for the relative velocity:

$$\bar{\mathbf{v}}^* = \mathbf{Q}\,\bar{\mathbf{v}}. \tag{2.18}$$

Also, the transformation rule for the traction $\mathbf{t}$ under a change in observer is

$$\mathbf{t}^* = \mathbf{Q}\,\mathbf{t}. \tag{2.19}$$

The relative velocity $\bar{\mathbf{v}}$ and the traction $\mathbf{t}$ are indifferent to a change in observer.

Next we define the *co-rotational derivative* $\mathbf{t}^\circ$ of $\mathbf{t}$, relative to an orthonormal basis $\{\mathbf{e}_i^s(t), i = 1,3\}$ at $\mathbf{x}^+$ at time t, with $\mathbf{e}_3^s(t) \equiv \mathbf{n}(t)$, as

$$\mathbf{t}^\circ \equiv \sum_i \dot{t}_i\,\mathbf{e}_i^s = \dot{\mathbf{t}} - \boldsymbol{\Omega}\,\mathbf{t}, \tag{2.20}$$

where $\boldsymbol{\Omega}(t)$ is the *twirl tensor*, defined by

$$\dot{\mathbf{e}}_i^s(t) = \boldsymbol{\Omega}(t)\,\mathbf{e}_i^s(t) \quad \text{with} \quad \boldsymbol{\Omega}(t) = -(\boldsymbol{\Omega}(t))^T \equiv \frac{\partial}{\partial\tau}\mathbf{R}_t(\tau)\Big|_{\tau=t}, \tag{2.21}$$

and the tensor $\mathbf{R}_t(\tau)$ is an incremental rotation tensor defined by

$$\mathbf{e}_i^s(\tau) = \mathbf{R}_t(\tau)\,\mathbf{e}_i^s(t), \tag{2.22}$$

with properties:

$$(\mathbf{R}_t(\tau))^T\,\mathbf{R}_t(\tau) = \mathbf{1}, \quad \det \mathbf{R}_t(\tau) = 1, \quad \mathbf{R}_t(t) = \mathbf{1}. \tag{2.23}$$

The vector $\mathbf{t}^\circ$ represents the time derivative of the traction *measured by an observer rotating with an orthonormal basis* $\{\mathbf{e}_i^s\}$ *attached to particle* $\mathbf{p}^+$. The co-rotational derivative $\mathbf{t}^\circ$ is indifferent to a change in observer[3].

Finally it is necessary to show that the quantities $\mathbf{R}_t(\tau)$ and $\boldsymbol{\Omega}(t)$ can be calculated given the motion $\hat{\mathbf{x}}_t^+(\mathbf{x}^+,\tau)$. As proposed by ANAND (1992), let us define the *surface deformation gradient* corresponding to a given motion and its polar decomposition by

$$\mathbf{F}_t{}^+(\mathbf{x}^+,\tau) = \frac{\partial}{\partial \mathbf{x}^+}\hat{\mathbf{x}}_t^+(\mathbf{x}^+,\tau), \quad \mathbf{F}_t{}^+(\mathbf{x}^+,\tau) = \mathbf{R}_t{}^+(\mathbf{x}^+,\tau)\,\mathbf{U}_t{}^+(\mathbf{x}^+,\tau). \tag{2.24}$$

Then, obvious choices for $\mathbf{R}_t(\tau)$ and $\boldsymbol{\Omega}(t)$ are:

$$\mathbf{R}_t(\tau) \equiv \mathbf{R}_t{}^+(\mathbf{x}^+,\tau), \tag{2.25}$$

and

$$\boldsymbol{\Omega}(t) \equiv \mathbf{W}^+(\mathbf{x}^+,t) = \frac{\partial}{\partial \tau}\mathbf{R}_t{}^+(\mathbf{x}^+,\tau)\Big|_{\tau=t}. \tag{2.26}$$

In conclusion, the objectivity of the interface constitutive model is guaranteed by using the indifferent pair $(\bar{\mathbf{v}},\mathbf{t}^\circ)$.

2.3 Interface Constitutive Model

The variables governing the response of an element of a contacting interface between a workpiece and a tool are taken to be the pair $(\mathbf{t},\boldsymbol{\alpha})$, where $\mathbf{t}$ is the traction and $\boldsymbol{\alpha}$ is the state of the intreface. The evolution equation for the traction $\mathbf{t}$ is taken as:

$$\dot{t}_N = -k_N\left(v_N^+ - v_N^-\right) = -k_N\bar{v}_N, \tag{2.27}$$

$$\mathbf{t}_T^\circ = -k_T\{\bar{\mathbf{v}}_T^a\} = -k_T\{\bar{\mathbf{v}}_T - \bar{\mathbf{v}}_T^s\}, \tag{2.28}$$

[3]A rigorous proof has been given by ANAND (1992).

where the relative tangential velocity $\bar{\mathbf{v}}_T$ has been decomposed into an adhering and a slipping part

$$\bar{\mathbf{v}}_T = (\bar{\mathbf{v}}_T)^a + (\bar{\mathbf{v}}_T)^s \,. \tag{2.29}$$

The parameters $k_N > 0$ and $k_T > 0$ are scalars, and are called the normal and tangential stiffness in adherance, respectively. In general these stiffnesses are expected to be functions of the state parameters $(\mathbf{t}, \boldsymbol{\alpha})$, but they are taken to be constants here. These parameters were introduced by MICHALOWSKI & MROZ (1978) as constitutive parameters, whereas they were introduced by CHENG & KIKUCHI (1985) as "penalty" parameters to resolve a "non-penetration" condition, $\bar{v}_N = 0$, and an "adherance" condition, $\bar{\mathbf{v}}_T = 0$, for contacting points. These constraint conditions are satisfied as $k_N \to \infty$ and $k_T \to \infty$, respectively. They can be satisfied rigorously using Lagrange multipliers, as implemented by BATHE & CHAUDHARY (1985) and ETEROVIC & BATHE (1991). However, as also noted by CHENG & KIKUCHI, the experiments of COURTNEY-PRATT & EISNER (1957) suggest a physical interpretation for k_T as a constitutive parameter describing a "shear modulus" of the interface. Also, the review of ODEN & MARTINS (1985) suggests the utility of modeling the normal as well the tangential response of metallic contact surfaces as "compliant interfaces". Although the interpretation of the parameters (k_N, k_T) as physical parameters describing a "shear modulus" and a "bulk modulus" of an interface (and also their physical measurement) remains to be investigated, we adopt the phenomenological formalism in equations (2.27) and (2.28) above for the evolution equations for the normal and tangential components of the traction. These equations may be written in compact form as

$$\mathbf{t}^\circ = -\{\mathbf{K}\bar{\mathbf{v}} - k_T \bar{\mathbf{v}}_T^s\} \,, \tag{2.30}$$

where $\bar{\mathbf{v}}$ is the relative velocity between the workpiece and the tool, $\bar{\mathbf{v}}_T^s$ is the relative

tangential slipping velocity, and

$$\mathbf{K} \equiv [k_T(\mathbf{1} - \mathbf{n} \otimes \mathbf{n}) + k_N(\mathbf{n} \otimes \mathbf{n})] \tag{2.31}$$

is the second order isotropic stiffness tensor for adherance.

The relative tangential slipping velocity $\bar{\mathbf{v}}_T^s$ is given by the *slip rule*:

$$\bar{\mathbf{v}}_T^s = \chi \bar{v}^s \mathbf{m}^s . \tag{2.32}$$

Here, $\mathbf{m}^s$ is a unit vector defining the "direction" of slip, and

$$\bar{v}^s \equiv \sqrt{\bar{\mathbf{v}}_T^s \cdot \bar{\mathbf{v}}_T^s} \geq 0 , \tag{2.33}$$

the magnitude of $\bar{\mathbf{v}}_T^s$, is an *effective relative tangential slipping velocity.* It is a positive valued scalar parameter which is determined by the *consistency condition* to be considered below.

The parameter χ is a switching parameter. When $\chi = 0$ we call the process *adhering*, and when $\chi = 1$ we call the process *slipping.* The conditions under which χ has a value 0 or 1 are based on the following notions of a yield condition and an unloading/loading criterion. Let s be a scalar variable called the *isotropic slip resistance* such that

$$s = \tilde{s}(p, \boldsymbol{\alpha}) \geq 0 , \tag{2.34}$$

where the scalar s is taken to have units of stress. Let also $f(\mathbf{t}, s)$ be a scalar valued function of the pair $(\mathbf{t}, s)$ with values

$$f(\mathbf{t}, s) \leq 0 . \tag{2.35}$$

Equation (2.35) defines a generic *slip condition* in the model. The surface $f(\mathbf{t}, s) = 0$ defines the current *slip surface* in traction space, and

$$\bar{\mathbf{m}} \equiv \frac{\partial f}{\partial \mathbf{t}} \tag{2.36}$$

is the outward normal to the slip surface at the current traction point. If the current traction is within the slip surface, or if it is on the slip surface and a *trial traction rate* $\{-\mathbf{K}\bar{\mathbf{v}}\}$ points towards the interior side of the tangent plane to the slip surface, that is, if $\bar{\mathbf{m}} \cdot \{-\mathbf{K}\bar{\mathbf{v}}\} \leq 0$, then the process is defined to be *adhering* and $\chi = 0$. Otherwise, $\chi = 1$, and the process is *slipping* :

$$\chi = \left\{ \begin{array}{ll} 0 & \text{if } f < 0, \text{ or if } f = 0 \text{ and } \bar{\mathbf{m}} \cdot \{-\mathbf{K}\bar{\mathbf{v}}\} \leq 0 \\ 1 & \text{if } f = 0 \text{ and } \bar{\mathbf{m}} \cdot \{-\mathbf{K}\bar{\mathbf{v}}\} > 0 \end{array} \right\} . \tag{2.37}$$

Next, we specialize the slip function f as

$$f(\mathbf{t}, s) = \bar{\tau} - s , \tag{2.38}$$

where $\bar{\tau} \equiv \sqrt{\mathbf{t}_T \cdot \mathbf{t}_T}$ is an *effective tangential traction*, and we replace $\boldsymbol{\alpha}$ in $s = \tilde{s}(p, \boldsymbol{\alpha})$ by a macroscopic scalar variable, $\bar{u}^s$, which we call the *accumulated relative tangential slip*, and take the evolution of this variable to be governed by

$$\dot{\bar{u}}^s \equiv \bar{v}^s , \quad \text{with initial value} \quad \bar{u}^s(0) = 0 . \tag{2.39}$$

The slip resistance s is then determined by the constitutive equation

$$s = \hat{s}(p, \bar{u}^s) \geq 0 , \tag{2.40}$$

where the function $\hat{s}$ is defined only for $p \geq 0$, with

$$\hat{s}(0, \bar{u}^s) = s_{th} \geq 0 . \tag{2.41}$$

The quantity s_{th} represents a threshold slip resistance under zero pressure[4]. Then, for the given slip function

$$\frac{\partial f}{\partial \mathbf{t}} = \frac{\partial \bar{\tau}}{\partial \mathbf{t}} - \frac{\partial \hat{s}}{\partial p} \frac{\partial p}{\partial \mathbf{t}} = (\mathbf{t}_T / \bar{\tau}) - \frac{\partial \hat{s}}{\partial p} (-\mathbf{n}) . \tag{2.42}$$

[4]In air most surfaces are contaminated; accordingly, it is expected that the threshold slip resistance under engineering conditions will be vanishingly small.

Let

$$\mathbf{m} \equiv (\mathbf{t}_T/\bar{\tau})\,, \tag{2.43}$$

and

$$h_N \equiv \frac{\partial \hat{s}}{\partial p}\,, \tag{2.44}$$

then the outward unit normal to the slip surface at the current traction point is

$$\bar{\mathbf{m}} = \mathbf{m} + h_N\,\mathbf{n}\,. \tag{2.45}$$

The direction of slip $\mathbf{m}^s$ is taken to be in the opposite direction of $\mathbf{m}$, that is:

$$\mathbf{m}^s = -\mathbf{m}\,. \tag{2.46}$$

Note that since we have chosen $\mathbf{m}^s \neq -\bar{\mathbf{m}}$, our flow rule is *non-associated.*

From equations (2.39, 2.40) the evolution equation for the slip resistance s is

$$\dot{s} = h_N\,\dot{p} + h_T\,\bar{v}^s\,, \tag{2.47}$$

where

$$h_N \equiv \frac{\partial \hat{s}}{\partial p} \qquad \text{and} \qquad h_T \equiv \frac{\partial \hat{s}}{\partial \bar{u}^s} \tag{2.48}$$

are hardening functions which account for changes in the slip resistance with changes in the contact pressure and the relative slip, respectively.

During a slipping process the pair $(\mathbf{t}, s)$ must continue to satisfy the slip condition $\bar{\tau} = s$. This is feasible only if the *consistency condition*

$$\dot{\bar{\tau}} = \dot{s} \tag{2.49}$$

is satisfied. Using the results

$$\dot{\bar{\tau}} = \mathbf{m}\cdot\dot{\mathbf{t}}_T \qquad \text{and} \qquad \frac{\partial f}{\partial \mathbf{t}}\cdot\dot{\mathbf{t}} = \frac{\partial f}{\partial \mathbf{t}}\cdot\mathbf{t}^\circ\,,$$

together with the evolution equation (2.47), we obtain the following condition for the evolution equation for the traction and the evolution equation for s to be "consistent":

$$\bar{v}^s = h_T^{-1}\{\mathbf{m}\cdot\mathbf{t}_T^\circ + h_N t_N^\circ\}\,. \tag{2.50}$$

Next, using (2.30), (2.31), (2.32), (2.36) and (2.46), we may write $\bar{v}^s$ as

$$\bar{v}^s = -g_T^{-1}\bar{\mathbf{m}}\cdot\{-\mathbf{K}\bar{\mathbf{v}}\}\,, \tag{2.51}$$

where

$$g_T = k_T + h_T\,. \tag{2.52}$$

In summary our isotropic, rate-independent, isothermal interface constitutive model consists of the following set of coupled evolution equations for the variables $(\mathbf{t}, s)$:

1. Evolution equation for the traction $\mathbf{t}$:

$$\mathbf{t}^\circ = -\{\mathbf{K}\bar{\mathbf{v}} - k_T\bar{\mathbf{v}}_T^s\}\,, \tag{2.53}$$

where

$$\mathbf{K} \equiv [k_T(\mathbf{1} - \mathbf{n}\otimes\mathbf{n}) + k_N(\mathbf{n}\otimes\mathbf{n})] \tag{2.54}$$

is the stiffness tensor for adherance and $\bar{\mathbf{v}}$ is the relative velocity between the workpiece and the tool. The relative tangential slipping velocity $\bar{\mathbf{v}}_T^s$ is given by the slip rule:

$$\bar{\mathbf{v}}_T^s = \chi\bar{v}^s(-\mathbf{m}) \tag{2.55}$$

where

$$\mathbf{m} \equiv (\mathbf{t}_T/\bar{\tau})\,, \tag{2.56}$$

is the unit vector in the direction of the tangential traction,

$$\bar{\tau} \equiv \sqrt{\mathbf{t}_T\cdot\mathbf{t}_T} \tag{2.57}$$

is an effective tangential traction or shear stress, and $\bar{v}^s$ is an effective relative tangential slipping velocity given by

$$\bar{v}^s = -g_T^{-1}\bar{\mathbf{m}} \cdot \{-\mathbf{K}\bar{\mathbf{v}}\}\,, \tag{2.58}$$

where

$$g_T = k_T + h_T\,, \tag{2.59}$$

and

$$\bar{\mathbf{m}} = \mathbf{m} + h_N\,\mathbf{n}\,, \tag{2.60}$$

is the normal to the slip surface $\bar{\tau} - s = 0$. The parameter χ is a switching parameter with values

$$\chi = \left\{ \begin{array}{ll} 0 & \text{if } f < 0, \text{ or if } f = 0 \text{ and } \bar{\mathbf{m}} \cdot \{-\mathbf{K}\bar{\mathbf{v}}\} \leq 0 \\ 1 & \text{if } f = 0 \text{ and } \bar{\mathbf{m}} \cdot \{-\mathbf{K}\bar{\mathbf{v}}\} > 0 \end{array} \right\}. \tag{2.61}$$

Note that by using (2.54), (2.55), (2.58) and (2.60), the evolution equation for the traction (2.53) may be expressed in compact form as

$$\mathbf{t}^\circ = -\mathbf{M}\bar{\mathbf{v}} \tag{2.62}$$

where

$$\mathbf{M} \equiv \mathbf{K} - \chi g_T^{-1}\{(-k_T\mathbf{m}) \otimes (-k_T\mathbf{m}) - h_N\,k_N\,(-k_T\mathbf{m}) \otimes \mathbf{n}\} \tag{2.63}$$

is the second order adhering-slipping stiffness tensor.

2. Evolution equation for the slip resistance s:

The slip resistance is assumed to be given by constitutive equation

$$s = \hat{s}(p, \bar{u}^s) \geq 0\,, \qquad \text{with} \qquad \hat{s}(0, \bar{u}^s) = s_{th} \geq 0\,, \tag{2.64}$$

where $p = -t_N$ is the contact pressure, s_{th} is a threshold value of the slip resistance, and $\bar{u}^s$ is an accumulated relative tangential slip whose evolution is governed by

$$\dot{\bar{u}}^s \equiv \bar{v}^s, \qquad \bar{u}^s(0) = 0. \tag{2.65}$$

The evolution of s is then governed by

$$\dot{s} = h_N \dot{p} + h_T \bar{v}^s, \tag{2.66}$$

where

$$h_N \equiv \frac{\partial \hat{s}}{\partial p} \quad \text{and} \quad h_T \equiv \frac{\partial \hat{s}}{\partial \bar{u}^s} \tag{2.67}$$

are hardening functions which account for changes in the slip resistance with changes in the contact pressure and the relative slip, respectively.

To complete this constitutive model for a particular tool-workpiece interface the constitutive parameters/functions that need to be specified are the tangential and normal stiffnesses in adherance, k_T and k_N, respectively, and the constitutive equation for the slip resistance s, or equivalently the initial value of the slip resistance and the hardening functions h_N and h_T.

The slip resistance function $\hat{s}(p, \bar{u}^s)$ used in the present work is

$$\hat{s}(p(\tau), \bar{u}^s(\tau)) = s^*(\bar{u}^s) \tanh\left[\frac{\mu(\bar{u}^s)p(\tau)}{s^*(\bar{u}^s)}\right]. \tag{2.68}$$

This functional form captures the essence of the pressure dependence of the slip resistance suggested by Bay, Wanheim & Avitzur (1987). At very low normal pressures, this expression reduces to:

$$s = \mu p, \tag{2.69}$$

with

$$\mu = \hat{\mu}(\bar{u}^s), \tag{2.70}$$

and thus μ, at a fixed relative sliding distance, represents the conventional coefficient of friction. At high pressures the expression reduces to:

$$s = s^*, \tag{2.71}$$

with

$$s^* = \hat{s}^*(\bar{u}^s), \tag{2.72}$$

and thus s^* represents the limit of interfacial shear stress at high contact pressure and at a given relative sliding distance. The evolution laws for μ and s^* can be put in incremental form as follows:

$$\dot{\mu}(\tau) = h_1 \bar{v}^s(\tau), \quad \mu(0) = \mu_0, \tag{2.73}$$

$$\dot{s}^*(\tau) = h_2 \bar{v}^s(\tau), \quad s^*(0) = s_0^*, \tag{2.74}$$

where

$$h_1 = \hat{h}_1(\mu(\tau)), \tag{2.75}$$

$$h_2 = \hat{h}_2(s^*(\tau)), \tag{2.76}$$

are hardening functions.

2.4 Time-integration Procedure

Assume that $\{\mathbf{t}(t), \bar{u}^s(t), \mathbf{n}(t), s(t)\}$[5] at time t are known, and that the *relative displacement increment*

$$\bar{\mathbf{u}}_t(\tau) \equiv \mathbf{u}_t^+(\mathbf{x}^+, \tau) - \mathbf{u}_t^-(\mathbf{x}^-, \tau), \tag{2.77}$$

together with the *rotation increment*

$$\mathbf{R}_t(\tau) \equiv \mathbf{R}_t^+(\mathbf{x}^+, \tau), \tag{2.78}$$

[5]In the following we will assume the evolution law for the slip resistance s to be that defined by eqns (2.68), (2.73) and (2.74).

which governs

$$\mathbf{n}(\tau) = \mathbf{R}_t(\tau)\,\mathbf{n}(t)\,, \tag{2.79}$$

are given. Then the problem is to integrate the evolution equations for $\mathbf{t}$, μ and s^* across a time increment $\Delta t = \tau - t$ and thereby calculate $\{\mathbf{t}(\tau), \bar{u}^s(\tau), \mathbf{n}(\tau), s(\tau)\}$ and march forward in time.

An algorithm to integrate the rate evolution equation for t should in general be consistent, numerically stable, and incrementally objective. Let us first consider the problem of consistency and objectivity. For two currently contacting points $\mathbf{x}^+ = \mathbf{x}^- \equiv \mathbf{x}$, the relative displacement increment $\bar{\mathbf{u}}_t(\tau)$ is *indifferent*:

$$\bar{\mathbf{u}}_t(\tau)^* = \mathbf{Q}(\tau)\bar{\mathbf{u}}_t(\tau)\,. \tag{2.80}$$

We define a transformed relative displacement increment

$$\tilde{\mathbf{u}}_t(\tau) \equiv (\mathbf{R}_t(\tau))^T\bar{\mathbf{u}}_t(\tau)\,, \tag{2.81}$$

where $\mathbf{R}_t(\tau)$ is the rotation tensor which carries $\mathbf{n}(t)$ to $\mathbf{n}(\tau)$. Using the fact that

$$\mathbf{R}_t(\tau)^* = \mathbf{Q}(\tau)\mathbf{R}_t(\tau)\,, \tag{2.82}$$

the displacement increment $\tilde{\mathbf{u}}_t(\tau)$ is *invariant* under a change in observer, that is:

$$\tilde{\mathbf{u}}_t(\tau)^* = \tilde{\mathbf{u}}_t(\tau)\,. \tag{2.83}$$

Also, the instantaneous time derivative of $\tilde{\mathbf{u}}_t(\tau)$ is equal to the relative velocity $\bar{\mathbf{v}}$:

$$\frac{\partial}{\partial\tau}\{\tilde{\mathbf{u}}_t(\tau)\}\bigg|_{\tau=t} = \bar{\mathbf{v}}(t)\,. \tag{2.84}$$

We consider next the definition of an *invariant* traction increment. Consider the transformed traction

$$\tilde{\mathbf{t}}(\tau) \equiv (\mathbf{R}_t(\tau))^T\,\mathbf{t}(\tau) \quad \text{with} \quad \tilde{\mathbf{t}}(t) = \mathbf{t}(t)\,. \tag{2.85}$$

The traction increment $\{\tilde{\mathbf{t}}(\tau) - \tilde{\mathbf{t}}(t)\}$ is invariant under a change in observer:

$$\left\{\tilde{\mathbf{t}}(\tau) - \tilde{\mathbf{t}}(t)\right\}^* = \left\{\tilde{\mathbf{t}}(\tau) - \tilde{\mathbf{t}}(t)\right\}, \tag{2.86}$$

and the instantaneous time derivative of this traction is

$$\frac{\partial}{\partial \tau}\left\{(\mathbf{R}_t(\tau))^T\,\mathbf{t}(\tau) - \mathbf{t}(t)\right\}\Big|_{\tau=t} = \dot{\mathbf{t}}(t) - \boldsymbol{\Omega}(t)\mathbf{t}(t) \equiv \mathbf{t}^\circ(t). \tag{2.87}$$

Thus the invariant traction increment $\{\tilde{\mathbf{t}}(\tau)-\tilde{\mathbf{t}}(t)\}$ is consistent with the co-rotational derivative of the traction $\mathbf{t}^\circ$.

To address the problem of stability, the stable Euler-backward method of integration will be used. Thus, from eqns (2.27), (2.28), (2.55), (2.73) and (2.74), and using the "rotation-neutralized" quantities defined above we obtain[6]

$$\tilde{t}_N(\tau) = t_N(t) + (-k_N)\Delta\tilde{u}_N\,, \tag{2.88}$$

$$\tilde{\mathbf{t}}_T(\tau) = \tilde{\mathbf{t}}_T^*(\tau) + (-k_T)\,\chi\Delta\bar{u}^s\,\tilde{\mathbf{m}}(\tau)\,, \tag{2.89}$$

$$\mu(\tau) = \mu(t) + \hat{h}_1(\mu(\tau))\Delta\bar{u}^s\,, \tag{2.90}$$

$$s^*(\tau) = s^*(t) + \hat{h}_2(s^*(\tau))\Delta\bar{u}^s\,, \tag{2.91}$$

where

$$\tilde{\mathbf{t}}_T^*(\tau) \equiv \tilde{\mathbf{t}}_T(t) + (-k_T)\Delta\tilde{\mathbf{u}}_T(\tau) \tag{2.92}$$

$$\Delta\bar{u}^s \equiv \Delta t\,\bar{v}^s(\tau) \tag{2.93}$$

and

$$\tilde{\mathbf{m}}(\tau) \equiv \tilde{\mathbf{t}}_T(\tau)\,/\,\bar{\tau}(\tau)\,. \tag{2.94}$$

[6]We note that if the slip resistance s is defined directly as a function of $\bar{u}^s$, equations (2.90) and (2.91) are replaced by:

$$s(\tau) = \hat{s}\{p(\tau),\,(\bar{u}^s(t) + \Delta\bar{u}^s)\}\,.$$

In this case the integration procedure, described in the work of ANAND, is slightly different.

The quantity $\tilde{\mathbf{t}}_T^*$ is a *trial* value for the shear traction at the end of the increment[7].

In a finite-element program $\Delta\tilde{\mathbf{u}}(\tau)$ can be computed from known kinematic information extrapolating from the solution at time t to obtain $\Delta\bar{\mathbf{u}}(\tau)$ and then using $\mathbf{R}_t(\tau)$ to calculate $\Delta\tilde{\mathbf{u}}(\tau)$ according to eqn (2.81). Thus, $\tilde{\mathbf{t}}_T^*(\tau)$ is known at the beginning of the increment. Also, using (2.79) and (2.85) the contact pressure at the end of the step is

$$p(\tau) \equiv -\mathbf{t}(\tau)\cdot\mathbf{n}(\tau) = -\mathbf{t}(\tau)\cdot\mathbf{R}_t(\tau)\mathbf{n}(\tau) = -\tilde{t}_N(\tau)\,, \tag{2.95}$$

and since all the quantities on the right end side of (2.88) are known, so also is the contact pressure p at time τ. To update the state variables using (2.89), (2.90) and (2.91), we need to calculate $\tilde{\mathbf{m}}(\tau)$, $\Delta\bar{u}^s$, $\mu(\tau)$ and $s^*(\tau)$. It is shown next that $\tilde{\mathbf{m}}(\tau)$ is known in terms of $\tilde{\mathbf{t}}_T^*(\tau)$, and, hence, it is also known at the beginning of the solution process.

From eqn (2.89), using $\tilde{\mathbf{t}}_T(\tau) = \bar{\tau}(\tau)\tilde{\mathbf{m}}(\tau)$ and rearranging, we obtain

$$(\bar{\tau}(\tau) + \chi k_T \Delta\bar{u}^s)\tilde{\mathbf{m}}(\tau) = \tilde{\mathbf{t}}_T^*(\tau)\,, \tag{2.96}$$

which shows that $\tilde{\mathbf{m}}(\tau)$ is parallel in direction to $\tilde{\mathbf{t}}_T^*(\tau)$. Hence,

$$\tilde{\mathbf{m}}(\tau) = \tilde{\mathbf{t}}_T^*(\tau)/\|\tilde{\mathbf{t}}_T^*(\tau)\| = \tilde{\mathbf{t}}_T^*(\tau)/\bar{\tau}^*(\tau)\,, \tag{2.97}$$

where

$$\bar{\tau}^*(\tau) = \sqrt{\tilde{\mathbf{t}}_T^*(\tau)\cdot\tilde{\mathbf{t}}_T^*(\tau)}\,. \tag{2.98}$$

Equation (2.97) may be rearranged to read

$$\tilde{\mathbf{t}}_T(\tau) = \eta(\tau)\tilde{\mathbf{t}}_T^*(\tau) \quad \text{where} \quad \eta(\tau) = \bar{\tau}(\tau)/\bar{\tau}^*(\tau)\,. \tag{2.99}$$

[7]Here and henceforth the superscript (*) on a quantity does not denote the transformation of the quantity under a change in observer.

We call $\eta(\tau)$ the "radial return factor". As an alternate to evaluating $\tilde{\mathbf{t}}_T(\tau)$ from (2.89), we can directly use (2.99). Thus, the problem reduces to finding $\bar{\tau}(\tau)$, $\mu(\tau)$ and $s^*(\tau)$.

From (2.89), during plastic sliding ($\chi = 1$), we obtain

$$\bar{\tau}(\tau) = \bar{\tau}^*(\tau) - k_T \Delta\bar{u}^s . \tag{2.100}$$

Further, using eqn (2.100) and the fact that $\bar{\tau} = s$ during plastic sliding, and substituting for $\Delta\bar{u}^s$ in (2.90) and (2.91), we obtain the pair of equations

$$\mu(\tau) - \mu(t) - \hat{h}_1(\mu(\tau))\frac{1}{k_T}\{\bar{\tau}^*(\tau) - \hat{s}(\mu(\tau), s^*(\tau), p(\tau))\} = 0 , \tag{2.101}$$

$$s^*(\tau) - s^*(t) - \hat{h}_2(s^*(\tau))\frac{1}{k_T}\{\bar{\tau}^*(\tau) - \hat{s}(\mu(\tau), s^*(\tau), p(\tau))\} = 0 . \tag{2.102}$$

The solution of this pair of equations yields the updated values of $\mu(\tau)$ and $s^*(\tau)$ with which it is possible to calculate the new value of the slip resistance $s(\tau) = \bar{\tau}(\tau)$ according to eqn (2.68). To complete the algorithm we need to perform the updates

$$\mathbf{t}(\tau) = \mathbf{R}_t(\tau)\left\{\eta(\tau)\,\tilde{\mathbf{t}}_T^*(\tau) + \tilde{t}_N(\tau)\mathbf{n}(t)\right\} , \tag{2.103}$$

$$\mathbf{n}(\tau) = \mathbf{R}_t(\tau)\,\mathbf{n}(t) , \tag{2.104}$$

and march forward in time.

2.4.1 Summary of Time-Integration Algorithm

1. Given (i) $\{\mathbf{t}(t), \bar{u}^s(t), \mathbf{n}(t), s(t), \mu(t), s^*(t);\}$, (ii) $\Delta t = \tau - t$, (iii) $\bar{\mathbf{u}}_t(\tau)$, and (iv) $\mathbf{R}_t(\tau) \equiv \mathbf{R}_t{}^+(\mathbf{x}^+, \tau)$

2. Calculate $\{\mathbf{t}(\tau), \bar{u}^s(\tau), \mathbf{n}(\tau), s(\tau), \mu(\tau), s^*(\tau);\}$ using the algorithm

   Step 1. Calculate the transformed relative displacement increment

   $$\tilde{\mathbf{u}}_t(\tau) = (\mathbf{R}_t(\tau))^T \bar{\mathbf{u}}_t(\tau) .$$

Step 2. Calculate the contact pressure

$$p(\tau) = -\tilde{t}_N(\tau) = -t_N(t) + k_T \Delta\tilde{u}_N .$$

Step 3. Calculate the trial tangential traction and its effective value

$$\begin{aligned} \tilde{\mathbf{t}}_T^*(\tau) &= \mathbf{t}_T(t) + (-k_T)\Delta\tilde{\mathbf{u}}_T(\tau) , \\ \bar{\tau}^*(\tau) &= \sqrt{\tilde{\mathbf{t}}_T^*(\tau) \cdot \tilde{\mathbf{t}}_T^*(\tau)} . \end{aligned}$$

Step 4. If

$$\bar{\tau}^*(\tau) < s(t) ,$$

then the process is adhering, and

$$\begin{aligned} \mathbf{t}(\tau) &= \mathbf{R}_t(\tau) \left\{ \tilde{\mathbf{t}}_T^*(\tau) + \tilde{t}_N(\tau)\mathbf{n}(t) \right\} , \\ \mu(\tau) &= \mu(t) , \\ s^*(\tau) &= s^*(t) , \\ \mathbf{n}(\tau) &= \mathbf{R}_t(\tau)\, \mathbf{n}(t) , \\ s(\tau) &= s(t) . \end{aligned}$$

Otherwise the process is slipping. Continue. Calculate $\mu(\tau)$ and $s^*(\tau)$ by solving

$$\begin{aligned} \mu(\tau) - \mu(t) - \hat{h}_1(\mu(\tau))\frac{1}{k_T}\{\bar{\tau}^*(\tau) - \hat{s}(\mu(\tau), s^*(\tau), p(\tau))\} &= 0 , \\ s^*(\tau) - s^*(t) - \hat{h}_2(s^*(\tau))\frac{1}{k_T}\{\bar{\tau}^*(\tau) - \hat{s}(\mu(\tau), s^*(\tau), p(\tau))\} &= 0 . \end{aligned}$$

Step 5. Calculate

$$s(\tau) = s^*(\tau) \tanh\left[\frac{\mu(\tau)p(\tau)}{s^*(\tau)}\right] ,$$

and set

$$\bar{\tau}(\tau) = s(\tau) .$$

Step 6. Calculate the radial return factor $\eta(\tau)$

$$\eta(\tau) = (\bar{\tau}(\tau)/\bar{\tau}^*(\tau)).$$

Step 7. Perform the updates

$$\begin{aligned} \mathbf{t}(\tau) &= \mathbf{R}_t(\tau)\left\{\eta(\tau)\,\tilde{\mathbf{t}}_T^*(\tau) + \tilde{t}_N(\tau)\mathbf{n}(t)\right\}, \\ \mathbf{n}(\tau) &= \mathbf{R}_t(\tau)\,\mathbf{n}(t). \end{aligned}$$

3. March forward in time.

2.5 The Linearization Moduli $\tilde{\mathbf{M}}$

With reference to Chapter 4, in order to implement the constitutive model and time-integration procedure in the general purpose finite element program ABAQUS, it is necessary to evaluate its linearized moduli $\tilde{\mathbf{M}}(\tau)$, defined as[8]:

$$\tilde{\mathbf{M}}(\tau) \equiv -\partial_{\Delta\bar{\mathbf{u}}_t}\tilde{\mathbf{t}}(\tau). \tag{2.105}$$

The linearization moduli depends on the constitutive equations and the time integration algorithm used to evaluate $\tilde{\mathbf{t}}(\tau)$.

Combining eqns (2.88) and (2.89), during loading we have

$$\tilde{\mathbf{t}}(\tau) = \tilde{\mathbf{t}}^*(\tau) - k_T\Delta t\,\bar{v}^s(\tau)\tilde{\mathbf{m}}(\tau) \tag{2.106}$$

where

$$\tilde{\mathbf{t}}^*(\tau) = \tilde{\mathbf{t}}_T^*(\tau) + \tilde{t}_N(\tau)\tilde{\mathbf{n}}(\tau), \tag{2.107}$$

and

$$\tilde{\mathbf{n}}(\tau) \equiv (\mathbf{R}_t(\tau))^T\,\mathbf{n}(\tau) = \mathbf{n}(t). \tag{2.108}$$

[8]This term is needed in the Newton-Raphson method for the solution of the finite element system of equations.

From (2.106), (2.88) and (2.89) we have

$$\tilde{\mathbf{M}}(\tau) = -\partial_{\Delta\tilde{\mathbf{u}}_t}\tilde{\mathbf{t}}^s(\tau) + k_T\,\Delta t\,[\tilde{\mathbf{m}}(\tau)\otimes\partial_{\Delta\tilde{\mathbf{u}}_t}\bar{v}^s(\tau) + \bar{v}^s(\tau)\partial_{\Delta\tilde{\mathbf{u}}_t}\tilde{\mathbf{m}}(\tau)]\,. \tag{2.109}$$

Using (2.88), (2.89), (2.97) and (2.98), straightforward calculations give

$$\partial_{\Delta\tilde{\mathbf{u}}_t}\tilde{\mathbf{t}}^s(\tau) = -\mathbf{K}\,, \tag{2.110}$$

$$\partial_{\Delta\tilde{\mathbf{u}}_t}\bar{\tau}^s(\tau) = -k_T\tilde{\mathbf{m}}(\tau)\,, \tag{2.111}$$

$$\partial_{\Delta\tilde{\mathbf{u}}_t}\tilde{\mathbf{m}}(\tau) = -\frac{k_T}{\bar{\tau}^s(\tau)}\,[\mathbf{1} - \tilde{\mathbf{m}}(\tau)\otimes\tilde{\mathbf{m}}(\tau)]\,, \tag{2.112}$$

$$\partial_{\Delta\tilde{\mathbf{u}}_t}t_N = -k_N\tilde{\mathbf{n}}(\tau)\,. \tag{2.113}$$

Substituting (2.110) and (2.112) into (2.109), and rearranging gives

$$\tilde{\mathbf{M}}(\tau) = \tilde{\mathbf{K}}(\tau) + \Delta t\left[k_T\tilde{\mathbf{m}}(\tau)\otimes\partial_{\Delta\tilde{\mathbf{u}}_t}\bar{v}^s(\tau) + \left(\frac{\bar{v}^s(\tau)}{\bar{\tau}^s(\tau)}\right)k_T\tilde{\mathbf{m}}(\tau)\otimes k_T\tilde{\mathbf{m}}(\tau)\right], \tag{2.114}$$

where

$$\tilde{\mathbf{K}}(\tau) \equiv k_T(\mathbf{1}\eta(\tau) - \tilde{\mathbf{n}}(\tau)\otimes\tilde{\mathbf{n}}(\tau)) + k_N(\tilde{\mathbf{n}}(\tau)\otimes\tilde{\mathbf{n}}(\tau))\,, \tag{2.115}$$

$$\eta(\tau) \equiv \left\{\frac{\bar{\tau}(\tau)}{\bar{\tau}^s(\tau)}\right\}. \tag{2.116}$$

Linearization of (2.90), (2.91) and (2.100) gives:

$$d\bar{\tau}(\tau) = d\bar{\tau}^s(\tau) - k_T\,\Delta t\,d\bar{v}^s(\tau)\,, \tag{2.117}$$

$$d\mu(\tau) = \bar{h}_1(\tau)\,\Delta t\,d\bar{v}^s(\tau)\,, \tag{2.118}$$

$$ds^s(\tau) = \bar{h}_2(\tau)\,\Delta t\,d\bar{v}^s(\tau)\,, \tag{2.119}$$

where

$$\bar{h}_1(\tau) \equiv \frac{h_1(\tau)}{1 - \frac{dh_1}{d\mu}|_\tau\,\Delta t\,\bar{v}^s(\tau)}\,, \tag{2.120}$$

$$\bar{h}_2(\tau) \equiv \frac{h_2(\tau)}{1 - \frac{dh_2}{ds^s}|_\tau\,\Delta t\,\bar{v}^s(\tau)}\,. \tag{2.121}$$

From (2.66)

$$ds(\tau) = -h_N(\tau)dt_N(\tau) + \bar{h}_T(\tau)\Delta t\, d\bar{v}^s(\tau)\,, \tag{2.122}$$

where

$$\bar{h}_T(\tau) = \partial_\mu s|_\tau \bar{h}_1(\tau) + \partial_{s^*} s|_\tau \bar{h}_2(\tau)\,. \tag{2.123}$$

Next, using the fact that $d\bar{\tau}^*(\tau) = ds(\tau)$, substituting (2.122) into (2.117) and solving for $d\bar{v}^s(\tau)$, gives

$$d\bar{v}^s(\tau) = \frac{d\bar{\tau}^*(\tau) + h_N(\tau)dt_N(\tau)}{\Delta t\,(k_T + \bar{h}_T(\tau))}\,. \tag{2.124}$$

Finally, using (2.111), (2.113) and (2.124) we obtain

$$\partial_{\Delta\tilde{\mathbf{u}}_t}\bar{v}^s(\tau) = \frac{-k_T\tilde{\mathbf{m}}(\tau) - h_N(\tau)k_N\tilde{\mathbf{n}}(\tau)}{\Delta t\,(k_T + \bar{h}_T(\tau))}\,. \tag{2.125}$$

Substitution of (2.125) into (2.114) gives

$$\tilde{\mathbf{M}}(\tau) = \tilde{\mathbf{K}}(\tau) - \bar{g}_T^{-1}(\tau)\,\{k_T\tilde{\mathbf{m}}(\tau)\otimes k_T\tilde{\mathbf{m}}(\tau)\} - \bar{g}_N^{-1}(\tau)\,\{k_T\tilde{\mathbf{m}}(\tau)\otimes k_N\tilde{\mathbf{n}}(\tau)\}\,, \tag{2.126}$$

where

$$\bar{g}_T^{-1}(\tau) = \frac{1}{k_T}\left\{\eta(\tau) - \frac{\bar{h}_T(\tau)}{k_T + \bar{h}_T(\tau)}\right\}, \tag{2.127}$$

$$\bar{g}_N^{-1}(\tau) = \frac{h_N(\tau)}{k_T + \bar{h}_T(\tau)}\,. \tag{2.128}$$

Note that the linearization moduli $\tilde{\mathbf{M}}$ has exactly the same form as the constitutive modulus $\mathbf{M}$ of eqn (2.63). However the incremental stiffness tensor $\tilde{\mathbf{K}}$, and the parameters $\bar{g}_T$ and $\bar{g}_N$ in the linearization moduli are different from the corresponding quantities in $\mathbf{M}$. Also, the directions $\tilde{\mathbf{n}}$ and $\tilde{\mathbf{m}}$ in the linearization moduli are evaluated at the end of the increment instead of the beginning of the increment. The use of $\mathbf{M}$ in the Newton procedure, instead of the appropriate linearization moduli $\tilde{\mathbf{M}}$, can lead to very slow convergence.

Chapter 3

Experimental Study

3.1 Introduction

This chapter presents a brief summary of the experimental work carried out at MIT to study the evolution of the slip resistance of dry metallic surfaces with sliding and its dependence on pressure[1]. Based on the results obtained in these experiments, the specific evolution law for the slip resistance as a function of the sliding distance and the pressure proposed in Chapter 2 is characterized, and its validity checked by comparison with additional experimental results.

The workpiece specimens used in the experiments are made of OFHC copper and the tool material is hardened AISI H13 steel.

The experimental procedure presented in the following represents a *direct* methodology in which one can independently control the normal contact pressure, temperature, relative tangential sliding distance and speed, and measure the shear stress response. In contrast, as reviewed by SCHEY (1983) and KALPAKJIAN (1991), the most widely used method for estimating frictional properties (a constant "friction coefficient, μ" or a constant "friction factor, m") in metalforming, is the ring compression

[1]This experimental work has been carried out by Dr. W. TONG and is more extensively discussed in a paper by ANAND, PISONI & TONG (1992).

test which is an *indirect* test procedure. According to this methodology, cylindrical ring specimens are compressed and curves corresponding to the reduction in internal diameter versus reduction in height are constructed. These curves are then compared against calibration curves obtained by solving a complete boundary value problem with an *assumed* constitutive response for the interface and the workpiece. Due to the assumptions and the approximations introduced in a particular solution procedure, the estimated value of μ or m can vary by as much as ± 50 % (SCHEY, 1983).

3.2 Experimental Approach

Friction experiments have been conducted using an INSTRON biaxial compression-torsion material testing machine. This testing facility has a capability of up to 50,000 lbs of axial load, 25,000 in $\times$ lb of torque, ± 2 in of linear stroke, and ± 80 degrees of angular stroke.

The experimental configuration for the fundamental experiments is shown in fig. (3.1). The set-up consists of an axisymmetric workpiece and a hardened AISI H13 solid cylindrical tool. The contacting region between the tool and the workpiece is annular. The tool and the workpiece are first compressed together to generate a normal pressure p, and they are then slid relative to each other by a rotation about the axis of symmetry.

For tests at low to moderate normal pressures (relative to the flow strength of the workpiece at a moderate plastic strain), the workpiece is made of a tapered, thin-walled cylinder (see fig. 3.1(a)), which results in an annular contact region. At large normal pressures this workpiece specimen is inadequate because of large geometry changes and flaring of the conical contacting region. Accordingly, for high normal

pressures, the workpiece is a thin annular disc (see fig. 3.1(b)). This disc is indented by a thin-walled cylinder made of the tool material against the solid cylindrical tool. The indenting thin-walled cylindrical piece has a rough but clean contacting surface, which gets "stuck" to the thin disk at high pressures. There is essentially no relative sliding between this disc and the thin-walled indenting cylindrical piece during the experiment. The area of contact between the thin disc-shaped workpiece and the solid cylindrical tool in such tests remains essentially constant even for very high normal pressures ($\sim$ 600 MPa for copper).

Before an experiment, the contacting surface of the solid cylindrical tool is lapped optically flat (up to 0.3 μm over a two-inch diameter circle), and then different surface roughnesses for the tool are produced by lapping with different grades of abrasive papers. The topography of all tool and workpiece contact surfaces are measured by using either a stylus-type profilometer, or a non-contacting profiler.

For the annular contact region with a mean diameter of $\sim$ 33 mm, the maximum sliding speed achievable in the experiments is about 25 mm/s, and the maximum unidirectional sliding distance is about 50 mm. Complete time histories of torque and rotation angle as well as axial load and displacement are simultaneously recorded during an experiment by a microcomputer-based digital data acquisition system. The same microcomputer also independently controls the prescribed histories of both the axial load and the angle of rotation.

The inner and outer diameters D_i and D_o, respectively, of the contacting annular region, are measured after each test. The normal pressure p, and the tangential stress τ, are computed by

$$p = F/A \text{ and } \tau = M/[A \times (D_i + D_o)/4], \tag{3.1}$$

where F and M are the measured axial load and torque, and $A = \pi(D_o^2 - D_i^2)/4$ is the area of contact. The relative sliding distance between the tool and workpiece is determined from:

$$\bar{u}^s = \theta \times (\pi/180) \times (D_i + D_o)/4\,, \tag{3.2}$$

where θ is the measured angle of rotation in degrees.

3.3 Results

Typical experimental results are shown in fig. (3.2) for dry contact between steel-copper, at a low and at a high contact pressure. Clearly, there is a strong "slip-hardening" effect on the interfacial shear stress during the initial stages of sliding. It is believed that factors such as plowing, wear particle formation, and the resulting change in the topography of the workpiece surface as well as sub-surface material strain-hardening are the major contributors to this slip-hardening behavior.

By conducting such experiments over a wide range of pressures, the dependence of the shear stress on the normal pressure at initiation of macroscopic sliding ($\bar{u}^s = 0.25$ mm), and that at "steady state" ($\bar{u}^s = 40$ mm) under monotonic conditions has been determined for the dry steel-copper interface, fig. (3.3). These data show that the shear stress at the tool-workpiece interface is proportional to the normal pressure (Coulomb's law) at very low contact pressures. As the normal pressure increases the shear stress tends to a saturation level at both small and large sliding distances. This fact is related to the variation of the real area of contact with the normal pressure: at low contact pressure the real area of contact is proportional to the normal load; at higher pressures the real area of contact tends to the maximum value of unity. This explanation also agrees with the experimentally observed gradual transition of the

shear stress response from the low to the high contact pressures regimes.

Fig. (3.4) shows the result of an interrupted sliding test on a dry steel-copper interface at a constant normal pressure and a constant slip-rate. The steel and copper are slid relative to each other for about 4 mm, and the experiment is then stopped. After a while, the sliding is resumed and then stopped and restarted once more during the test. The loading/unloading/reloading and slip-hardening behavior of the interface is very similar to the elastic-plastic strain hardening of the bulk material.

3.4 Estimation of Model Parameters

A schematic of the dependence of τ on p and $\bar{u}^s$ based on the conducted experiments is shown in fig. (3.5). The projections of the "frictional resistance surface" of Fig 3.5 on the p-τ plane and on the $\bar{u}^s$-τ plane are shown in fig. (3.6) and fig. (3.7), respectively. The simple interface constitutive model introduced in Chapter 2 is able to account for the effects of both contact pressure and relative sliding distance shown by these experimental results. Based on this model the shear stress during monotonic sliding is taken to be governed by:

$$\tau = \hat{s}(p, \bar{u}^s) = s^*(\bar{u}^s) \tanh\left[\frac{\mu(\bar{u}^s)\, p}{s^*(\bar{u}^s)}\right] . \tag{3.3}$$

We notice again that at very low normal pressures, this expression reduces to $\tau = \mu p$ while at high pressures the expression reduces to $\tau = s^*$.

The given functional form for $\tau = \hat{s}(p, \bar{u}^s)$ provides the following simple means for determining the functions $\hat{\mu}(\bar{u}^s)$ and $\hat{s}^*(\bar{u}^s)$ by two experiments: an experiment at a "low" constant normal pressure to determine $\hat{\mu}(\bar{u}^s)$, and a second experiment at a "high" constant normal pressure to determine $\hat{s}^*(\bar{u}^s)$. For dry, clean steel-copper the following specific functional forms for $\hat{\mu}(\bar{u}^s)$ and $\hat{s}^*(\bar{u}^s)$ are found to provide a good

representation of the observed slip-hardening behavior:

$$\hat{\mu}(\bar{u}^s) = \mu_0 + (\mu_s - \mu_0)[1 - \exp(-\bar{u}^s/u_1)] , \tag{3.4}$$

$$\hat{s}^*(\bar{u}^s) = s_0^* + (s_s^* - s_0^*)[1 - \exp(-\bar{u}^s/u_2)] , \tag{3.5}$$

where $\{\mu_0, \mu_s, u_1\}$ and $\{s_0^*, s_s^*, u_2\}$ are constants of the model. These constants have been determined from the results shown in fig. (3.2) for dry steel-copper interface. Curve fitting gives:

$$\mu_0 = 0.33 , \quad \mu_s = 0.627 , \quad u_1 = 1.5 \text{ mm} , \tag{3.6}$$

and

$$s_0^* = 108 \text{ MPa} , \quad s_s^* = 220 \text{ MPa} , \quad u_2 = 5.0 \text{ mm} . \tag{3.7}$$

The quality of the curve fit is shown in fig. (3.8). Differentiating eqns (3.4) and (3.5) gives the incremental form of the evolution equations for μ and s^*, namely:

$$\dot{\mu}(\tau) = h_1 \bar{v}^s(\tau) , \quad \mu(0) = \mu_0 , \tag{3.8}$$

$$\dot{s}^*(\tau) = h_2 \bar{v}^s(\tau) , \quad s^*(0) = s_0^* , \tag{3.9}$$

where

$$h_1 = \hat{h}_1(\mu(\tau)) = h_{10} \left\{ 1 - \frac{\mu(\tau)}{\mu_s} \right\} , \tag{3.10}$$

$$h_2 = \hat{h}_2(s^*(\tau)) = h_{20} \left\{ 1 - \frac{s^*(\tau)}{s_s^*} \right\} , \tag{3.11}$$

are the hardening functions. Also we have $h_{10} = \mu_s/u_1$ and $h_{20} = s_s^*/u_2$ so that, using the values given in (3.6), (3.7), we get

$$h_{10} = 0.418 \text{ mm}^{-1} , \quad h_{20} = 44.0 \text{ MPa/mm} .$$

Predictions from the model and comparison with experiments for the dependence of τ on p at "small" and "large" sliding distances are shown in fig. (3.9), for a step-change pressure test in fig. (3.10), and for a cyclic sliding test (the sliding direction is reversed a few times) in fig. (3.11). The major features of the interfacial friction resistance between the surfaces of steel and copper are reasonably well captured by the simple constitutive model for $\tau = \hat{s}(p, \bar{u}^s)$.

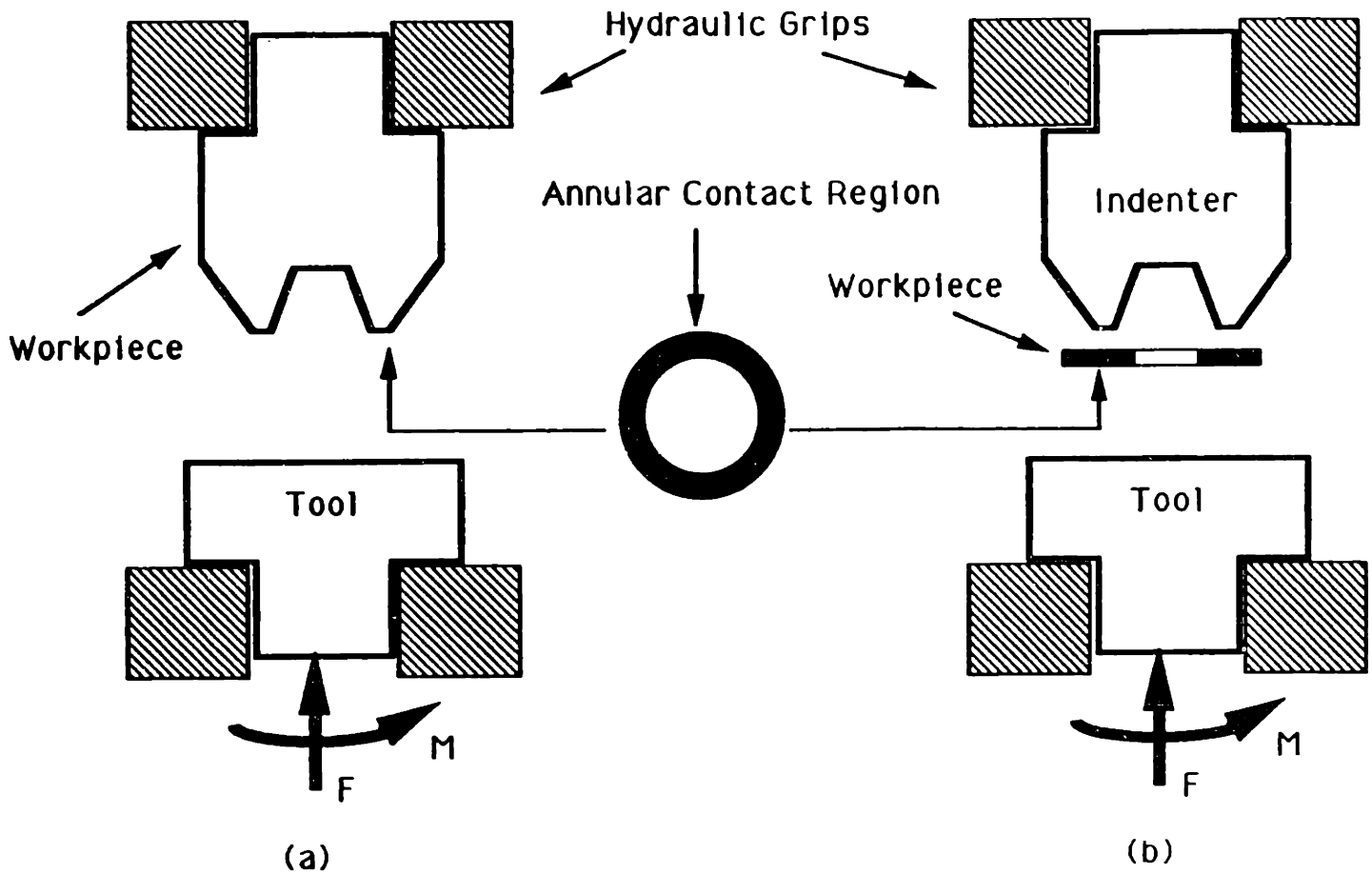

Figure 3.1: Experimental setups for friction testing: (a) low and moderate contact pressure range; (b) high contact pressure range.

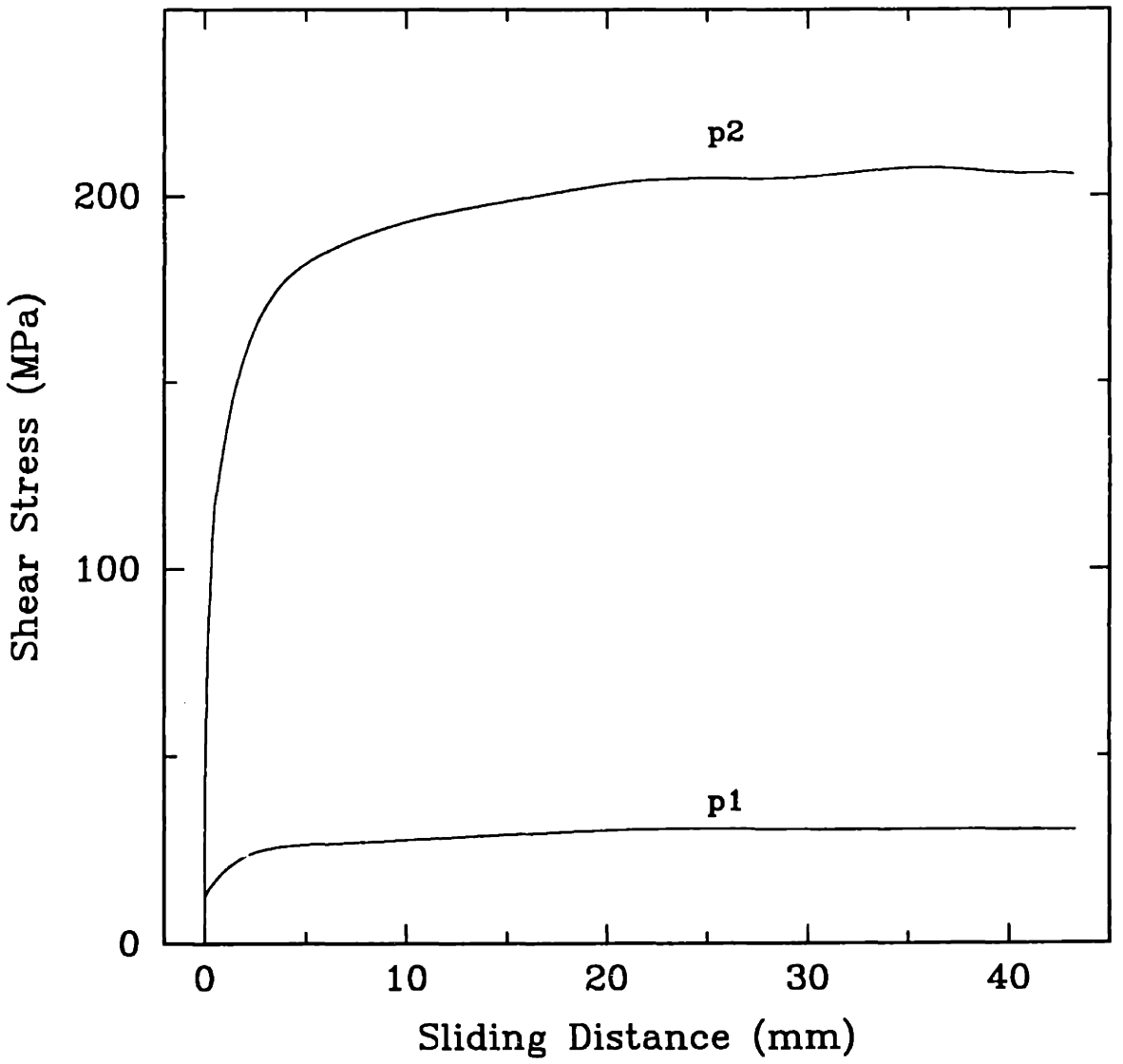

Figure 3.2: Friction tests at low and high contact pressures: $p_1 = 40$ MPa, $p_2 = 540$ MPa, dry steel-copper interface, $v = 0.3$ mm/sec.

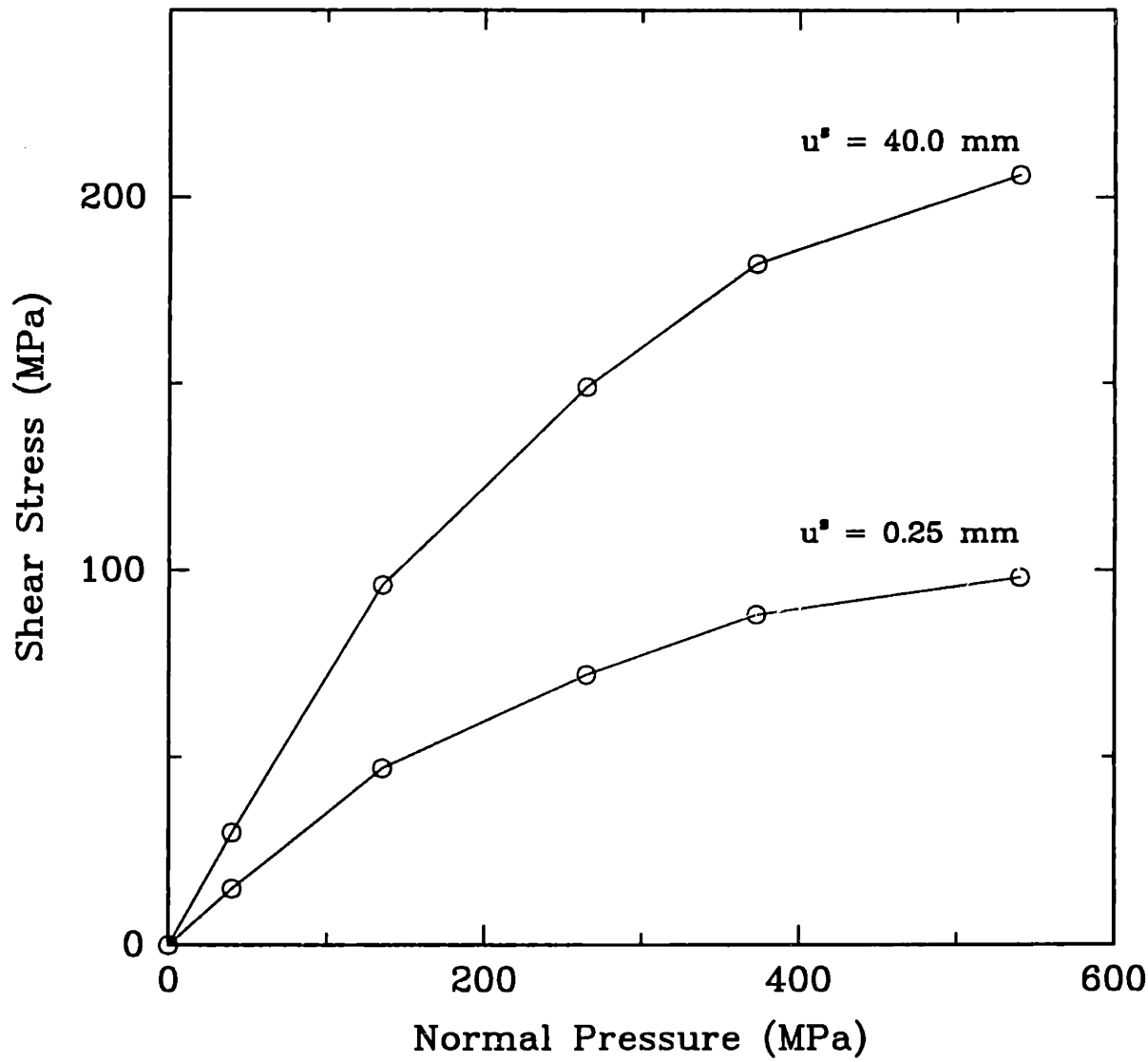

Figure 3.3: Pressure-dependence of frictional resistance for small and large sliding distances, dry steel-copper interface, $v = 0.3$ mm/sec.

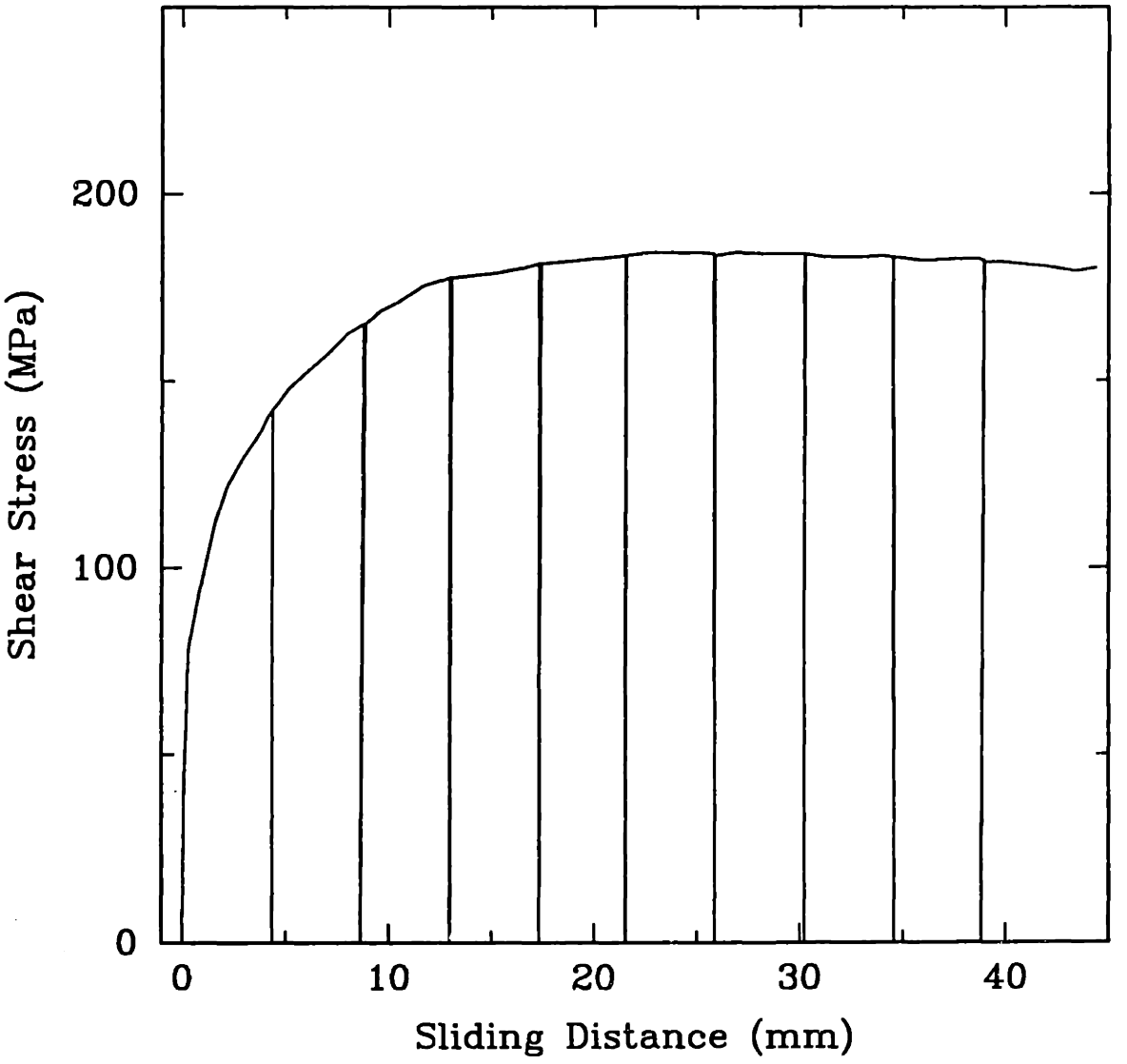

Figure 3.4: Interrupted friction test on a dry steel-copper interface: $p = 339$ MPa, $v = 0.3$ mm/sec.

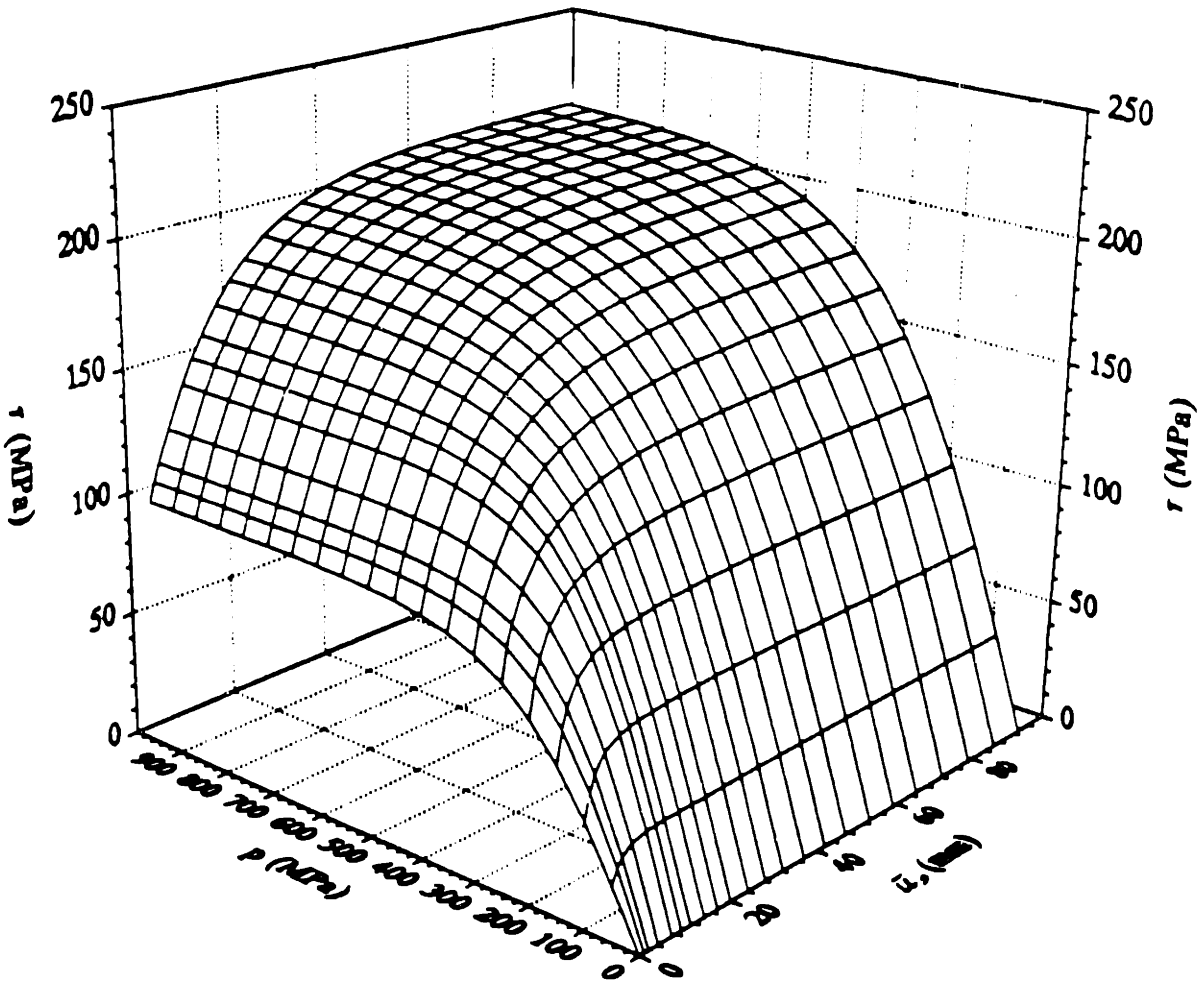

Figure 3.5: Schematic of frictional resistance surface.

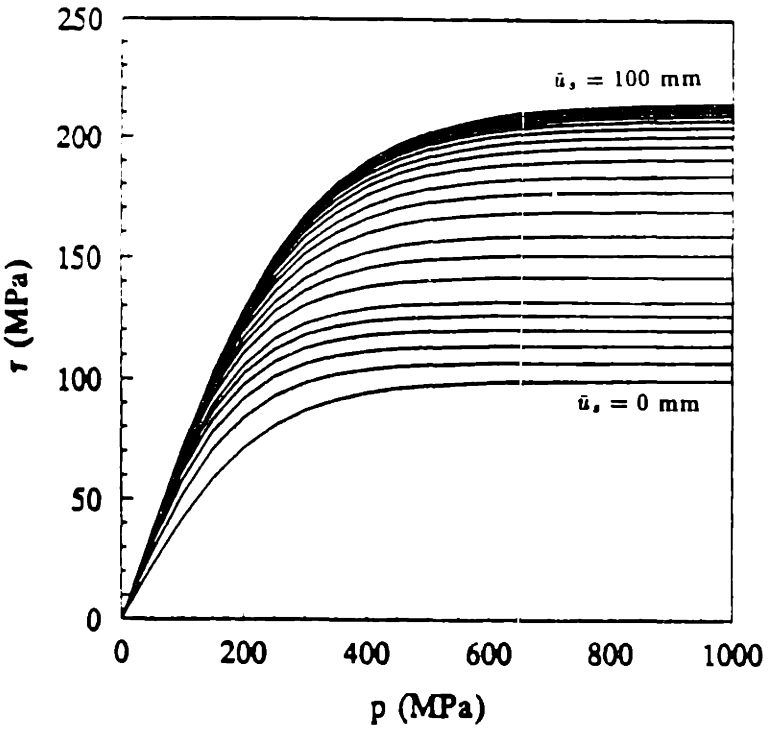

Figure 3.6: Schematic of pressure-dependence of frictional resistance.

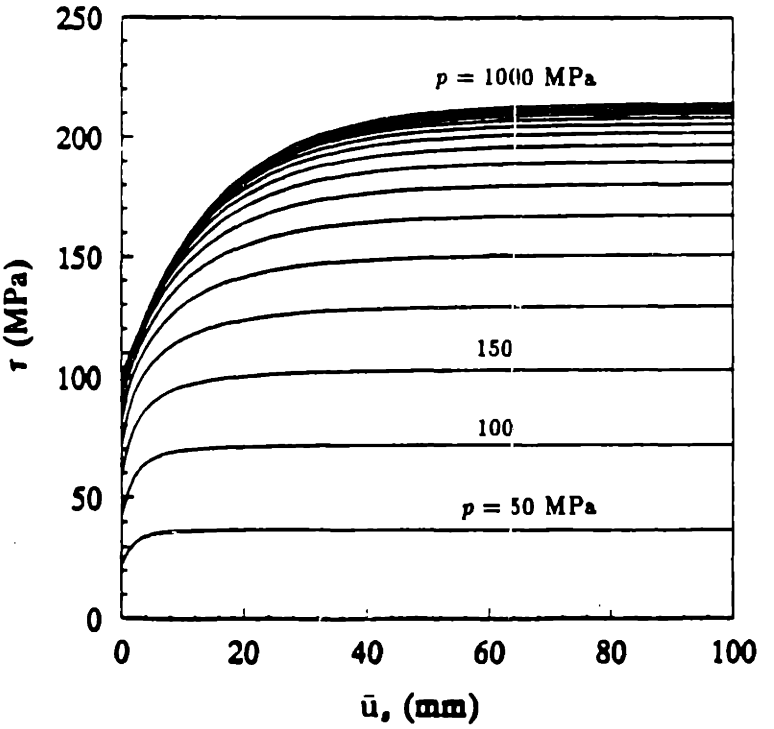

Figure 3.7: Schematic of the dependence of the frictional resistance on the sliding distance.

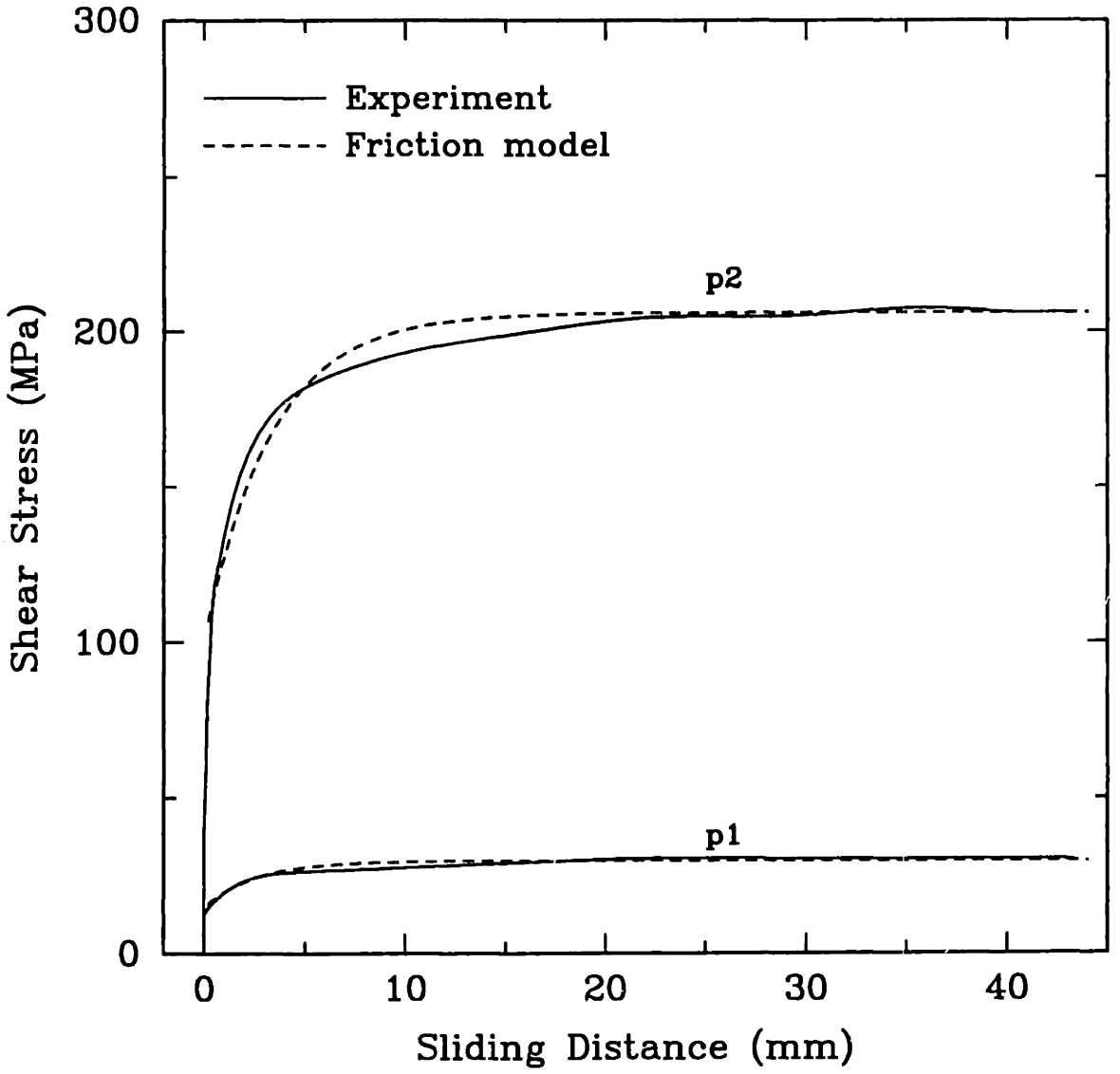

Figure 3.8: Identification of friction model parameters for the dry steel-copper interface: $\mu_0 = 0.33$, $\mu_s = 0.624$, $u_1 = 1.5$ mm, $\tau_0 = 108$ MPa, $\tau_s = 220$ MPa, $u_2 = 5.0$ mm.

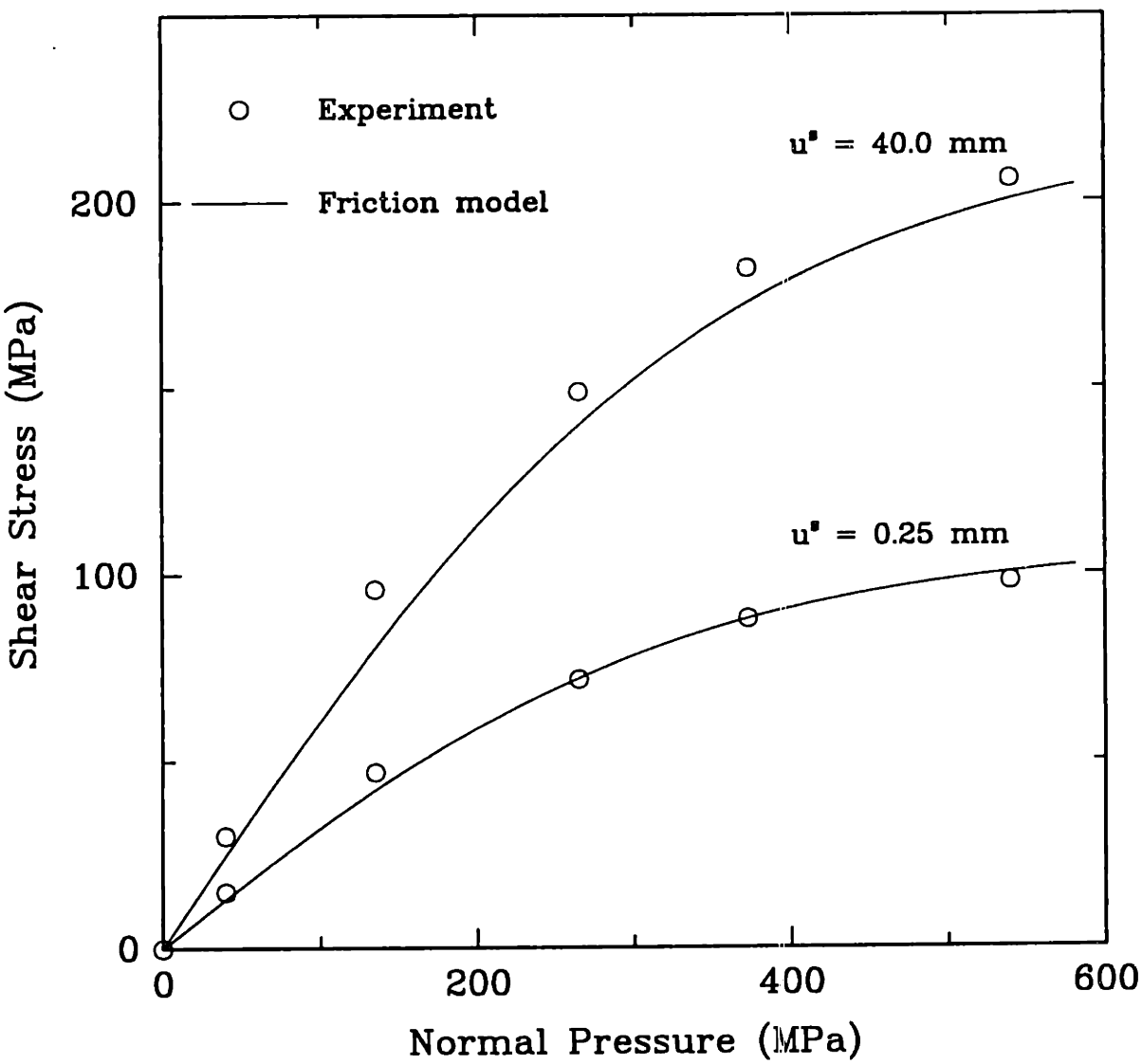

Figure 3.9: Comparison of model prediction and experiment on pressure-dependence of frictional resistance, dry steel-copper interface.

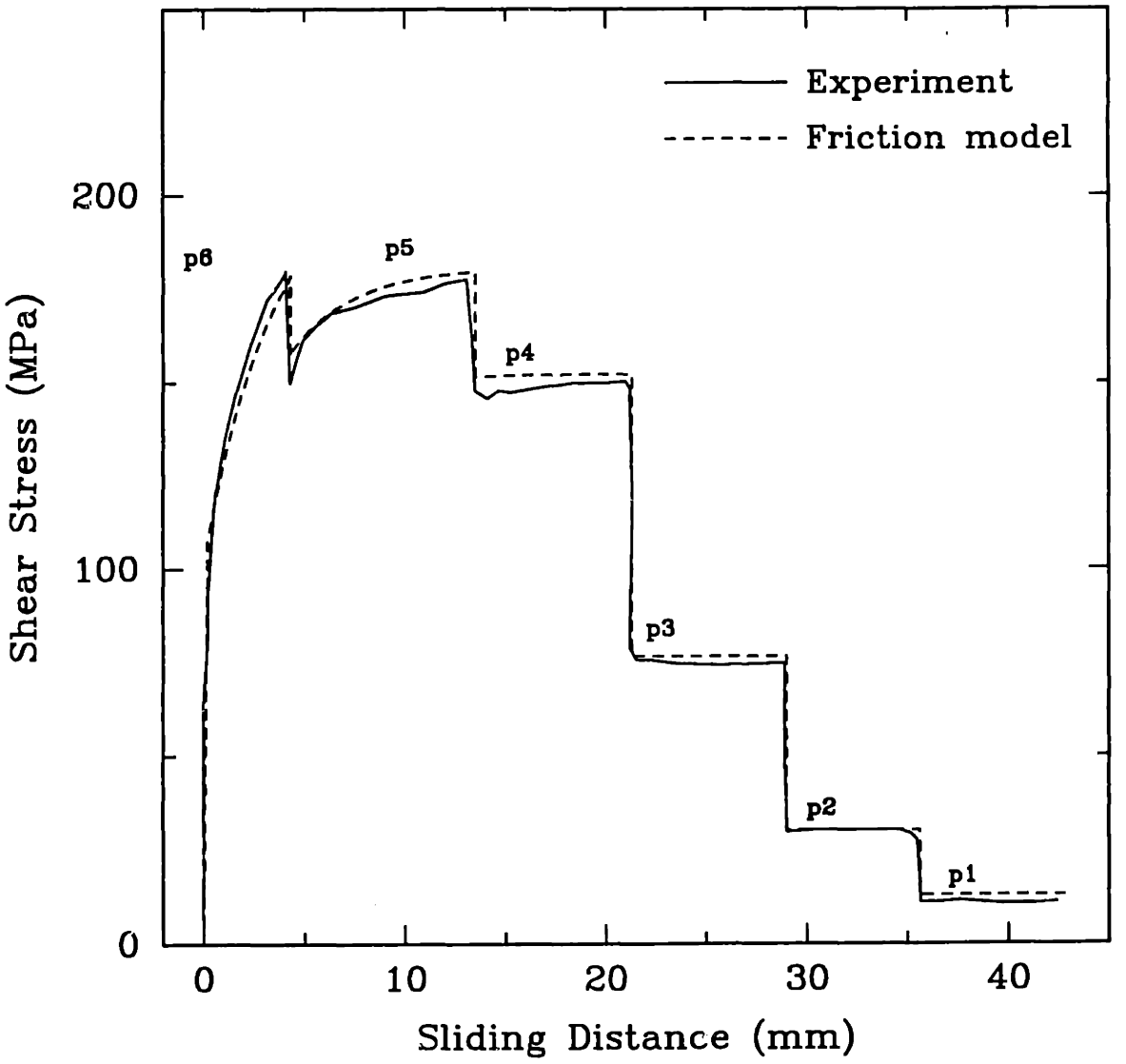

Figure 3.10: Comparison of model prediction and experiment on step-changes in normal pressure, dry steel-copper interface, $v = 0.3$ mm/sec, $p_6 = 570$ MPa, $p_5 = 352$ MPa, $p_4 = 255$ MPa, $p_3 = 110$ MPa, $p_2 = 41$ MPa and $p_1 = 17$ MPa.

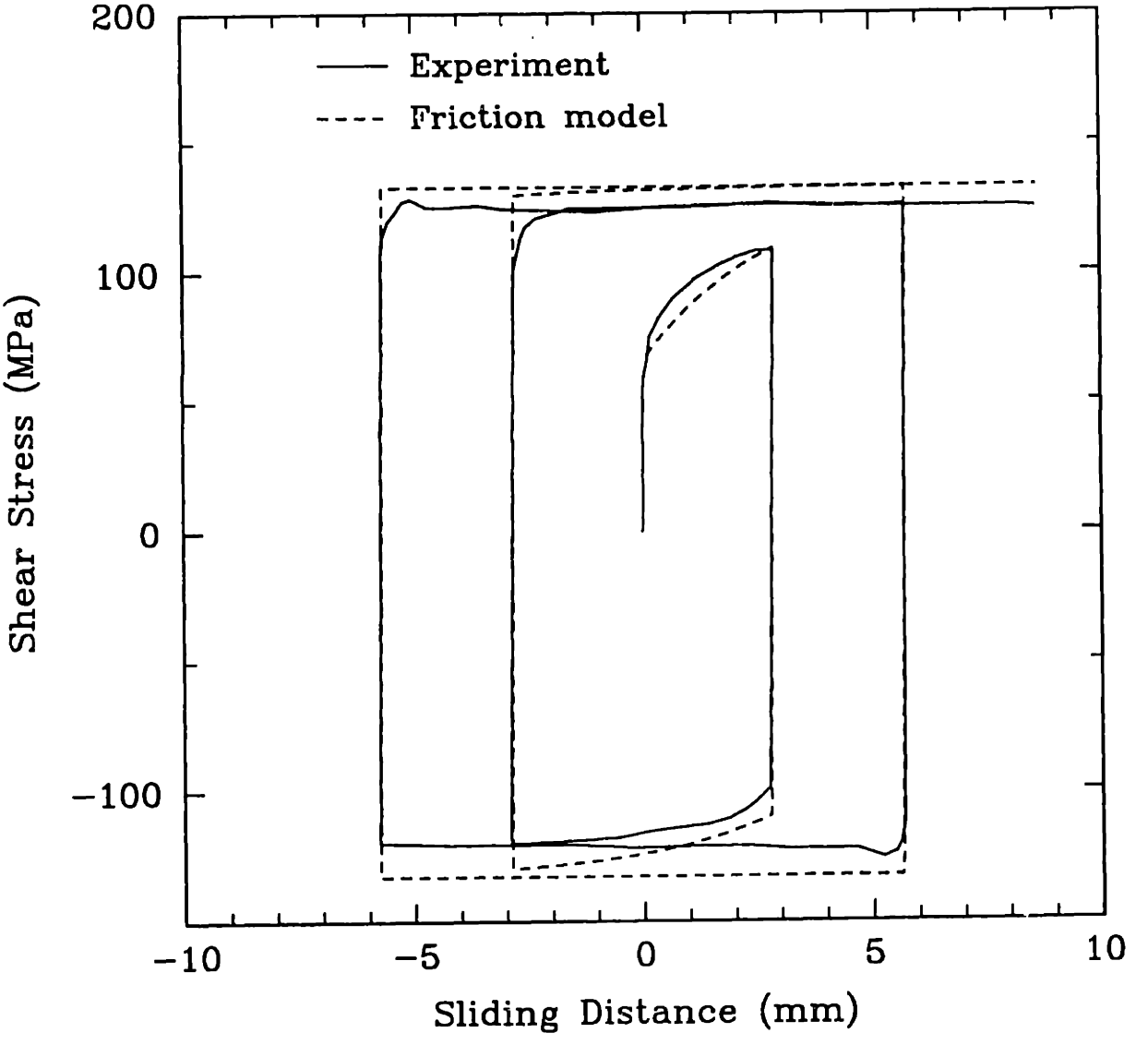

Figure 3.11: Comparison of model prediction and experiment for cyclic sliding, dry steel-copper interface: $p = 207$ MPa, $v = 0.3$ mm/sec.

Chapter 4

Finite Element Implementation

4.1 Introduction

This chapter discusses the implementation of the new interface constitutive model and the time-integration procedure into the implicit finite element program ABAQUS (Development Version 5.1). Also, several numerical examples are solved and the results are presented and discussed.

In metal forming operations the workpiece is in general much softer than the tool. The workpiece deforms plastically while the tool remains in the elastic domain. It is profitable to take advantage of this fact by modeling the tool as a rigid surface. ABAQUS provides a library of interface elements which model the contact between a deforming body and a rigid body (see ABAQUS Reference Manuals, 1990). At each integration point of these contact elements a measure of overclosure (numerical penetration of the point on the surface of the deforming body into the rigid surface) and measures of relative shear sliding are constructed. These kinematic measures are then used, together with specific surface interaction theories (contact and friction) to determine the contribution of the surface of contact to the overall system of finite element equations.

4.2 User Friction Subroutine

The rate-independent frictional constitutive equations and time-integration procedures described in Chapter 2 have been implemented in the implicit finite element code ABAQUS (Development Version 5.1) by writing a friction subroutine, FRIC. Concerning the normal contact, ABAQUS allows a "softened" surface to be defined, for which, as schematically shown in fig. (4.1), the pressure p transmitted between the surfaces increases exponentially as the surfaces come into contact. Thus the normal traction is not given in a rate form, as in the developed model, but is given instead as a direct function of the "overclosure"(or clearance), h, of the surfaces (the interpenetration of the surfaces). This corresponds to using a normal stiffness k_N which varies with the overclosure h. The specific functional form for p and k_N are completely defined by specifying the clearance c at which the contact pressure is zero and the pressure $p_0 = p(h)|_{h=0}$ at zero clearance:

$$\begin{aligned}
p &= 0 && \text{for } h \geq c \\
p &= \tfrac{p_0}{(\exp(1)-1)}\left[\left(\tfrac{h}{c}+1\right)\left(\exp\left(\tfrac{h}{c}+1\right)-1\right)\right] && \text{for } -6c < h < c \\
p &= \tfrac{p_0}{(\exp(1)-1)}\left[7\exp(7)-1+\left(\tfrac{h}{c}-6\right)(8\exp(7)-1)\right] && \text{for } h < -6c
\end{aligned}$$

and

$$\begin{aligned}
k_N &= \tfrac{dp}{dh} = 0 && \text{for } h \geq c \\
k_N &= \tfrac{dp}{dh} = \tfrac{p_0}{(\exp(1)-1)}\left[\tfrac{1}{c}\left(\tfrac{h}{c}+2\right)\exp\left(\tfrac{h}{c}+1\right)-\tfrac{1}{c}\right] && \text{for } -6c < h < c \\
k_N &= \tfrac{dp}{dh} = \tfrac{p_0}{(\exp(1)-1)}\left[\tfrac{8}{c}\exp(7)-\tfrac{1}{c}\right] && \text{for } h < -6c
\end{aligned}$$

The FRIC subroutine is called once for each integration point of every contact element in the model for every global iteration. The input provided to FRIC consists of the following quantities:

(i) the components with respect to the tangential orthonormal basis $\{\mathbf{e}^s_\alpha(\tau), \alpha =$

$1,2\}$, of the tangential traction $\mathbf{t}_T(t)$ rotated by $\mathbf{R}_t(\tau)$:

$$\tau_\alpha(t) \;=\; [\mathbf{R}_t(\tau)\,\mathbf{t}_T(t)] \cdot \mathbf{e}^s_\alpha(\tau)\,. \tag{4.1}$$

Using eqn (2.22) we note that $\tau_\alpha(t)$ are also the components of $\mathbf{t}_T(t)$ with respect to $\mathbf{e}^s_\alpha(t)$:

$$\tau_\alpha(t) \;=\; \mathbf{t}_T(t) \cdot \left[\mathbf{R}^T_t(\tau)\,\mathbf{e}^s_\alpha(\tau)\right] \;=\; \mathbf{t}_T(t) \cdot \mathbf{e}^s_\alpha(t)\,; \tag{4.2}$$

(*ii*) the pressure at the beginning and at the end of the increment, $p(t)$ and $p(\tau)$;

(*iii*) the components of the relative displacement increment $\bar{\mathbf{u}}_t(\tau)$ with respect to $\mathbf{e}^s_\alpha(\tau)$, which are also the components of the rotation-neutralized relative displacement increment $\tilde{\mathbf{u}}_t(\tau)$ with respect to $\mathbf{e}^s_\alpha(t)$:

$$\begin{aligned}\Delta\gamma_\alpha(\tau) \;\equiv\; \bar{\mathbf{u}}_t(\tau) \cdot \mathbf{e}^s_\alpha(\tau) \;=\; \bar{\mathbf{u}}_t(\tau) \cdot [\mathbf{R}_t(\tau)\,\mathbf{e}^s_\alpha(t)] \;=\; \\ \left[\mathbf{R}^T_t(\tau)\bar{\mathbf{u}}_t(\tau)\right] \cdot \mathbf{e}^s_\alpha(t) \;=\; \tilde{\mathbf{u}}_t(\tau) \cdot \mathbf{e}^s_\alpha(t)\,;\end{aligned} \tag{4.3}$$

(*iv*) the internal variable $\bar{u}^s(t)$ at the beginning of the increment.

With reference to the time-integration algorithm given in Chapter 2, we then have:

Step 1 The transformed relative displacement increment $\tilde{\mathbf{u}}_t(\tau)$ is provided as an input to FRIC in terms of its components $\Delta\gamma_\alpha(\tau)$ (see eqn 4.3).

Step 2 The contact pressure $p(\tau)$ is calculated prior to the call to FRIC and provided as an input.

Step 3 The trial tangential traction $\tilde{\mathbf{t}}^*_T(\tau)$is calculated in terms of its components with respect to $\mathbf{e}^s_\alpha(t)$:

$$\tilde{\tau}^*_\alpha(\tau) \;=\; \tau_\alpha(t) \;+\; (-k_T)\,\Delta\gamma_\alpha(\tau)\,,$$

where $\tau_\alpha(t)$ are the components of $\mathbf{t}_T(t)$ with respect to $\mathbf{e}^s_\alpha(t)$. The effective value of the trial tangential traction is computed according to

$$\bar{\tau}^* = \sqrt{\sum_{\alpha=1}^{2} (\tilde{\tau}^*_\alpha(\tau))^2}\,.$$

Step 4 If

$$\bar{\tau}^* < s(t)$$

then the process is adhering and $\mathbf{t}_T(\tau)$ is given in terms of its components with respect to $\mathbf{e}^s_\alpha(\tau)$:

$$\begin{aligned}\tau_\alpha(\tau) &= \left[\mathbf{R}_t(\tau)\,\tilde{\mathbf{t}}^*_T(\tau)\right]\cdot\mathbf{e}^s_\alpha(\tau) = \tilde{\mathbf{t}}^*_T(\tau)\cdot\left[\mathbf{R}_t{}^T(\tau)\,\mathbf{e}^s_\alpha(\tau)\right] = \\ &\tilde{\mathbf{t}}^*_T(\tau)\cdot\mathbf{e}^s_\alpha(t) = \tilde{\tau}^*_\alpha(\tau)\,,\end{aligned}$$

Also,

$$\begin{aligned}\mu(\tau) &= \mu(t)\,,\\ s^*(\tau) &= s^*(t)\,,\\ s(\tau) &= s(t)\,.\end{aligned}$$

Otherwise the process is slipping. The parameters $\mu(\tau)$ and $s^*(\tau)$ are calculated by solving

$$\begin{aligned}\mu(\tau) - \mu(t) - \hat{h}_1(\mu(\tau))\frac{1}{k_T}\{\bar{\tau}^*(\tau) - \hat{s}(\mu(\tau), s^*(\tau), p(\tau))\} &= 0\,,\\ s^*(\tau) - s^*(t) - \hat{h}_2(s^*(\tau))\frac{1}{k_T}\{\bar{\tau}^*(\tau) - \hat{s}(\mu(\tau), s^*(\tau), p(\tau))\} &= 0\,.\end{aligned}$$

Step 5 The effective traction $\bar{\tau}(\tau) = s(\tau)$ is calculated as

$$\bar{\tau}(\tau) = s^*(\tau)\tanh\left[\frac{\mu(\tau)p(\tau)}{s^*(\tau)}\right],$$

Step 6 The radial return factor $\eta(\tau)$ is calculated as

$$\eta(\tau) = (\bar{\tau}(\tau)/\bar{\tau}^*(\tau)) .$$

Step 7 The components of $\mathbf{t}_T(\tau)$ with respect to $\mathbf{e}^s_\alpha(\tau)$ are calculated as follows:

$$\tau_\alpha(\tau) = \left\{\mathbf{R}_i(\tau)\left[\eta(\tau)\,\tilde{\mathbf{t}}^*_T(\tau)\right]\right\}\cdot\mathbf{e}^s_\alpha(\tau) = \left[\eta(\tau)\,\tilde{\mathbf{t}}^*_T(\tau)\right]\cdot\mathbf{e}^s_\alpha(t) = \eta(\tau)\,\tilde{\tau}^*_\alpha(\tau) .$$

An additional output expected from FRIC consists of the frictional components of the contribution $\tilde{\mathbf{M}}$ to the Jacobian matrix used in the Newton scheme for global equilibrium (see Section 2.5). Also, we notice that the operation $\mathbf{n}(\tau) = \mathbf{R}(\tau)\,\mathbf{n}(t)$ is performed in the main prior to the call to FRIC.

4.3 Numerical Simulations

In this section example calculations, performed using ABAQUS and the new frictional model and time-integration procedure are presented for: (a) Simple sliding with superposed rigid body rotation. This calculation is performed to verify the objectivity of the constitutive model and the time-integration procedure. (b) The ring compression test. This test is the most widely used experiment to indirectly assess the frictional properties of interfaces in metalworking. Predictions from the computational procedures show excellent agreement with experimental results. (c) Extrusion of a cylindrical billet. This calculation illustrates the effect of extensive sliding on the frictional properties of the interface. (d) Formation of central damage in the form of central bursts during drawing of a rod. This calculation extends the work of Zavaliangos & Anand (1992) by including the effect of heating generated at the sliding interfaces between the die and the workpiece. These examples show

the versatility of the constitutive model and the robustness of the time-integration procedure.

The subroutine FRIC is given in Appendix C. Also, all the ABAQUS input files are given in Appendix D.

4.3.1 Simple Sliding with Superposed Rotation

With respect to a rectangular cartesian coordinate system with origin $\mathbf{o}$ and orthonormal base vectors $\{\mathbf{e}_i | \, i = 1,3\}$, a simple translational motion in the $\mathbf{e}_1$-direction is described by

$$\mathbf{x} = \mathbf{p} + (\dot{\delta}t)\mathbf{e}_1 \,, \tag{4.4}$$

or in component form,

$$x_1 = p_1 + (\dot{\delta}t), \qquad x_2 = p_2, \qquad x_3 = p_3, \tag{4.5}$$

with $\dot{\delta} \geq 0$ a constant.

In order to study the incremental objectivity of our friction constitutive model and the time-integration procedure, consider the motion of two bodies which are undergoing relative sliding together with superposed rigid rotation. Let superscripts $(+)$ and $(-)$ refer to the "workpiece" and the "tool", respectively. Then, the relative motions of these two bodies under consideration are given by

$$\mathbf{x}^+ = \mathbf{o} + \mathbf{Q}(t)[\mathbf{p}^+ + (\dot{\delta}t)\mathbf{e}_1(0)] \,, \tag{4.6}$$

$$\mathbf{x}^- = \mathbf{o} + \mathbf{Q}(t)[\mathbf{p}^- - \mathbf{o}] \,, \tag{4.7}$$

where

$$\mathbf{Q}(t) = (\mathbf{e}_1 \otimes \mathbf{e}_1 + \mathbf{e}_2 \otimes \mathbf{e}_2)\cos(\dot{\theta}t) + (\mathbf{e}_1 \otimes \mathbf{e}_2 - \mathbf{e}_2 \otimes \mathbf{e}_1)\sin(\dot{\theta}t) + \mathbf{e}_3 \otimes \mathbf{e}_3 \,, \tag{4.8}$$

is an anti-clockwise rotation by an angle $(\dot{\theta}t)$ about $\mathbf{e}_3$.

The position of the contacting points at time τ is described by

$$\boldsymbol{\xi}^+ = \mathbf{o} + \mathbf{Q}(\tau)[\mathbf{p}^+ + (\dot{\delta}\tau)\mathbf{e}_1(0)], \tag{4.9}$$

$$\boldsymbol{\xi}^- = \mathbf{o} + \mathbf{Q}(\tau)[\mathbf{p}^- - \mathbf{o}]. \tag{4.10}$$

From (4.6) and (4.7) we have that

$$\mathbf{p}^+ = \mathbf{Q}^T(t)(\mathbf{x}^+ - \mathbf{o}) - (\dot{\delta}t)\mathbf{e}_1(0), \tag{4.11}$$

$$\mathbf{p}^- = \mathbf{o} + \mathbf{Q}^T(t)(\mathbf{x}^- - \mathbf{o}). \tag{4.12}$$

Substituting (4.11) and (4.12) in (4.9) and (4.10), respectively, and recalling that $\mathbf{R}_t(\tau) = \mathbf{Q}(\tau)\mathbf{Q}^T(t)$, the motion of the contacting points relative to the current configurations $\mathcal{B}_t^+$ and $\mathcal{B}_t^-$ of the workpiece and the tool are described by

$$\boldsymbol{\xi}^+ = \mathbf{o} + \mathbf{R}_t(\tau)[(\mathbf{x}^+ - \mathbf{o}) + (\dot{\delta}\Delta t)\mathbf{e}_1(t)], \tag{4.13}$$

$$\boldsymbol{\xi}^- = \mathbf{o} + \mathbf{R}_t(\tau)(\mathbf{x}^- - \mathbf{o}). \tag{4.14}$$

Next the incremental displacements of each of the two bodies are

$$\mathbf{u}_t^+(\tau) = \boldsymbol{\xi}^+ - \mathbf{x}^+ = \mathbf{R}_t(\tau)[(\mathbf{x}^+ - \mathbf{o}) + (\dot{\delta}\Delta t)\mathbf{e}_1(t)] - (\mathbf{x}^+ - \mathbf{o}), \tag{4.15}$$

$$\mathbf{u}_t^-(\tau) = \boldsymbol{\xi}^- - \mathbf{x}^- = \mathbf{R}_t(\tau)(\mathbf{x}^- - \mathbf{o}) - (\mathbf{x}^- - \mathbf{o}), \tag{4.16}$$

and therefore the relative displacement between the two bodies is

$$\bar{\mathbf{u}}_t(\tau) = \mathbf{u}_t^+(\tau) - \mathbf{u}_t^-(\tau) = \mathbf{R}_t(\tau)(\dot{\delta}\Delta t)\mathbf{e}_1(t), \tag{4.17}$$

and the rotation-neutralized displacement

$$\tilde{\mathbf{u}}_t(\tau) = \mathbf{R}_t(\tau)^T\bar{\mathbf{u}}_t(\tau) = (\dot{\delta}\Delta t)\mathbf{e}_1(t). \tag{4.18}$$

Eqn (4.18) indicates that the relative displacement increment at a particular pair of points in contact, upon which the frictional forces depend, is given by:

$$\Delta\gamma_1 = (\tilde{\mathbf{u}}_t(\tau)) \cdot \mathbf{e}_1(t) \equiv \dot{\delta}\Delta t\,. \tag{4.19}$$

Turning our attention to the tangential traction vector, we have:

$$\tilde{\mathbf{t}}_T(\tau) = \mathbf{R}_t(\tau)^T \mathbf{t}_T(\tau)\,, \tag{4.20}$$

and

$$\tilde{\mathbf{t}}_T(t) = \mathbf{t}_T(t)\,. \tag{4.21}$$

Let $\mathbf{e}_2(t) \equiv \mathbf{n}(t)$. Then:

$$\sigma_{12} = \mathbf{e}_1 \cdot \mathbf{T}(t)\mathbf{e}_2(t) \equiv \tilde{\tau}_1(t)\,, \tag{4.22}$$

where $\mathbf{T}(t)$ is the stress tensor and $\tilde{\tau}_1(t)$ is the component of the traction $\mathbf{T}(t)\mathbf{e}_2(t)$ in the $\mathbf{e}_1$-direction, or simply the shear stress, both evaluated at time t. Next, according to the algorithm:

$$\tilde{\tau}_1(\tau) = \tilde{\tau}_1(t) + (-k_T)[\Delta\gamma_1 - \chi\Delta\gamma_1^s(\tilde{\tau}_1(\tau))]\,, \tag{4.23}$$

where $\tilde{\tau}_1(\tau)$ is the shear stress at time τ with respect to the basis $\mathbf{e}_\alpha(t)$, that is:

$$\tilde{\mathbf{t}}_T(\tau) = \tilde{\tau}_1(\tau)\mathbf{e}_1(t)\,. \tag{4.24}$$

Finally,

$$\mathbf{t}_T(\tau) = \mathbf{R}_t(\tau)\tilde{\mathbf{t}}_T(\tau) = \tilde{\tau}_1(\tau)\mathbf{e}_1(\tau)\,. \tag{4.25}$$

This problem was simulated using ABAQUS by modeling the workpiece as a single four-noded plane strain element (ABAQUS type CPE4) and the tool as a rigid surface. A single contact element (ABAQUS type IRS21) was used to model the contact. A

constant pressure of 10 MPa was imposed at the interface by defining the pressure-overclosure function such that $p(h)|_{h=0} = 10$ MPa and maintaining an overclosure $h = 0$. The slip resistance was set to be $s = \mu p$, with $\mu = 0.1$. The penalty parameter was chosen to be $k_T = 2$ MPa/mm, so that, for a given total relative displacement of 1 mm, half of the process would be adhering and half slipping[1]. The element nodes and the rigid surface were then subjected to the motion defined by eqns (4.6), (4.7), and (4.8) by means of the ABAQUS user subroutine DISP, also given in appendix B. This motion allows for no relative displacement between the nodes of the element representing the workpiece, and thus the internal stresses were all zero. The calculation was performed with $\dot{\theta} = 2\pi$ radians per second, $\dot{\delta} = 1$ mm per second, and $t \in [0, 1]$ seconds. A fixed time step of $\Delta t = 0.1$ seconds was used, corresponding to a rotation of $\Delta\theta = 36°$ and a relative sliding $\Delta\delta = 0.1$ mm.

Fig. (4.2) shows the "tool-workpiece" configuration at time $t = 0$ sec, and at the end of each one of the 10 increments. We see that the final position corresponds to a simple translation from the initial configuration. Fig. (4.3) shows the shear stress as a function of the sliding. The "exact" solution to the problem is:

$$\tau = \begin{cases} k_T \delta & \text{for} \quad \delta < 0.5 \text{ mm} \\ \mu p & \text{for} \quad \delta > 0.5 \text{ mm} \end{cases} . \tag{4.26}$$

The calculated curve matches this solution.

The problem was also solved using the slip resistance function and evolution law proposed in Chapter 2, and the frictional parameters determined experimentally for the copper-steel interface as described in Chapter 3. Here, as in the following example problems, the tangential stiffness in adherance was chosen to be[2] $k_T = 10^4$ MPa/mm.

[1]Here the value of the parameter k_T was so chosen exclusively on the basis of numerical convenience. In general its choice requires some care: the convergence of the solution is more rapid when it is small, but the larger its value the better it simulates the actual behavior.

[2]This value appears to be of the same order of magnitude as the value which can be derived from

Fig. (4.4) shows the shear stress as a function of the sliding, in the case of a simple sliding motion and in the case of the sliding motion with superposed rigid body rotation. The two curves practically coincide.

4.3.2 Ring Compression Problem

As a simple metal-forming example, the problem of isothermal compression of a ring specimen was solved. This test has been the most widely-used technique for determining friction in metal forming process, particularly for bulk plastic deformation processes such as forging (KALPAKJIAN, 1991). The basis for this technique is that the amount of change in the inner diameter of a ring specimen for a given reduction in height is a sensitive parameter of the interface friction. Numerical values for the coefficient of friction μ or the friction factor m are then obtained by comparison of experimental reduction in internal diameter versus reduction in height curves, with calibration curves obtained analytically, either by using upper-bound limit analyses or finite element calculations (see SCHEY, 1983).

The dimensions of the specimen were as follows: {outer diameter 0.9 in, inner diameter 0.45 in, height 0.3 in}, corresponding to the ratio $\{6 : 3 : 2\}$, which is the most common geometry for specimens used in this application. The constitutive model adopted to describe the bulk material behavior was the rate-independent isotropic elastic-plastic with isotropic hardening model available in ABAQUS. The material parameters and the stress versus plastic strain law, needed in this model to describe the hardening of the material, were taken from BRONKHORST (1991). A value of $E = 123$ GPa was used for copper's Young's modulus. The Poisson's ra-

the interrupted friction test described in chapter 3. Furthermore, for all the problems that were analysed, it was noticed that higher values of k_T would yield the same results while increasing the computational cost of the analysis.

tio was taken to be $\nu = 0.33$. The stress-strain curve is shown in fig. (4.5). The penalty parameter needed in the frictional constitutive model, was again taken to be $k_T = 10^4$ MPa/mm. The parameters needed to describe the evolution of the isotropic slip resistance with sliding were determined experimentally as described in Chapter 3. Specifically these are

$$\mu_0 = 0.33,\ \mu_s = 0.627,\ h_{10} = 0.418\ \text{mm}^{-1},$$

and

$$s_0^* = 108\ \text{MPa},\ s_s^* = 220\ \text{MPa},\ h_{20} = 44\ \text{MPa/mm}.$$

Fig. (4.6) shows a schematic of the ring specimen and the finite element mesh containing 270 four-noded axisymmetric elements[3] (ABAQUS type CAX4). We note that symmetry allows us to model only one quarter of the specimen. Near the corners, where fold-over is expected to occur, the mesh is much finer. The die face was modeled as a rigid surface and the external surface of the model was covered with interface elements (ABAQUS type IRS21A) to model the contact conditions.

Fig. (4.7) shows the deformed finite element mesh after a height reduction of 50 %. The inner surface of the ring is seen to expand inward, while the outer surface expands outward. This is an effect due to the presence of friction: in frictionless conditions both surfaces expand outward. Fig. (4.8) shows the history of total die force versus die displacement. The experimental load versus displacement curve matches very well with the simulation. Fig. (4.9) shows the percentage of reduction in internal diameter versus reduction in height. Here again it is seen that the simulation matches very well with the experimental results. Fig. (4.10)(a,b) shows the contact pressure and the

[3]These elements in ABAQUS address the problem of mesh-locking in (near) incompressible situations by using the method of NAGTEGAAL, PARKS and RICE (1974).

contact shear stress at a height reduction of 60%. We note the characteristic "hill" in the pressure distribution (SCHEY, 1983), and the inversion of the shear stress at the point of no sliding. Also it can be seen that the shear slip resistance is dependent on the position of the point in contact since each point experiences a different amount of sliding.

The problem was also solved using ABAQUS frictional algorithm, with a constant coefficient of friction $\mu = 0.33$ and a shear stress limit $\tau_{lim} = 108$ MPa. These values correspond to the *initial* values for μ amd s^* used in our model, and were chosen since they approximate the slip resistance-pressure curves at zero sliding distance, determined experimentally for the two materials, as shown in fig. (4.11). This is justified in view of the results which show the distance slid to be less then 1 mm at most points of the interface up to 50 % upsetting.

The load versus displacement curve obtained using the existing ABAQUS friction model was seen to practically coincide with the curve obtained using the developed frictional constitutive model, fig. (4.8). However, as shown in fig. (4.12), somewhat higher reductions in internal diameter for a given height reduction were obtained using the ABAQUS friction model. This is in agreement with the the slip resistance versus pressure curve which results from the chosen values of μ and τ_{lim} (see fig. 4.11), which predicts a higher shear stress for a given pressure. Figure (4.13) compares the contact pressure and the contact shear stress distribution at a height reduction of 60% for the case of the new frictional model and the capped Coulomb model. We note that the slip-hardening phenomenon results in higher values of pressure and shear stress.

4.3.3 Extrusion of a Cylindrical Billet

The ring-compression test is a good test to study the accuracy of the assumed slip resistance-pressure curve for small relative sliding. However, due to the minimal sliding experienced by the contacting points, this problem is not an optimal test to verify the "slip-hardening" feature of our friction constitutive model. In an extrusion process on the other hand, the contacting points experience extensive amount of sliding before the material exits the die, and this therefore represents a better problem to investigate the evolution of the frictional resistance with sliding.

The rate-independent isotropic elastic-plastic with isotropic hardening constitutive model was again chosen for the bulk material. The same stress-strain curve as in the case of the ring compression test was used. The penalty parameter for the friction model was again taken to be $k_T = 10^4$ MPa/mm, and the same parameters as for the ring compression test were chosen to describe the evolution of the slip resistance.

Fig. (4.14) shows the finite element mesh containing 240 four-noded axisymmetric elements (ABAQUS type CAX4). Symmetry allows us to model only one half of the billet. The die face was modeled as a rigid surface and the external surface of the model was covered with interface elements (ABAQUS type IRS21A).

Fig. (4.15) shows the deformed finite element mesh at different stages of the analysis, while fig. (4.16) shows the history of total punch force versus punch displacement. Also plotted in the same graph is the experimental load-displacement curve. To simulate the initial gap between the die and the billet (of the order of ~ 0.03 mm) the straight portion of the mesh is not initially in contact with the rigid surface. This is reflected in the load-displacement curve by the abrupt change in slope which takes place when full contact between the billet and the die takes place, both for the exper-

imental data and for the prediction. Unfortunately, for the case of dry friction and for the given dimensions, the pressure inside the die becomes very large (over 1500 MPa for copper), and billet material is back-extruded, filling the gap which exists between the punch and the die. Since the gap is very small in comparison to the radius of the billet ($\sim$ 0.01 mm *vs.* $\sim$ 5 mm), it is impossible to simulate this event using the current finite element method. Therefore the action of the punch on the billet was simulated by displacing all the nodes on the bottom face of the billet, so that no back-extrusion was allowed to occur. Thus, meaningful comparison between predicted and experimental load-displacement curves is limited to the initial part of the extrusion process (up to 6 mm of punch displacement), where it can be assumed that back-extrusion is minimal.

The problem was also solved using ABAQUS frictional algorithm, with a coefficient of friction $\mu = .33$ and a shear stress limit $\tau_{lim} = 108$ MPa, and with a coefficient of friction $\mu = .627$ and a shear stress limit $\tau_{lim} = 220$ MPa. As shown in fig. (4.17), the two cases correspond to the initial and final values for μ and s^* used in our friction model.

With reference to fig. (4.18), we note that while the curve obtained using the slip-hardening model more closely follows the experimental curve the other two curves either underestimate or overestimate the load history. It seems reasonable to infer from this that the slip-hardening behavior plays an important role in metal forming operations which involve relative large amounts of sliding, particularly in the case of dry contact of metals. Furthermore the determination of the coefficient of friction or the friction factor by means of the ring compression test can lead to an underestimation of the maximum frictional forces.

4.3.4 Rod Drawing

In this section the focus of the study is shifted to examine the effect of heating due to friction in a metal-forming operation, namely the drawing of a rod. This problem has been very recently analysed by ZAVALIANGOS & ANAND (1992) to study the development of internal damage in the form of central bursts in porous metals. This type of defect is determined by growth of microvoids caused by the rise of large hydrostatic tension on the rod axis in the die zone. Using a new thermo-elasto-viscoplastic constitutive model for isotropic porous metals, these authors succesfully predicted the increase of porosity in the center of a rod undergoing a two-step frictionless drawing operation, by means of a finite element analysis. They showed that the heat generation due to plastic dissipation in a porous aluminum rod drawn at a speed of 10 m/s, although causing an increase in temperature of approximately 25 K for the region in the vicinity of the surface of the rod, did not have a significant effect on the values of hydrostatic tension and porosity. Nevertheless, as they suggest, in realistic situations friction at the interface between the workpiece and the die may be a more important source of heat generation than plastic deformation. In the present work the heat generated due to friction between the die and the workpiece was included in the analysis.

The material being drawn was taken to be the same aluminum alloy with the same material parameters considered by ZAVALIANGOS & ANAND, and their constitutive model for viscoplasticity of porous materials was used. Also the same dimensions were considered: the initial radius of the rod was taken to be 100 mm while the die was assumed to have a semi-cone angle of 15^{o} corresponding to a 16.3% reduction in area. While ZAVALIANGOS & ANAND assumed no heat transfer between the workpiece and the die and the die to be rigid, a *deformable and heat conducting* die was

considered in the present analysis. The die material was assumed to be steel, and perfectly elastic behavior was assumed. The geometry of the drawing operation, and the deformed finite element mesh are shown in figures (4.19) and (4.20), respectively. Because of the symmetry of the process, only one half of the problem was modeled. The rod was modeled with 287 4-noded coupled temperature-displacement elements (ABAQUS type CAX4T). The die was modeled with 33 of the same type of elements. The surface of the rod was covered with 2-noded coupled axisymmetric contact elements (ABAQUS type ISL21T). Friction at the interface was modeled using the developed constitutive model. As discussed in Appendix B, the constitutive parameters $\{\mu_0,\ \mu_s,\ h_{10},\ s_0^*,\ s_s^*,\ h_{20}\}$ were extrapolated from a set of experimental data derived for a *lubricated*[4] steel-aluminum interface. Specifically these are:

$$\mu_0 = 0.09,\ \mu_s = 0.25,\ h_{10} = 0.0833\ \text{mm}^{-1}\,,$$

and

$$s_0^* = 40\ \text{MPa},\ s_s^* = 80\ \text{MPa},\ h_{20} = 40\ \text{MPa/mm}\,.$$

The rod is gripped at the stepped-down end and pulled through the drawing dies at a rate of[5] 10 m/sec.

The results obtained by ZAVALIANGOS & ANAND, in the frictionless case and with non-conducting dies, are shown in fig. (4.21). These results show that a substantial hydrostatic tension can develop along the axis of the billet, and it is this hydrostatic tension that promotes void growth. Also we note that the porosity, set initially at $f_o = 0.01$, has increased to $f = 0.018$, and that the temperature increase, due to heating caused by plastic dissipation, is limited to approximately $25K$. The results

[4]Although the model was developed for dry interfaces, it was seen to be applicable to lubricated interfaces as well.

[5]This is the speed used by ZAVALIANGOS & ANAND in their thermo-mechanically coupled analysis.

obtained from the present analysis, which includes frictional heating and conduction through the dies, are shown in fig. (4.22)-fig. (4.24). The maximum temperature increase in the rod is now of the order of $100K$. Based on the model developed by ZAVALIANGOS & ANAND, an increase in temperature would tend to limit the increase in porosity. This fact is reflected in the results of fig. (4.22), which show that the porosity has increased only up to $f = 0.015$ instead of $f = 0.018$ as in the case of neglect of heat generation due to friction. Nevertheless this value is not much smaller than that obtained by ZAVALIANGOS & ANAND in frictionless conditions. The reason for this is that the maximum increase in temperature occurs near the surface where frictional heating takes place, while the temperature increase at the rod axis, where the hydrostatic tension develops to promote void growth, is limited.

Fig. (4.25) shows the pulling load as a function of the pulling displacement. Also shown is the load-displacement curve in the case of frictionless condition. As expected, the presence of friction *substantially* increases the load required for the operation.

The problem of void growth in porous metals due to hydrostatic tension is only one of the numerous phenomena in metal forming operations influenced by frictional heating. The temperature rise caused by frictional heating can in many cases be so high to affect several physical properties of the workpiece. The study of the effect of temperature on the frictional properties of the interface itself and the inclusion of frictional heating in the numerical simulation of forming problems is of substantial importance.

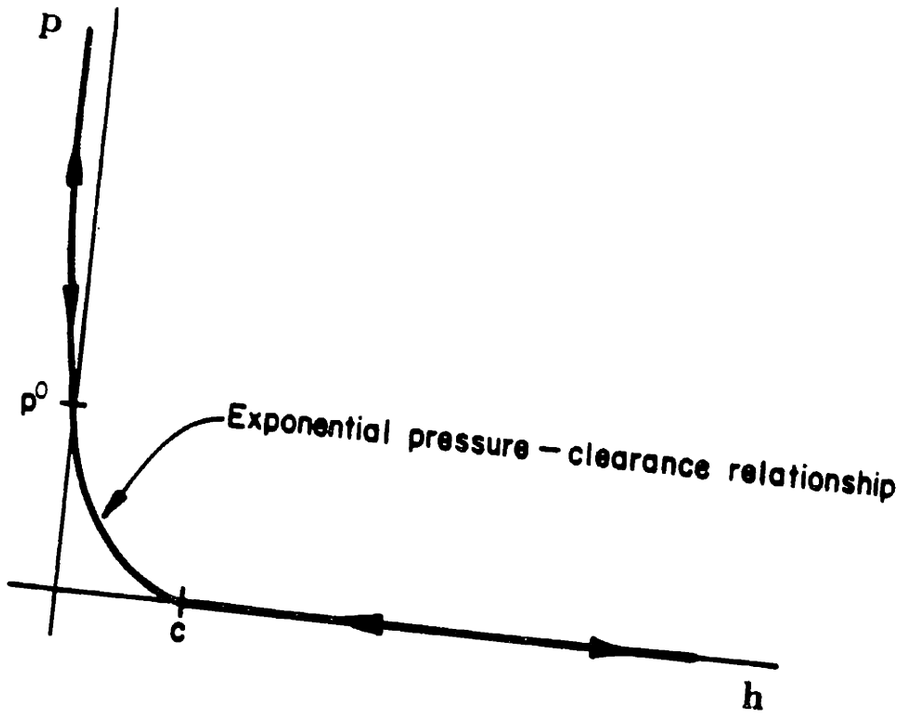

Figure 4.1: "Softened" pressure-clearance relationship for ABAQUS interface elements.

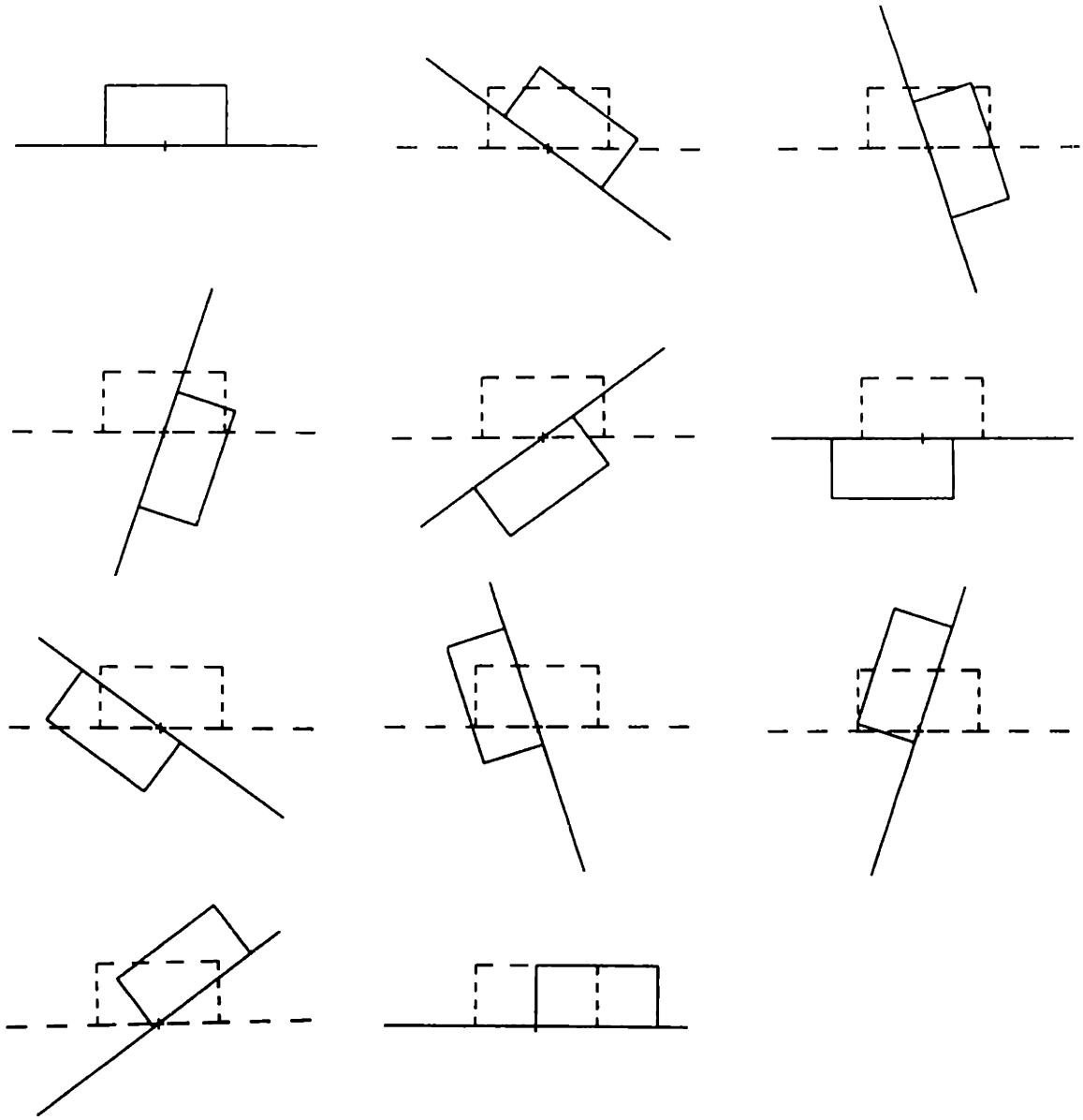

Figure 4.2: Simple sliding with superposed rigid body rotation: the total amount of sliding is $\delta = 1.0$ mm, and the total rotation is $\theta = 360^o$. The motion is imposed in ten increments $\dot{\delta}\,\Delta t = 0.1$ mm and $\dot{\theta}\,\Delta t = 36^o$.

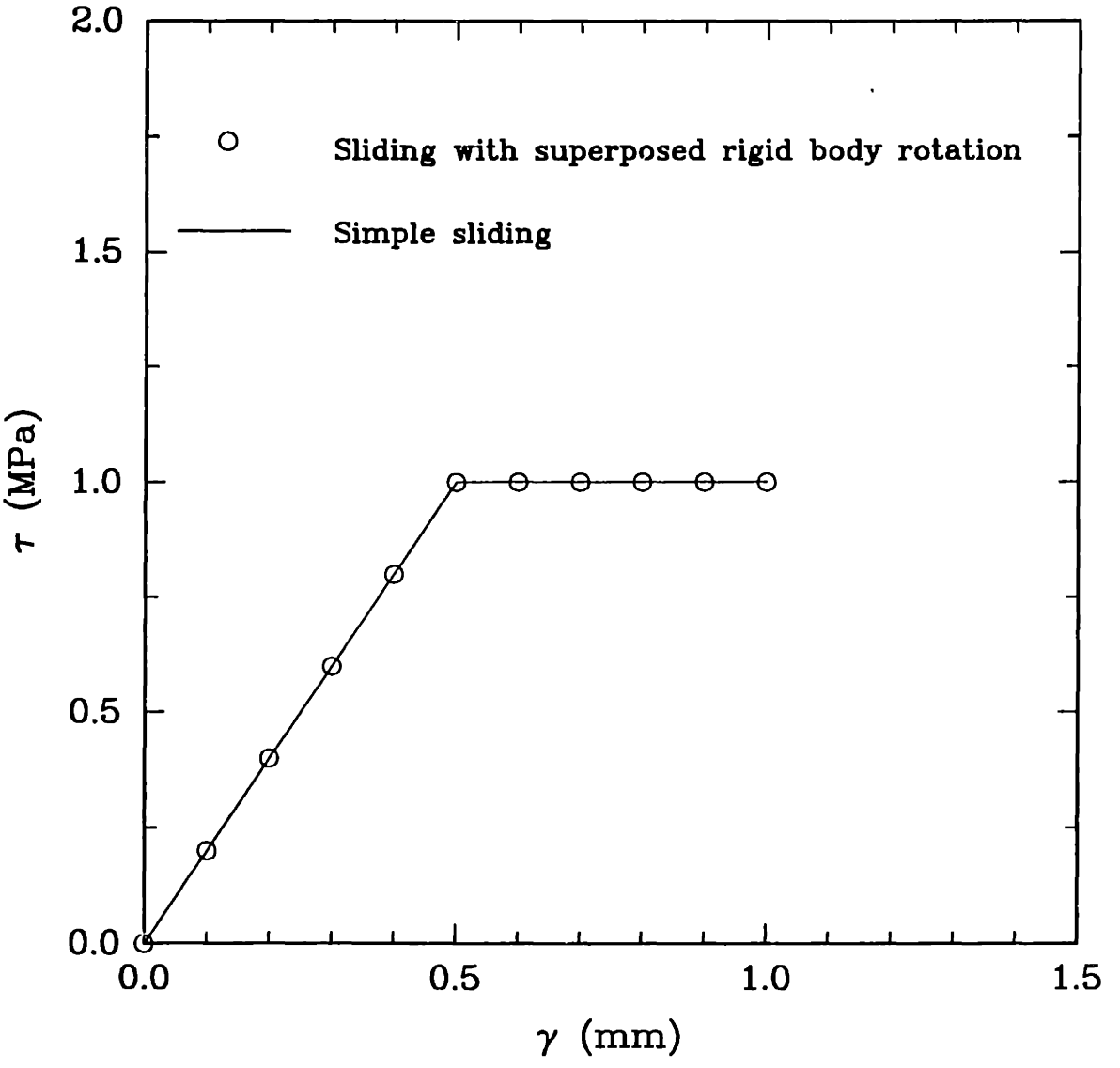

Figure 4.3: Simple sliding with superposed rigid body rotation (non-hardening friction): contact shear stress *vs.* sliding.

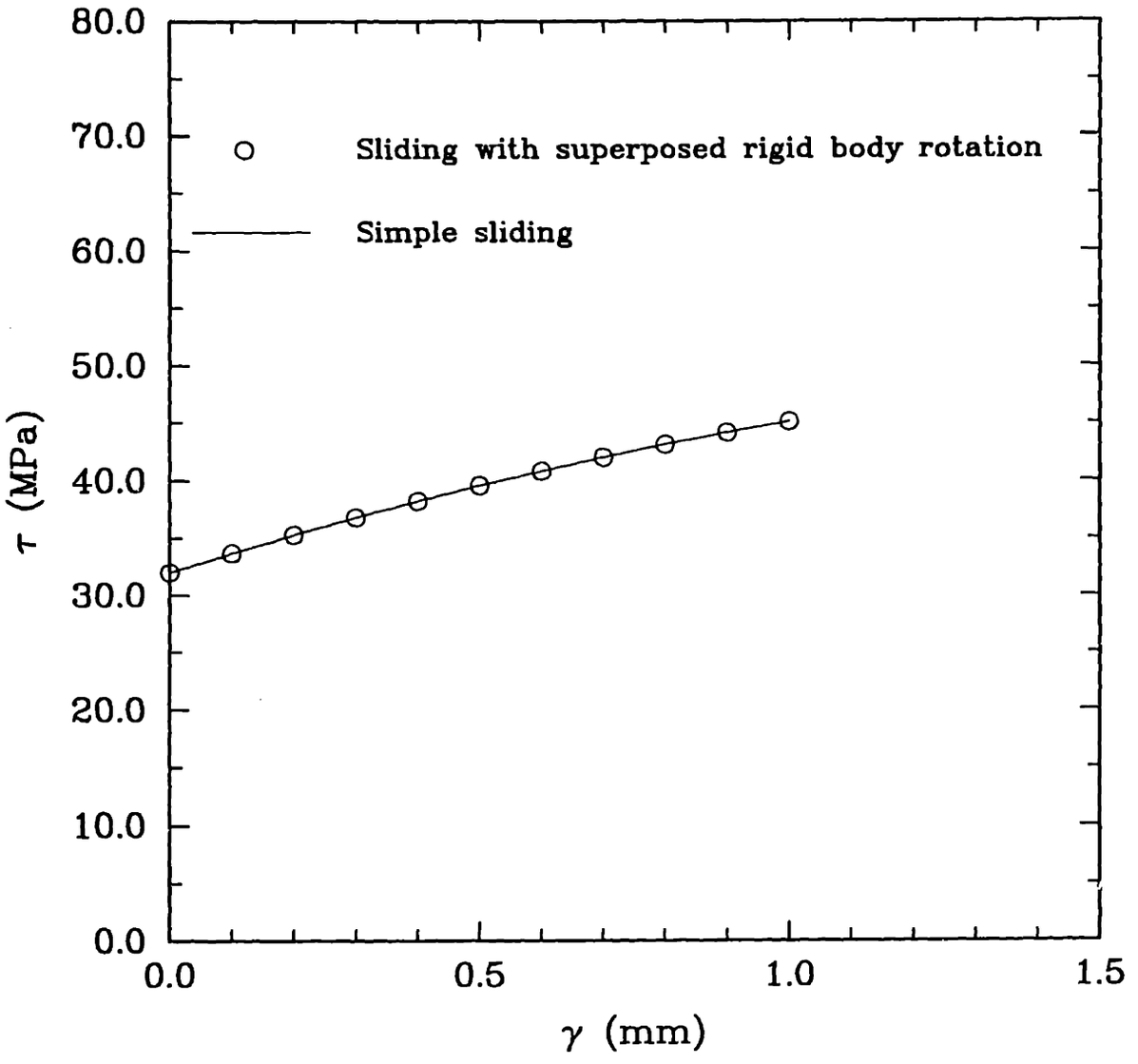

Figure 4.4: Simple sliding with superposed rigid body rotation (hardening friction): contact shear stress *vs.* sliding.

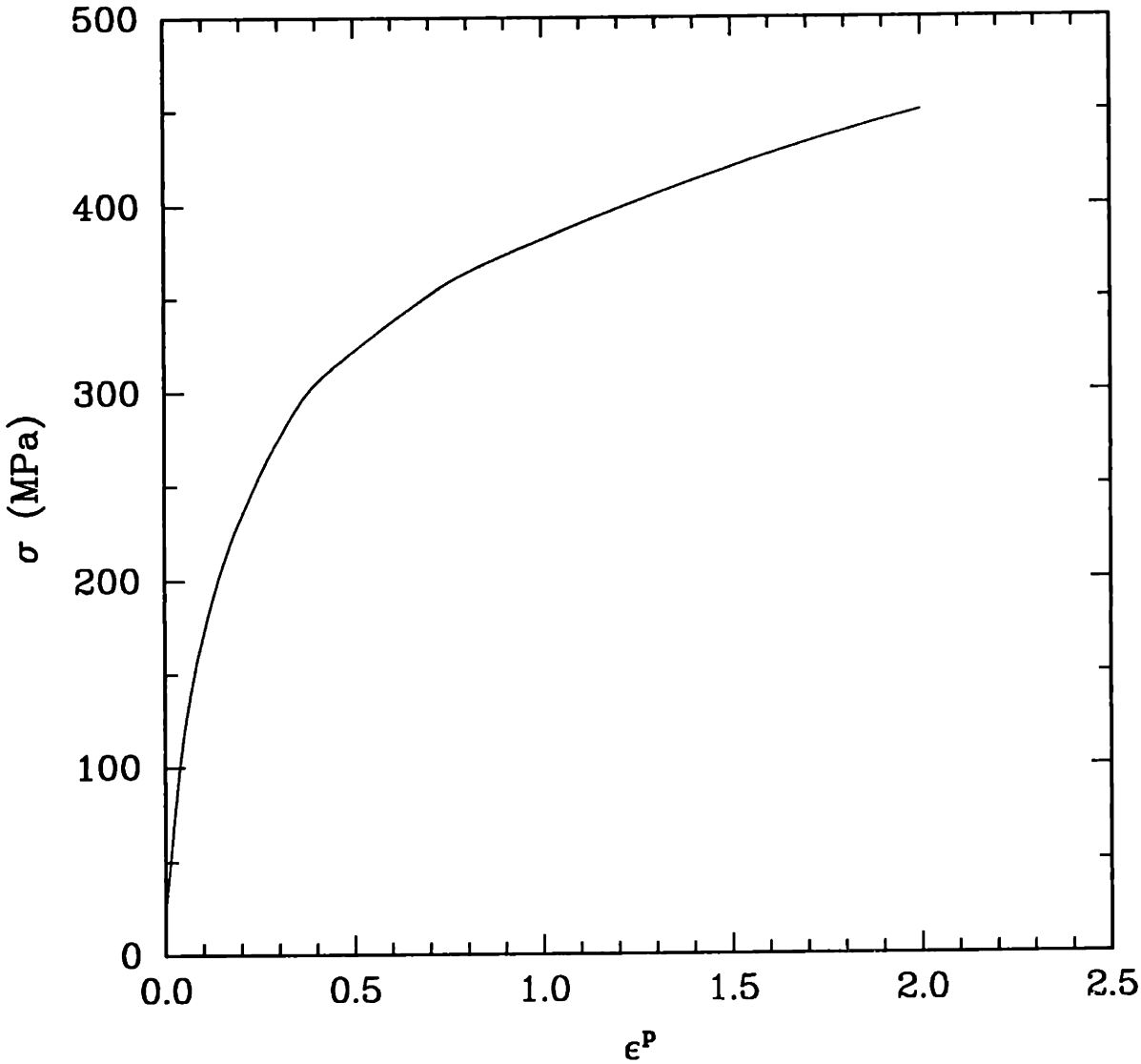

Figure 4.5: Stress versus plastic strain curve for copper.

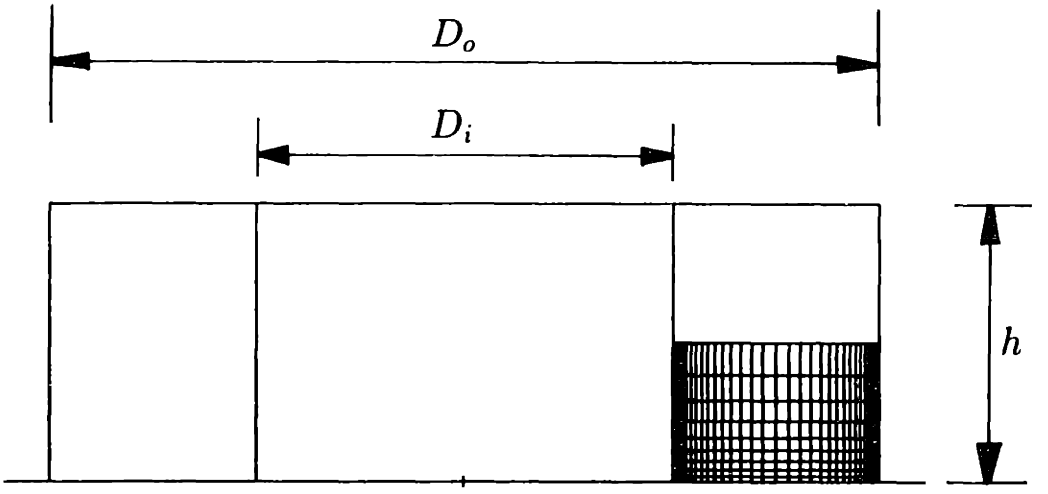

Figure 4.6: Schematic of the ring specimen and meshed portion. $D_o = 0.9$ in, $D_i = 0.45$ in, $h = 0.3$ in.

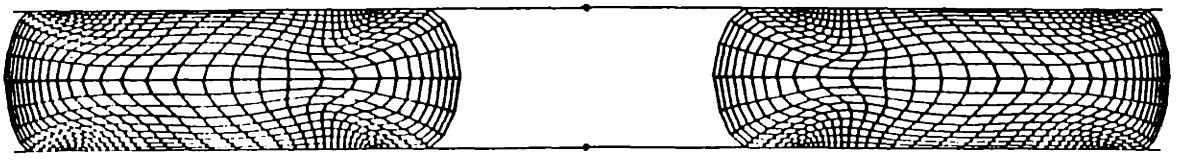

Figure 4.7: Deformed mesh for the ring compression problem (copper) after height reduction of 50%.

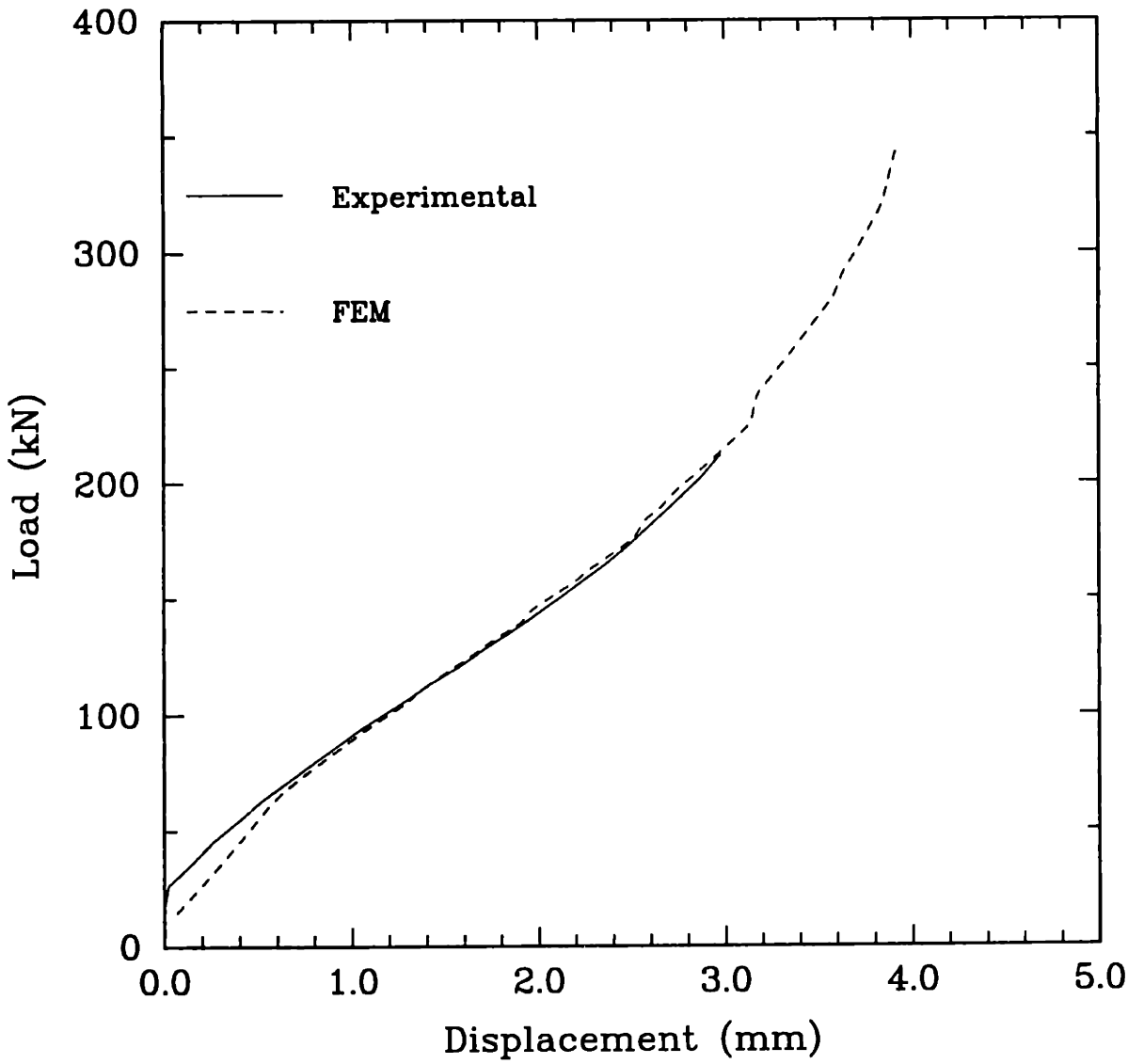

Figure 4.8: Load versus displacement curve for the ring compression of a copper specimen. Comparison between experimental and FE results.

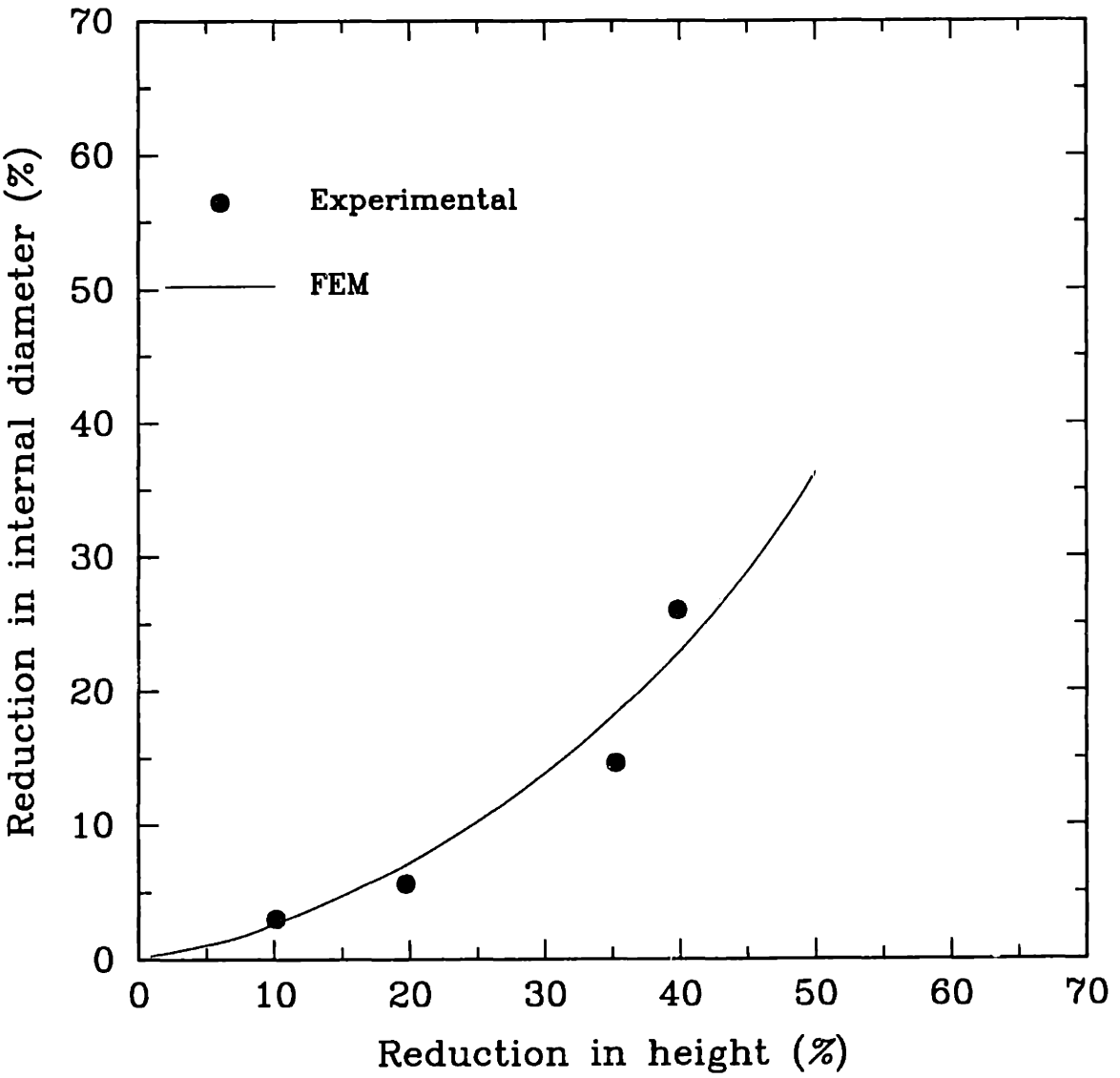

Figure 4.9: Reduction in internal diameter versus reduction in height for the ring compression of a copper specimen. Comparison between experimental and FE results.

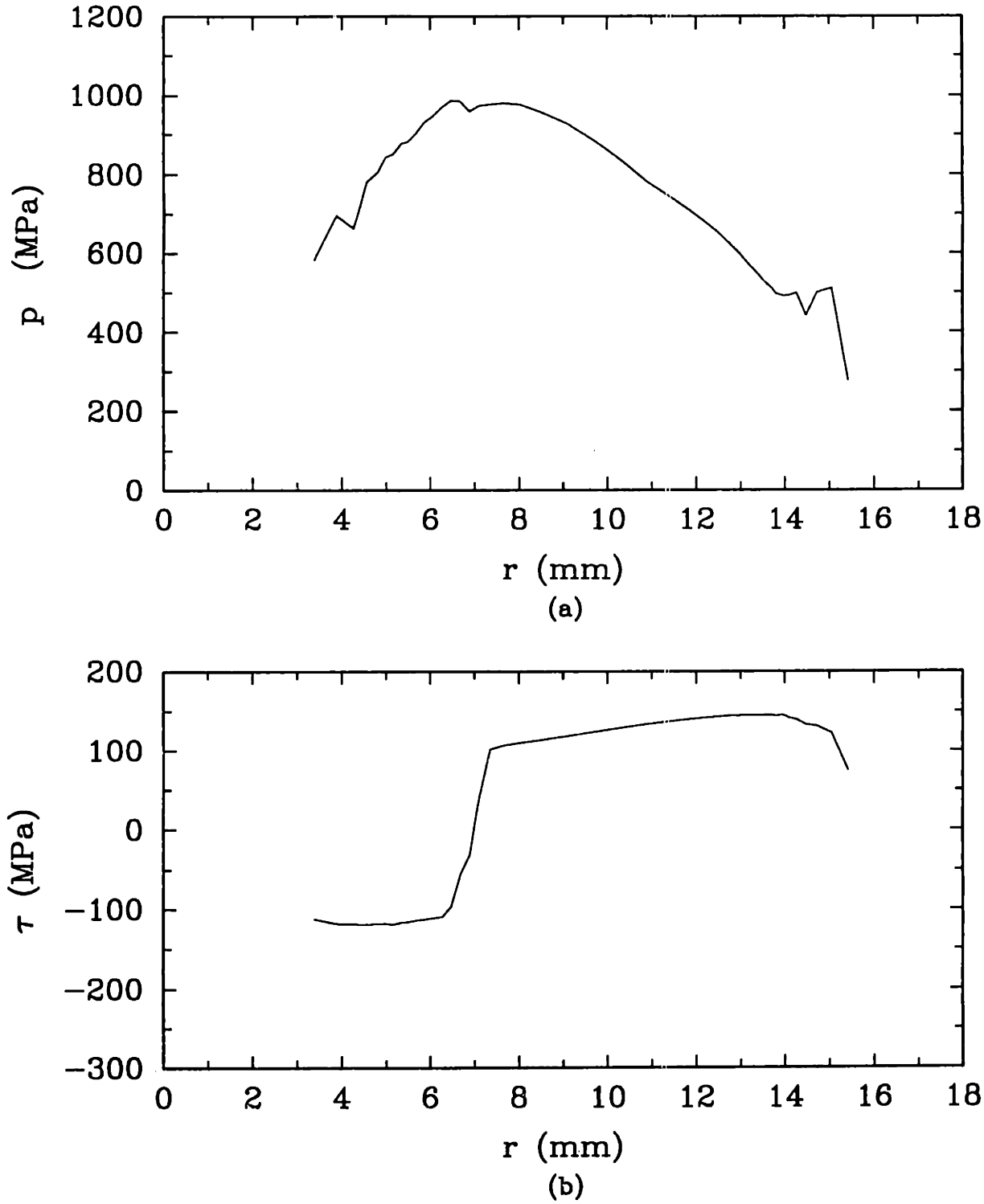

Figure 4.10: Ring compression of a copper specimen: (a) contact pressure, and (b) contact shear stress, at 60% upsetting. FE results.

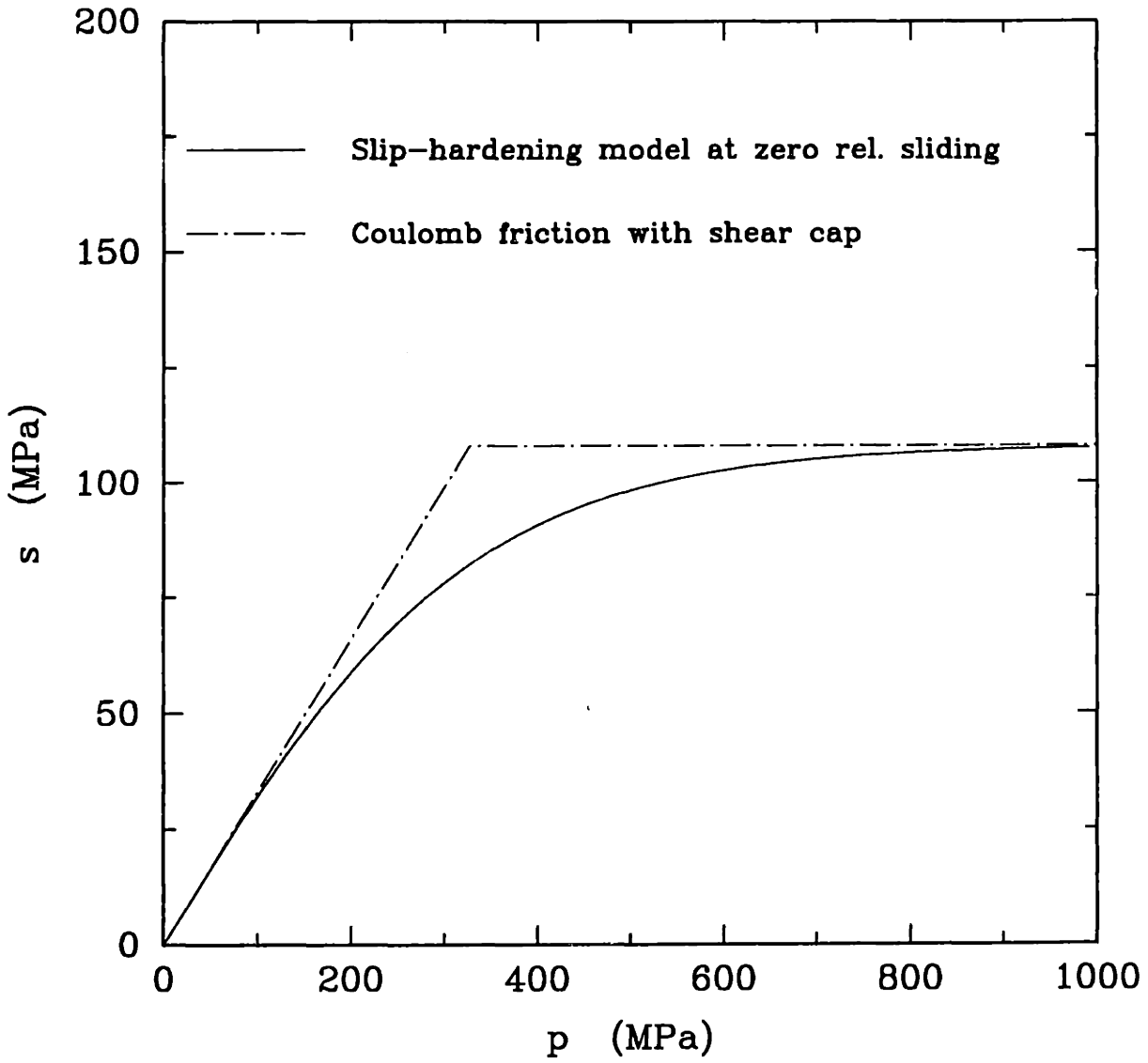

Figure 4.11: Slip resistance-pressure curve at zero sliding for the copper-steel interface.

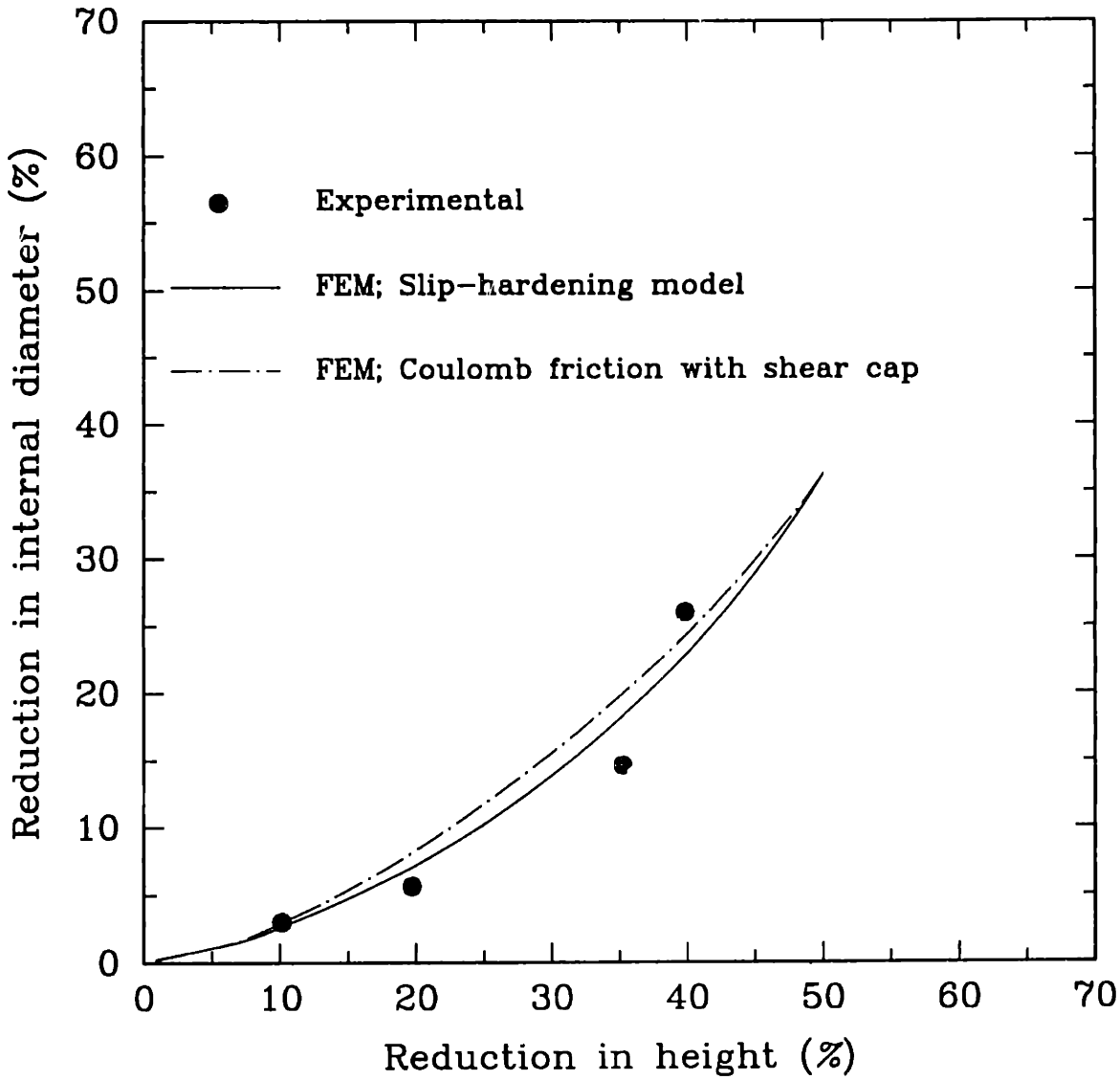

Figure 4.12: Reduction in internal diameter versus reduction in height for the ring compression of a copper specimen. Comparison between experimental and FE results.

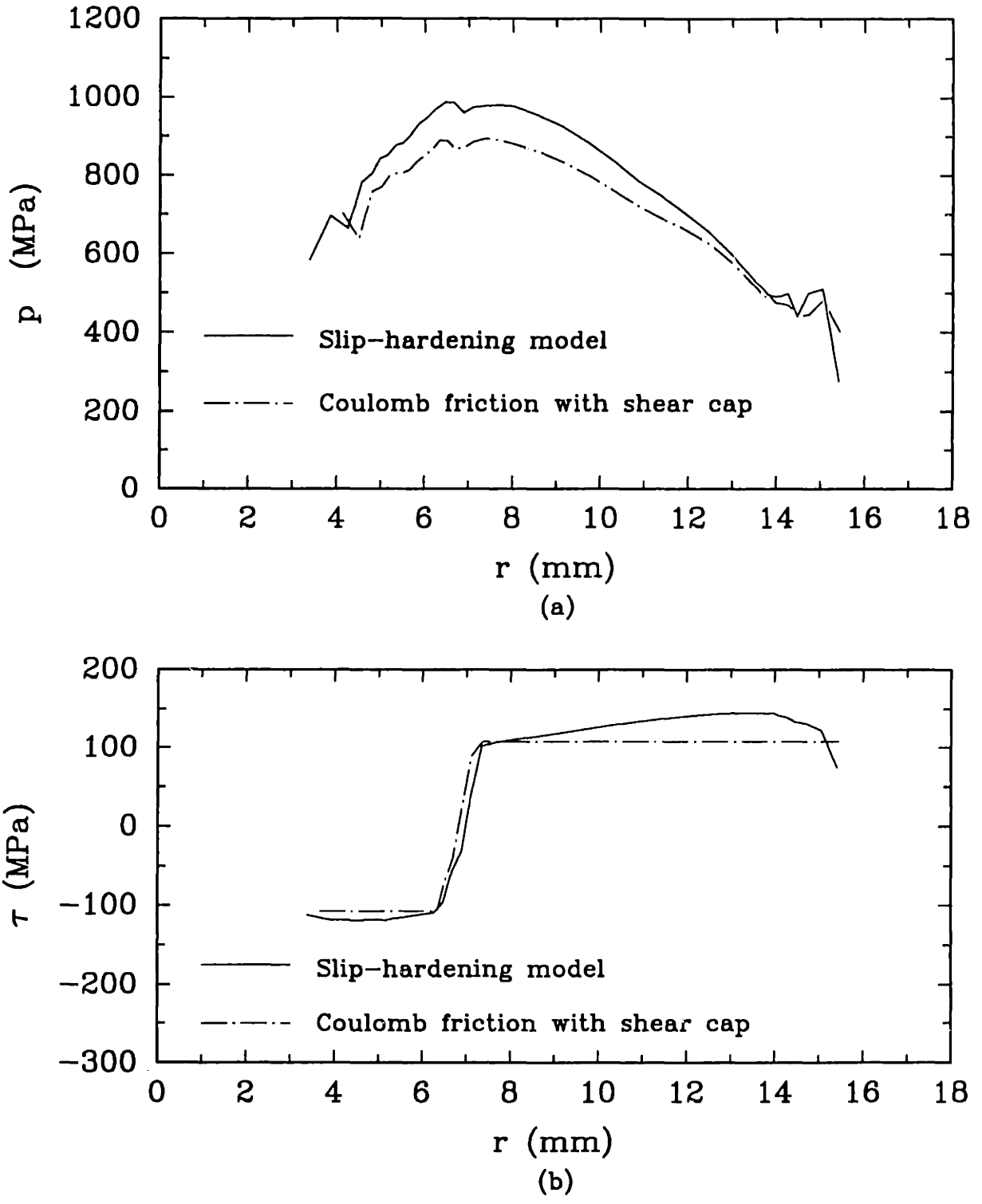

Figure 4.13: Ring compression of a copper specimen: (a) contact pressure, and (b) contact shear stress, at 60% upsetting. Comparison between FE results.

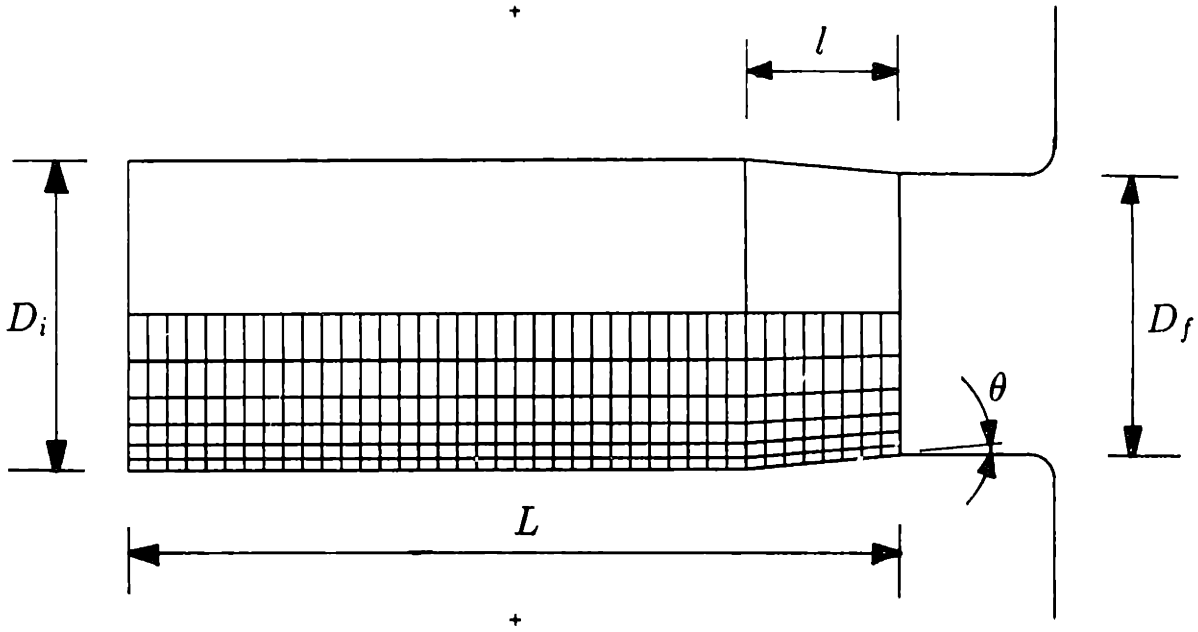

Figure 4.14: Schematic of the extrusion specimen and meshed portion. $D_i = 10$ mm, $D_f = 9.2$ mm, $L = 25.4$ mm, $l = 5.1$ mm, $\theta = 5^o$.

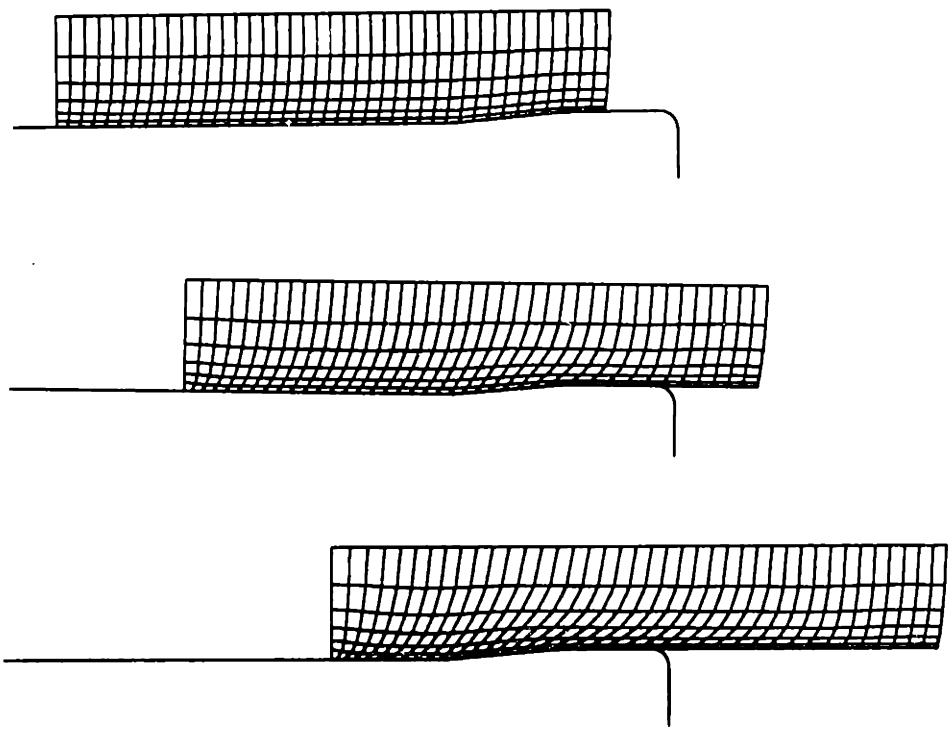

Figure 4.15: Deformed mesh for the extrusion problem at three successive stages of the analysis.

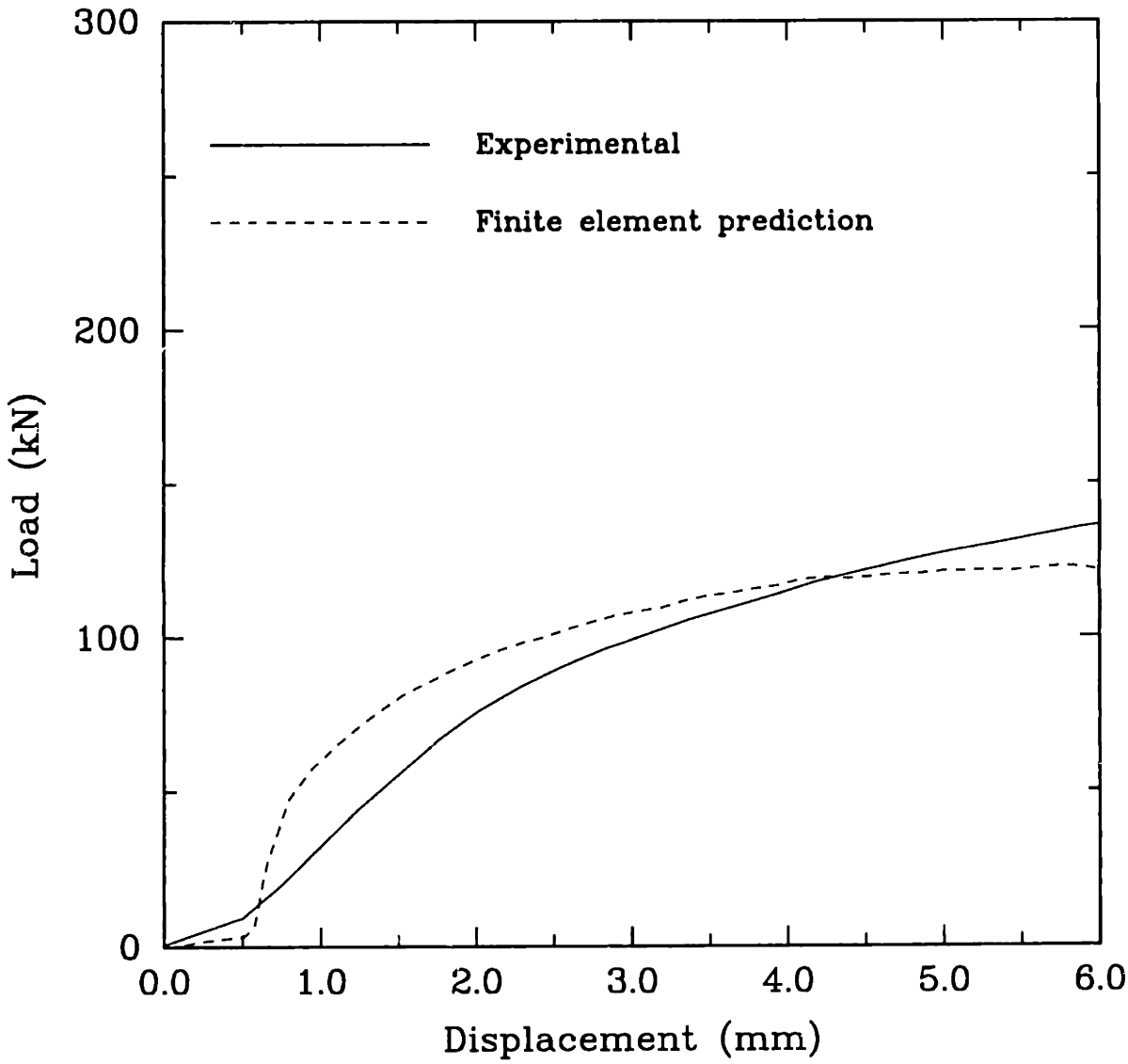

Figure 4.16: Load versus displacement curve for the extrusion of a copper specimen. Comparison between experimental and FE results.

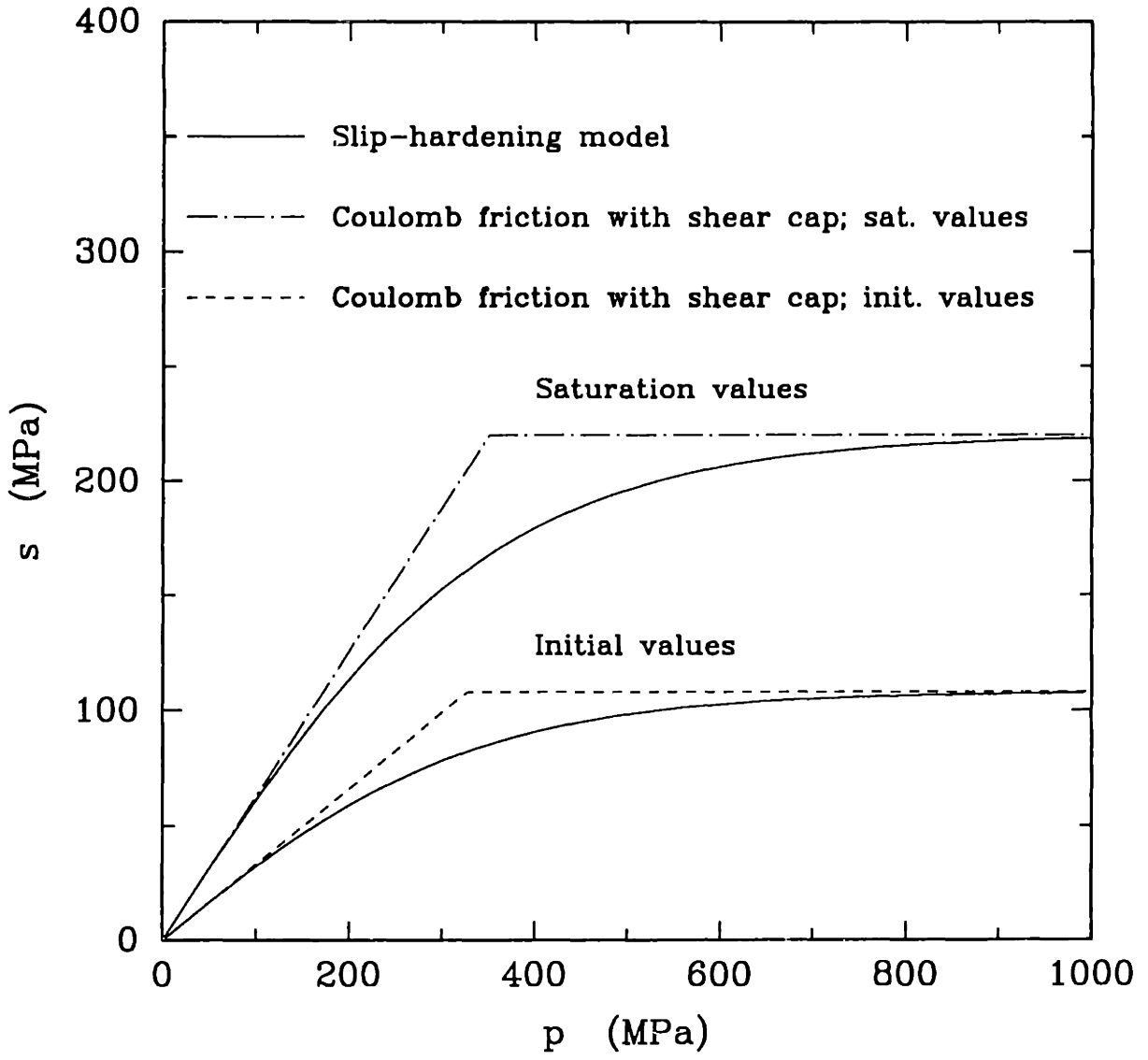

Figure 4.17: Slip resistance-pressure curve at zero sliding and at saturation for the copper-steel interface.

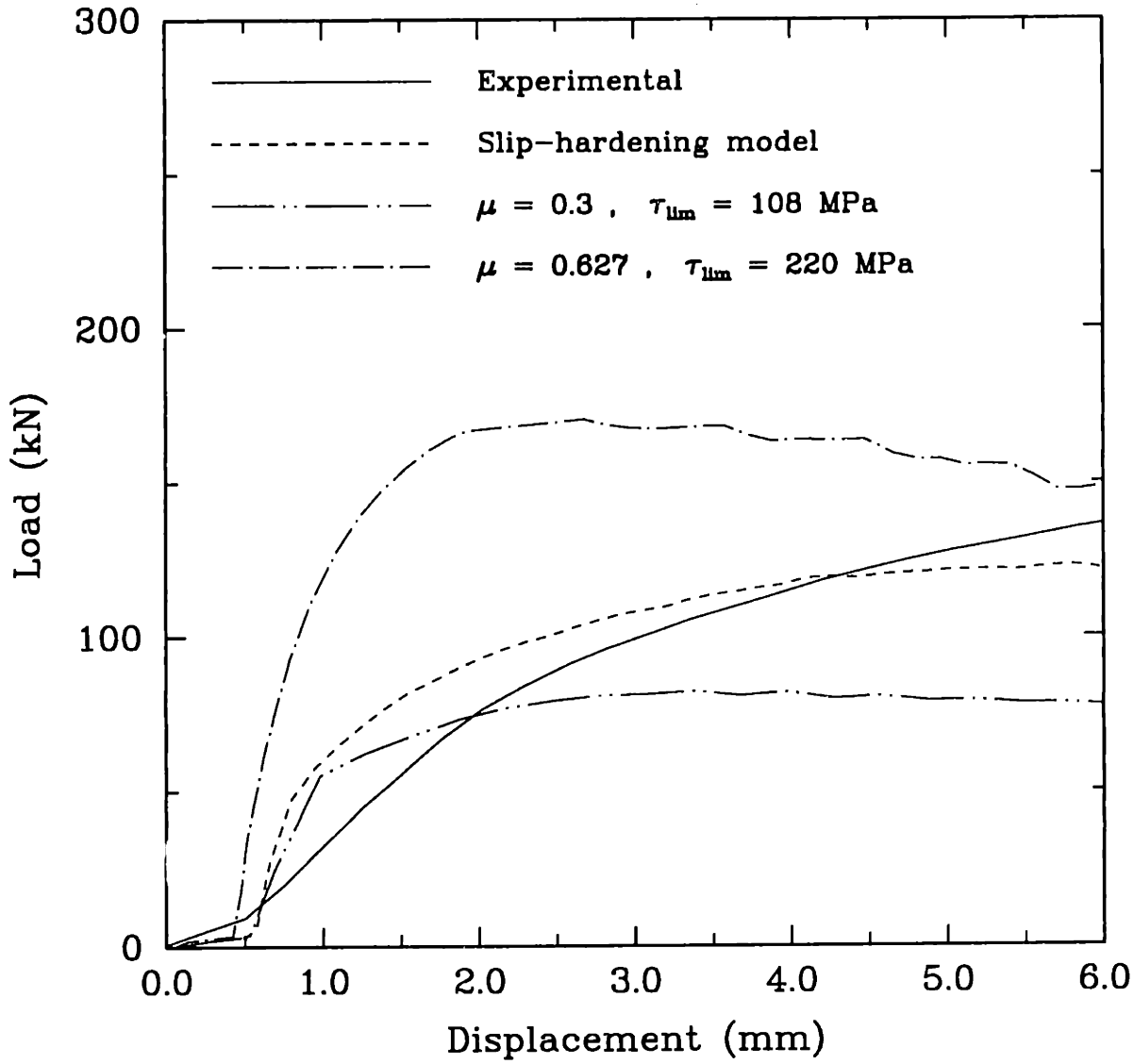

Figure 4.18: Load versus displacement curve for the extrusion of a copper specimen. Comparison between experimental and FE results.

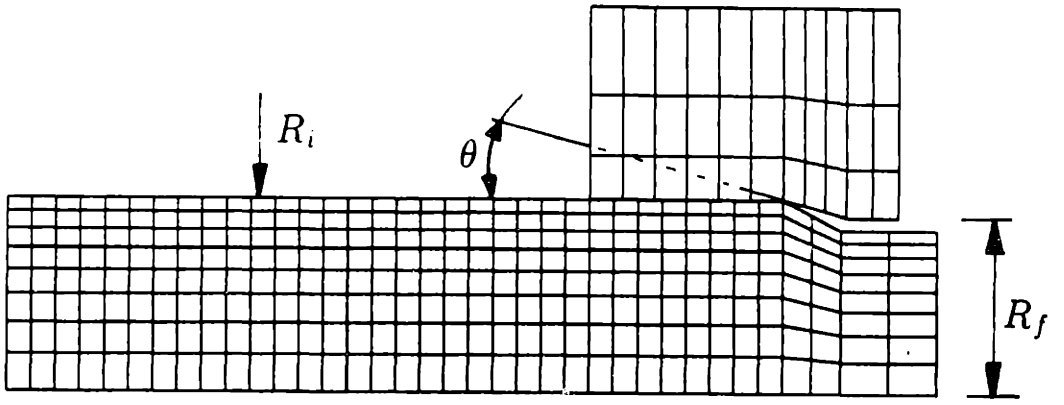

Figure 4.19: Geometry of axisymmetric drawing simulation; $R_i = 100$ mm, $R_f = 91.5$ mm, $\theta = 15°$, corresponding to a reduction in area of 16.3%. The nodes on the stepped-down end were given a horizontal pulling velocity of 10 m/sec, to simulate the drawing operation.

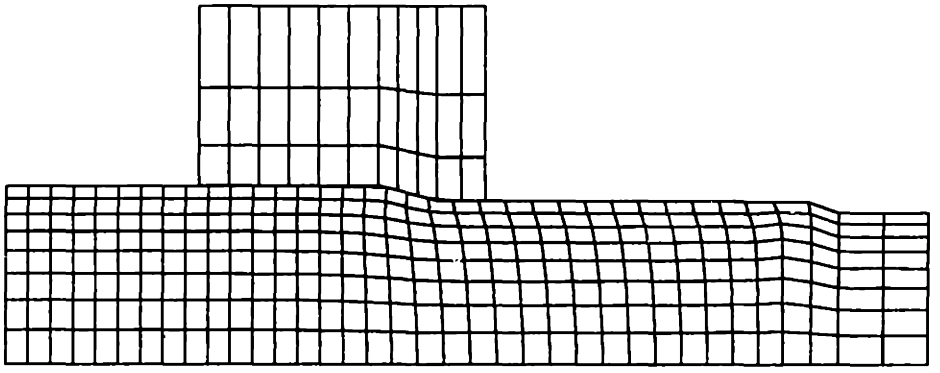

Figure 4.20: Drawing simulation: deformed mesh.

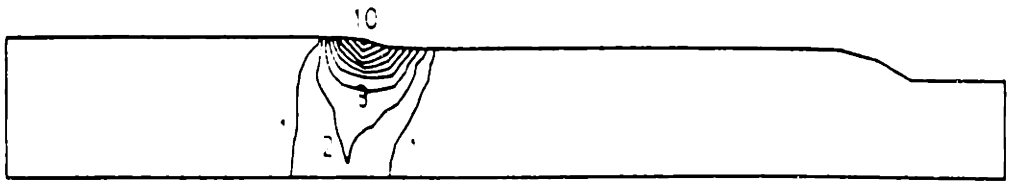

(a)

I.D.	$\dot{\epsilon}^p_m$ (s^{-1})
1	14.
2	28.
3	42.
4	56.
5	70.
6	84.
7	98.
8	112.
9	126.
10	140.

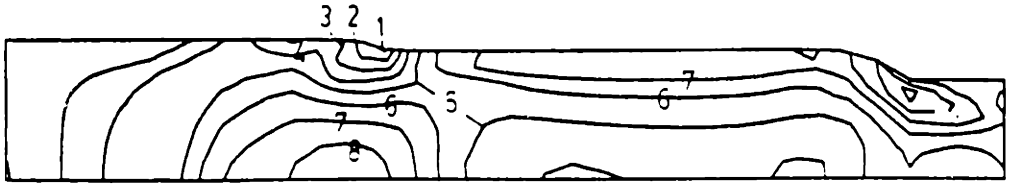

(b)

I.D.	Σ_h/s
1	-1.0
2	-0.8
3	-0.6
4	-0.4
5	-0.2
6	0.0
7	0.2
8	0.4
9	0.6
10	0.8

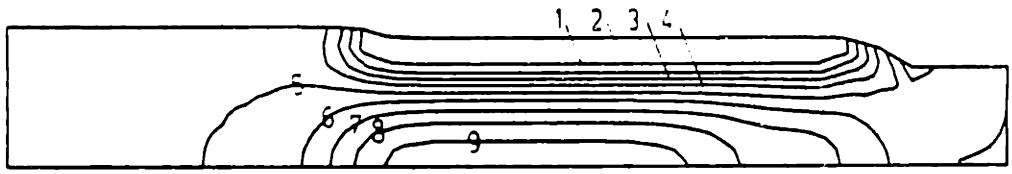

(c)

I.D.	f
1	0.002
2	0.004
3	0.006
4	0.008
5	0.010
6	0.012
7	0.014
8	0.016
9	0.018
10	0.020

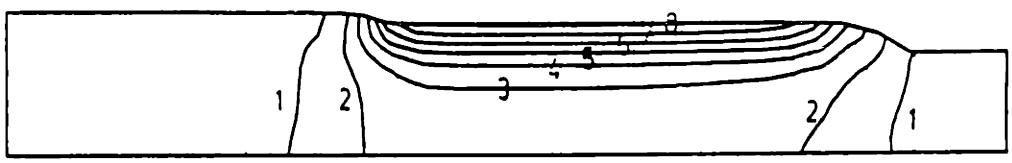

(d)

I.D.	θ (°K)
1	299.
2	302.5
3	306.
4	309.5
5	313.
6	316.5
7	320.
8	323.5

Figure 4.21: Defect formation in rod drawing (frictionless case): (a) contours of the equivalent plastic strain rate in the rod, (b) normalized pressure contours, (c) porosity contours, and (d) temperature contours. Taken from the work of Zavaliangos and Anand (1992).

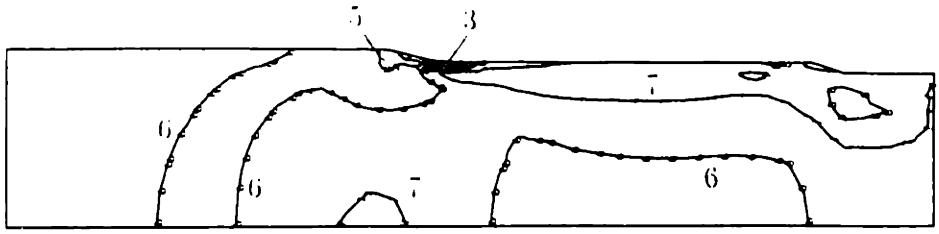

(a)

I.D.	Σ_h/s
1	−3.0
2	−2.4
3	−1
4	−1
5	−0.8
6	−0.2
7	0.3
8	0.9
9	1.4
10	2.0

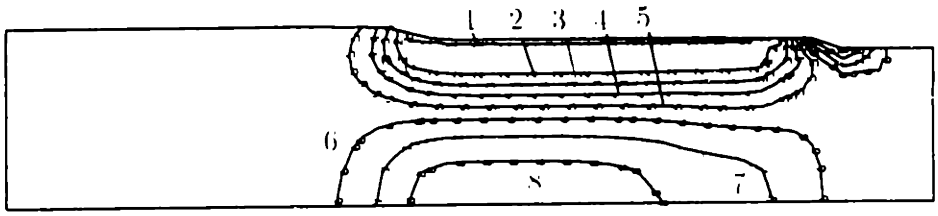

(b)

I.D.	f
1	0.000
2	0.002
3	0.004
4	0.007
5	0.009
6	0.011
7	0.013
8	0.015
9	0.018
10	0.020

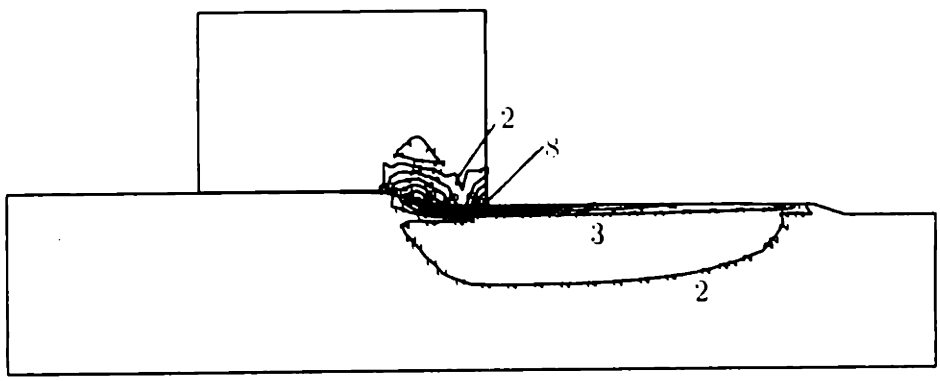

(c)

I.D.	$\partial(K)$
1	290.
2	305.
3	321.
4	337.
5	352.
6	368.
7	384.
8	400.

Figure 4.22: Defect formation in rod drawing (heating due to friction included): (a) normalized pressure contours, (b) porosity contours, and (c) temperature contours. Compare with fig. (4.21).

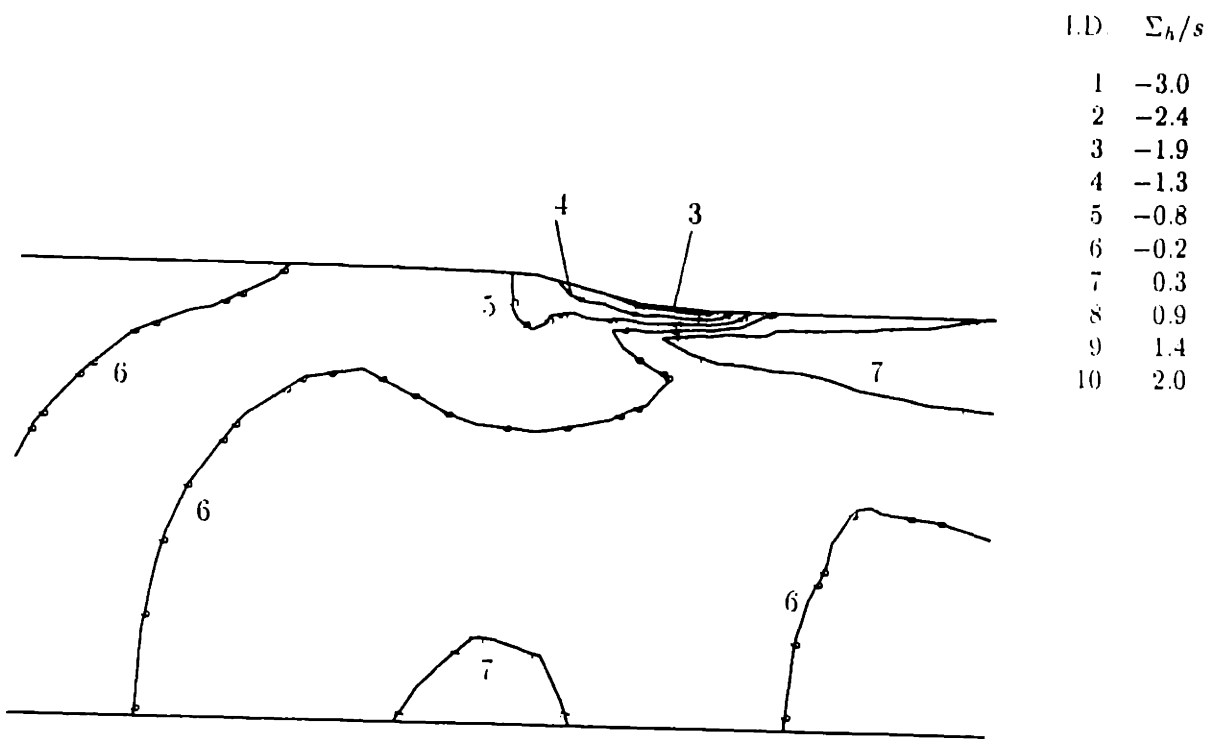

Figure 4.23: Defect formation in rod drawing (enlarged): normalized pressure contours. Compare with fig. (4.21)-(b).

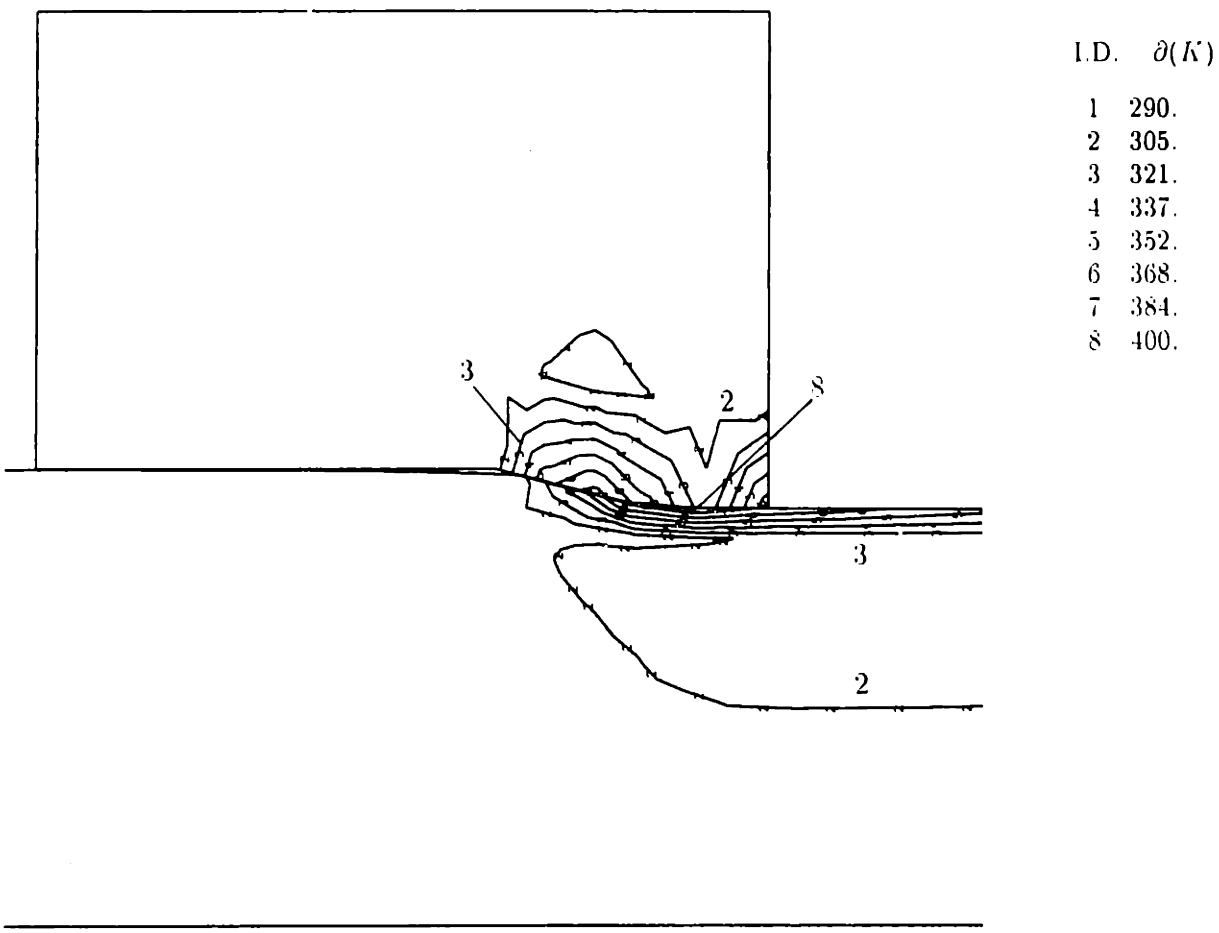

Figure 4.24: Defect formation in rod drawing (enlarged): temperature contours. Compare with fig. (4.21)-(d).

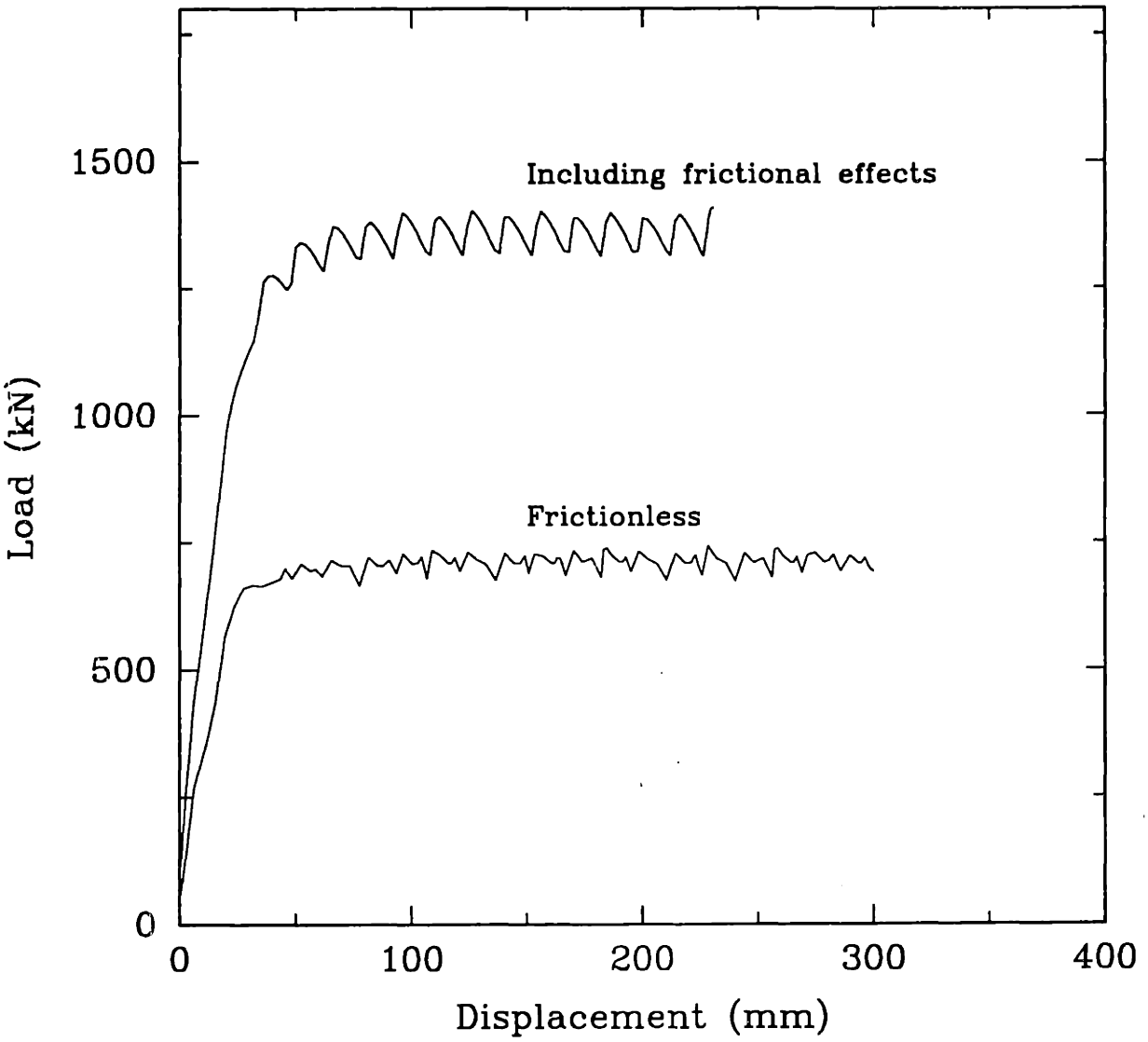

Figure 4.25: Load versus displacement curves for the drawing of a porous aluminum rod.

Chapter 5

Closure

In any metal-working application the properties of the interfaces influence dramatically the forces required to obtain the desired product and its final characteristics. In performing numerical simulations of metal-working operations it is therefore essential to have the capabilitiy to describe the phenomena of contact and sliding of deformable bodies in an efficient and accurate manner. To this end, the present research, based on the work of ANAND (1992), makes the following contributions:

- A fully three-dimensional, rate-independent, isotropic and isothermal constitutive model for interface friction is proposed.
- An incrementally objective implicit time-integration procedure for the model is formulated.
- A specific evolution law for the slip resistance of the interface of dry metallic surface pairs in contact is proposed. Based on this evolution law, specific material parameters, needed to complete the model for a particular tool-workpiece pair are given for copper as the workpiece material and a hardened steel as the tool.

- The developed constitutive model and time-integration procedure have been implemented in a commercial finite element program, and several example calculations have been performed. These calculations show the versatility of the constitutive model and the robustness of the time-integration procedure. Numerical predictions also match well with corresponding experimental results where available.

The present work lays the foundation for additional important contributions to the field of friction modeling for the simulation of metal-working operations. Namely, the proposed constitutive model can be generalized to include other effects, such as:

- Slip rate effects. To this end a rate-dependent constitutive model, described in Appendix A, has been formulated. Experimental work to determine the effect of the slip rate on the slip resistance has to be carried out and the model, along with a suitable time-integration procedure, has to be implemented in a finite element code. Slip rate effects could be important when modeling lubricated interfaces.

- Temperature effects. The temperature at the interface directly influences the value of the slip resistance. Again, although the extension of the constitutive framework presented here to include the effect of temperature on the frctional properties of an interface is reasonably simple, much work needs to be done in choosing specific forms of the various constitutive functions in the model.

Bibliography

[1957] COURTNEY-PRATT, J. S., EISNER, E.; *The Effect of a Tangential Force on the Contact of Metallic Bodies*, Procedings of the Royal Society A, 238, 529 - 550.

[1965] RABINOWICZ, E.; *Friction and Wear of Materials*, Wiley, New York.

[1974] NAGTEGAAL, J., PARKS, D. M., and RICE, J. R.; *On Numerically Accurate Finite Element Solutions in the Fully Plastic Range*, Computer Methods in Applied Mechanics and Engineering, 4, 153 - 177.

[1976] FREDRIKSSON, B.; *Finite Element Solution Of surface Nonlinearities in Structural Mechanics Problems*, Computers & Structures, 6, 281 - 290.

[1978] MICHALOWSKI, R., and MROZ Z.; *Associated and Non-Associated Sliding Rules in Contact Friction Problems*, Archives of Mechanics, 30, 259 - 276.

[1981] SUH, N. P., SIN, H. C.; *The Genesis of Friction*, Wear, 69, 91 - 114.

[1983] SCHEY, J.; *Tribology in Metalworking: Friction, Lubrication, and Wear*, American Society for Metals, Metals Park, Ohio.

[1985] CHENG, J.H., and KIKUCHI, N.; *An Incremental Constitutive Relation Of Unilateral Contact Friction For Large Deformation Analysis*, ASME Journal of Applied Mechanics, 52, 639 - 648.

[1985] ODEN, J. T., MARTIN, J. A. C.; *Models and Computational Methods for Dynamic Friction Phenomena*, Computer Methods in Applied Mechanics and Engineering, 52, 527 - 634.

[1985] RUINA, A. L.; *Constitutive Relations for Frictional Slip*, Mechanics of Geomaterials, Z. Bazant (ed.), John Wiley & Sons Ltd., London, 169 - 188.

[1985] BATHE, K. J., CHAUDHARY, A.; *A Solution Method for Planar and Axisymmetric Contact Problems*, International Journal for Numerical Methods in Engineering, 21, 65 - 88.

[1986] SUH, N. P.; *Tribophysics*, Prentice-Hall, Englewood Cliffs, New Jersey.

[1987] BAY, N., WANHEIM, T., and AVITZUR, B.; *Models for Friction In Metal Forming*, Manufacturing Technology Review 2, SME Press, Dearborn, Michigan, 372 - 378.

[1989] PLESHA, M. E., BALLARINI R., and PARULEKAR, A.;*Constitutive Model and Finite Element Procedure for Dilatant Contact Problems*, Journal of Engineering Mechanics, 115, 2649 - 2668.

[1990] ABAQUS, Reference Manuals, Hibbitt, Karlson and Sorenson Inc., Providence, RI.

[1991] KALPAKJIAN, S., *Manufacturing Processes for Engineering Materials*, 2nd Edition, Addison-Wesley, Reading, MA.

[1991] ETEROVIC A. L., BATHE, K. J.; *On the treatment of Inequality Constraints Arising from Contact Conditions in Finite Element Analysis*, Computers & Structures, 40, 203 - 209.

[1991] BRONKHORST, C.; *Plastic Deformation and Crystallographic Texture Evolution in Face-Centered Cubic Metals*, Ph.D. Thesis, MIT.

[1992] ANAND, L.; *A Constitutive Model for Interface Friction*, submitted to Computational Mechanics.

[1992] ZAVALIANGOS, A., ANAND, L.; *Thermo-Elasto-Viscoplasticity of Isotropic Porous Metals*, submitted to Journal of the Mechanics and Physics of Solids.

[1992] ANAND, L., PISONI, A. C., TONG, W.; to be published.

Appendix A

Rate-Dependent Interface Constitutive Model

A.1 Interface Constitutive Model

By paralleling arguments to those of Chapter 2, the rate-dependent constitutive model with isotropic hardening of the slip resistance consists of the following evolution equations for the state variables $(\mathbf{t}, s)$:

1. Evolution equation for the traction $\mathbf{t}$:

$$\mathbf{t}^{\circ} = -\{\mathbf{K}\bar{\mathbf{v}} - k_T\bar{\mathbf{v}}_T^s\}\,. \tag{A.1}$$

The relative tangential slipping velocity $\bar{\mathbf{v}}_T^s$ is given by the slip rule:

$$\bar{\mathbf{v}}_T^s = \bar{v}^s(-\mathbf{m})\,, \tag{A.2}$$

where

$$\mathbf{m} \equiv (\mathbf{t}_T/\bar{\tau})\,, \tag{A.3}$$

is the unit vector in the direction of the tangential traction,

$$\bar{\tau} \equiv \sqrt{\mathbf{t}_T \cdot \mathbf{t}_T} \tag{A.4}$$

is an effective tangential traction or shear stress, and $\bar{v}^s$ is an effective relative tangential slipping velocity given by

$$\bar{v}^s = f(\bar{\tau}, s). \tag{A.5}$$

2. Evolution equation for the slip resistance s:

$$\dot{s} = g(\bar{\tau}, s). \tag{A.6}$$

To complete this constitutive model for a particular tool-workpiece interface the constitutive parameters/functions that need to be specified are the tangential and normal stiffnesses in adherance, k_T and k_N, respectively, the constitutive function (A.5) for the effective relative tangential velocity and the initial value and evolution function (A.6) for the slip resistance.

Note that in the rate-dependent model there is no switching parameter which turns the sliding off or on; sliding is assumed to occur at all values of shear stress which exceed a threshold value[1] s_{th}. Further, the effective relative tangential slipping velocity, which is determined by the consistency condition in the rate-independent model, needs to be prescribed by a constitutive function. Since there is no slip condition to be satisfied in the rate-dependent model, there is also no consistency condition which needs to be satisfied in this model.

If a slip resistance function $\hat{s}(p, \bar{u}^s)$ of the same form as (2.68) is used than the parameters $\mu(\tau)$ and $s^*(\tau)$ are to be specified by evolution equations of the following type:

$$\dot{\mu} = g_1(\bar{\tau}, s), \tag{A.7}$$

$$\dot{s}^* = g_2(\bar{\tau}, s). \tag{A.8}$$

[1]In air most surfaces are contaminated; accordingly, it expected that the threshold slip resistance under engineering conditions will be vanishingly small.

A.2 Time-integration Procedure

From eqns (A.1)-(A.6), by paralleling arguments of Section 3.3 we obtain:

$$p(\tau) \equiv -\tilde{t}_N(\tau) = -t_N(t) + k_N \Delta t\, \tilde{v}_N(\tau), \tag{A.9}$$

$$\tilde{\mathbf{t}}_T(\tau) = \tilde{\mathbf{t}}_T^*(\tau) + (-k_T)\, \Delta t\, \bar{v}^s(\tau)\, \tilde{\mathbf{m}}(\tau), \tag{A.10}$$

$$\tilde{\mathbf{m}}(\tau) \equiv \tilde{\mathbf{t}}_T(\tau) \,/\, \bar{\tau}(\tau), \tag{A.11}$$

$$\bar{\tau}^*(\tau) = \sqrt{\tilde{\mathbf{t}}_T^*(\tau) \cdot \tilde{\mathbf{t}}_T^*(\tau)}, \tag{A.12}$$

$$\tilde{\mathbf{t}}_T(\tau) = \eta(\tau) \tilde{\mathbf{t}}_T^*(\tau), \tag{A.13}$$

$$\eta(\tau) = \bar{\tau}(\tau)/\bar{\tau}^*(\tau), \tag{A.14}$$

$$\bar{v}^s(\tau) = f(\bar{\tau}(\tau), s(\tau)), \tag{A.15}$$

$$\bar{\tau}(\tau) = \bar{\tau}^*(\tau) - k_T \Delta t\, \bar{v}^s(\tau), \tag{A.16}$$

$$\mu(\tau) = \mu(t) + \Delta t\, g_1(\bar{\tau}(\tau), s(\tau)), \tag{A.17}$$

$$s^*(\tau) = s(\tau) + \Delta t\, g_2(\bar{\tau}(\tau), s(\tau)), \tag{A.18}$$

Thus, unlike the procedure for the rate-independent model, here we have to solve for $\bar{\tau}(\tau)$, $\mu(\tau)$ and $s^*(\tau)$ from the set of equations

$$\mu(\tau) - \mu(t) + \Delta t\, g_1(\bar{\tau}(\tau), s(\tau)) = 0, \tag{A.19}$$

$$s^*(\tau) - s(\tau) + \Delta t\, g_2(\bar{\tau}(\tau), s(\tau)) = 0, \tag{A.20}$$

$$\bar{\tau}(\tau) - \bar{\tau}^*(\tau) + \Delta t\, f(\bar{\tau}(\tau), s(\tau)) = 0, \tag{A.21}$$

A.2.1 Summary of Time-Integration Algorithm

The algorithm is identical to that for the rate-independent model, except, replace **Step 4** in that algorithm by:

Step 4. Calculate $\bar{\tau}(\tau)$, $\mu(\tau)$ and $s^*(\tau)$ by solving

$$\mu(\tau) - \mu(t) + \Delta t\, g_1(\bar{\tau}(\tau), s(\tau)) = 0, \tag{A.22}$$

$$s^*(\tau) - s(\tau) + \Delta t\, g_2(\bar{\tau}(\tau), s(\tau)) = 0, \tag{A.23}$$

$$\bar{\tau}(\tau) - \bar{\tau}^*(\tau) + \Delta t f(\bar{\tau}(\tau), s(\tau)) = 0. \tag{A.24}$$

A.3 Linearization Moduli $\tilde{\mathbf{M}}$

From (2.114) we note that the only difference in $\tilde{\mathbf{M}}$ between the rate-independent and the rate-dependent model arises from the difference between the values for the term $\partial_{\Delta \bar{u}_t} \bar{v}^s(\tau)$. In what follows we evaluate this term for the rate-dependent model. Linearization of (A.16) gives

$$d\bar{\tau}(\tau) = d\bar{\tau}^*(\tau) - k_T \Delta t\, d\bar{v}^s(\tau). \tag{A.25}$$

The quantity $d\bar{\tau}(\tau)$ is obtained by linearizing (A.19), (A.20) and (A.21) and solving the resulting set of equations. This gives

$$d\bar{\tau}(\tau) = c_1(\tau) d\bar{\tau}^*(\tau) - k_N\, c_2(\tau) dt_N, \tag{A.26}$$

where the expressions for $c_1(t)$ and $c_2(t)$ are given by the following

$$c_1(\tau) = \frac{A_1}{D}, \tag{A.27}$$

$$c_2(\tau) = \frac{A_1 d_1 + A_2 d_2 + A_3 d_3}{D}, \tag{A.28}$$

where

$$A_1 = b_3c_2 - b_2c_3\,, \tag{A.29}$$

$$A_2 = b_1c_3 - b_3c_1\,, \tag{A.30}$$

$$A_3 = b_2c_1 - b_1c_2\,, \tag{A.31}$$

$$D = c_1(a_3b_2 - a_2b_3) + c_2(a_1b_3 - a_3b_1) + c_3(a_2b_1 - a_1b_2)\,, \tag{A.32}$$

with

$$a_1 \equiv 1 + k_T\,\Delta t\partial_{\bar\tau} f|_\tau\,, \tag{A.33}$$

$$a_2 \equiv -\Delta t\partial_{\bar\tau} g_1|_\tau\,, \tag{A.34}$$

$$a_3 \equiv -\Delta t\partial_{\bar\tau} g_2|_\tau\,, \tag{A.35}$$

$$b_1 \equiv \Delta t\partial_\mu f|_\tau\,, \tag{A.36}$$

$$b_2 \equiv 1 - \Delta t\partial_\mu g_1|_\tau\,, \tag{A.37}$$

$$b_3 \equiv -\Delta t\partial_\mu g_2|_\tau\,, \tag{A.38}$$

$$c_1 \equiv \Delta t\partial_{s^\bullet} f|_\tau\,, \tag{A.39}$$

$$c_2 \equiv -\Delta t\partial_{s^\bullet} g_1|_\tau\,, \tag{A.40}$$

$$c_3 \equiv 1 - \Delta t\partial_{s^\bullet} g_2|_\tau\,, \tag{A.41}$$

$$d_1 \equiv -\Delta t\partial_p f|_\tau\,, \tag{A.42}$$

$$d_2 \equiv \Delta t\partial_p g_1|_\tau\,, \tag{A.43}$$

$$d_3 \equiv \Delta t\partial_p g_2|_\tau\,. \tag{A.44}$$

Substituting (A.26) into (A.25) for $d\bar\tau(\tau)$, solving for $d\bar u^s(\tau)$ and using (2.111) we obtain

$$\partial_{\Delta\tilde{\mathrm{u}}_t}\bar v^s(\tau) = -\frac{(1-c_1(\tau))\tilde{\mathrm{m}}(\tau)}{\Delta t} - \frac{k_N\,c_2(\tau)\tilde{\mathrm{n}}(\tau)}{k_T\,\Delta t}\,. \tag{A.45}$$

Subtitution of (A.45) into (2.114) gives

$$\tilde{\mathbf{M}}(\tau) = \tilde{\mathbf{K}}(\tau) - \bar{g}_T^{-1}(\tau)\{k_T\tilde{\mathbf{m}}(\tau) \otimes k_T\tilde{\mathbf{m}}(\tau)\} - \bar{g}_N^{-1}(\tau)\{k_T\tilde{\mathbf{m}}(\tau) \otimes k_N\tilde{\mathbf{n}}(\tau)\} , \tag{A.46}$$

where

$$\bar{g}_T^{-1}(\tau) = \frac{1}{k_T}\{\eta(\tau) - c_1(\tau)\} , \tag{A.47}$$

$$\bar{g}_N^{-1}(\tau) = c_2(\tau) . \tag{A.48}$$

Appendix B

Evaluation of Constitutive Parameters for the Lubricated Aluminum-Steel Interface.

In contrast to the frictional parameter evaluation procedure given in Chapter 3 for the dry copper-steel interface, the constitutive parameters for the lubricated aluminum-steel interface were estimated from a step-change pressure test. The test was carried out using the same experimental apparatus described in Chapter 3. An aluminum workpiece, covered with lubricant[1], was compressed and slid against a steel tool. The compressive load was increased during the test to generate step-like changes in the contact pressure, fig. (B.1). Using eq. (3.1), the measured torque was transformed into the contact shear stress. A plot of the contact shear stress versus the distance slid is presented in fig. (B.2). The parameters for the frictional constitutive model were then determined using the evolution law for the slip resistance given by eqns. (3.3), (3.4) and (3.5) and curve fitting the contact shear stress versus sliding distance curve, until satisfactory agreement was achieved. The chosen values are

$$\mu_0 = 0.09,\ \mu_s = 0.25,\ h_{10} = 0.0833\ \text{mm}^{-1},$$

[1]The composition of the lubricant was: 75% of 20 W motor oil and 25% of STP oil.

and

$$s_0^* = 40 \text{ MPa}, \; s_s^* = 80 \text{ MPa}, \; h_{20} = 40 \text{ MPa/mm}.$$

The quality of the curve fit is shown in fig. (B.3).

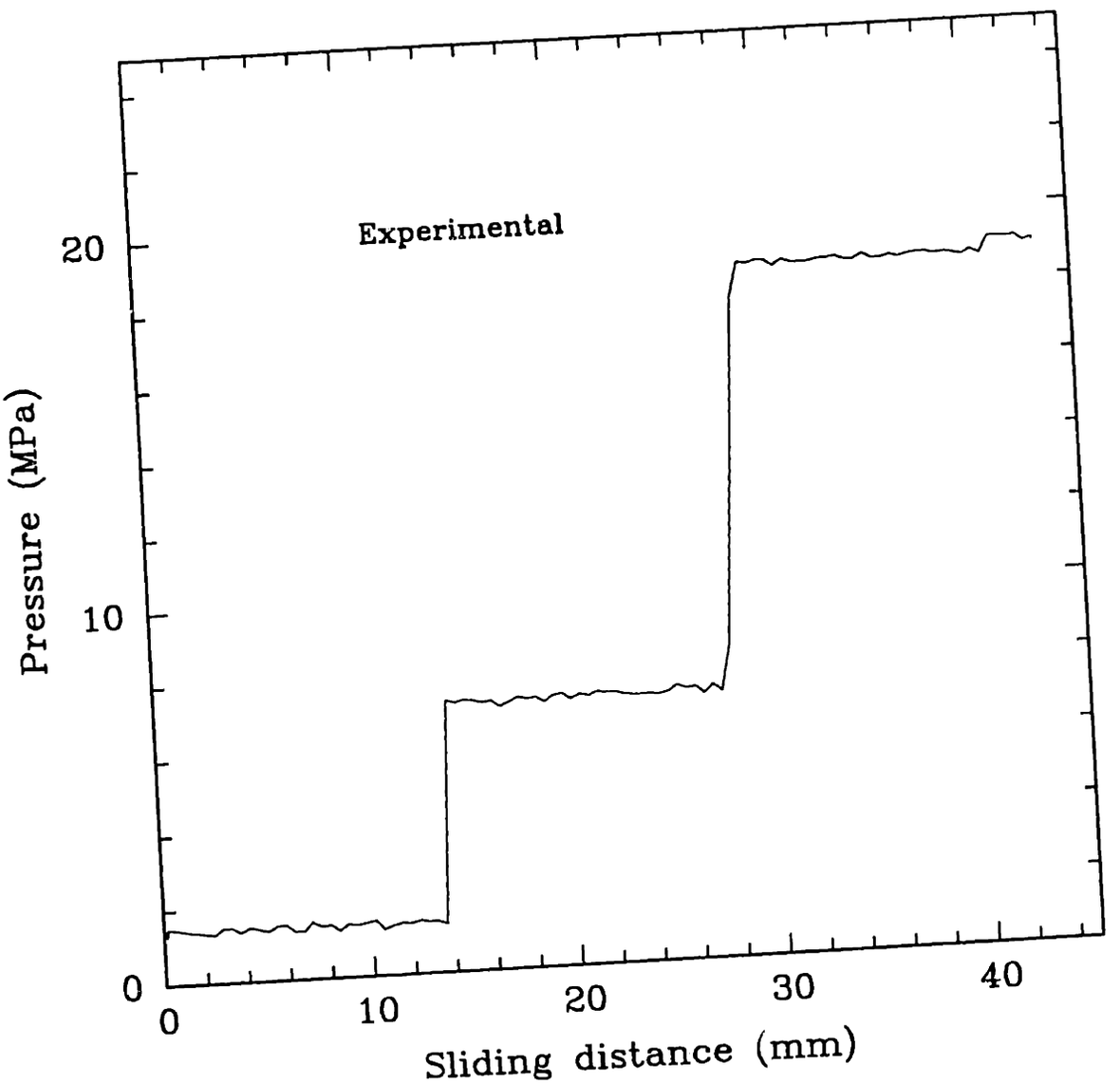

Figure B.1: Step changes in normal pressure, lubricated aluminum-steel interface.

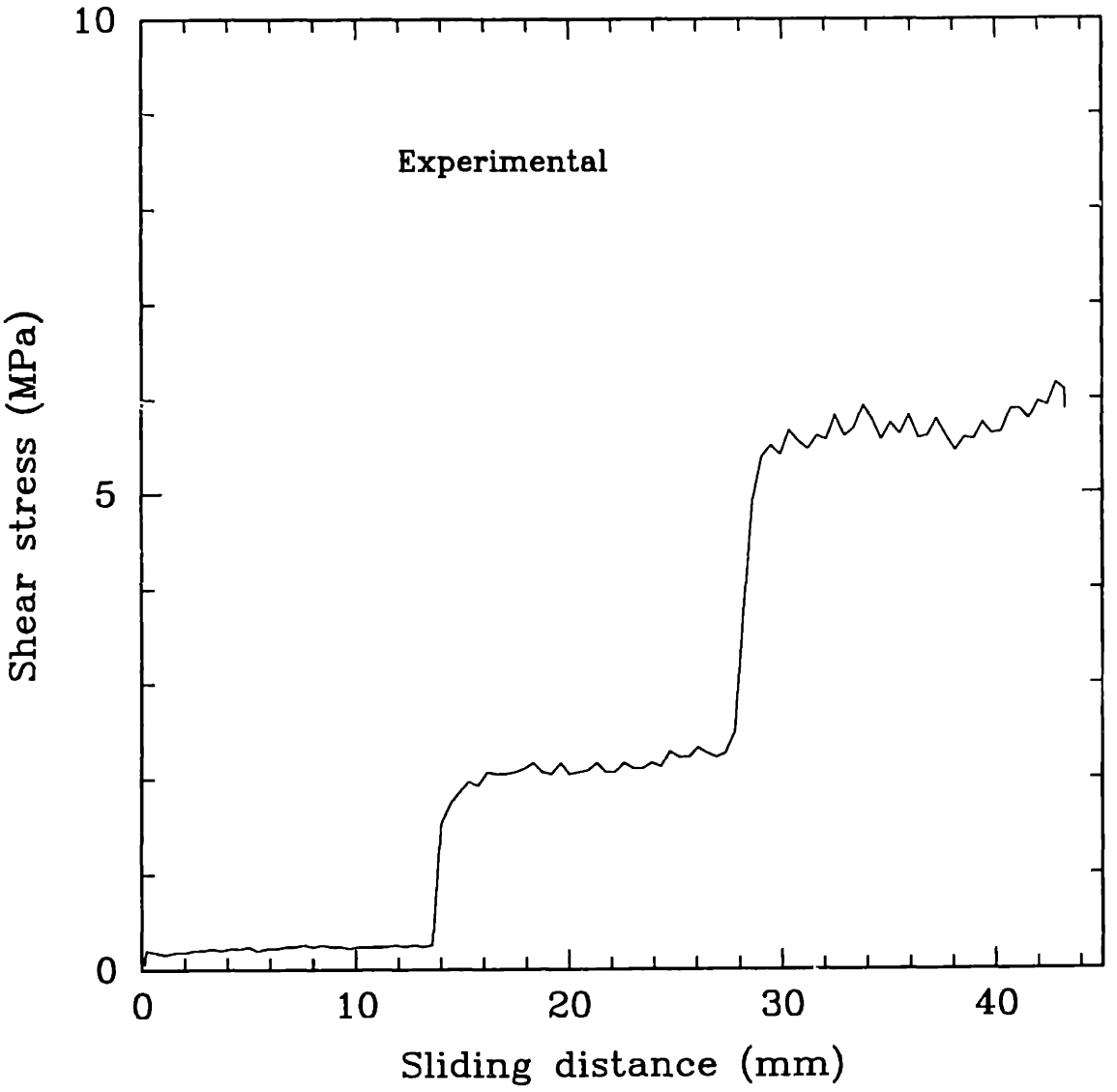

Figure B.2: Tangential stress versus sliding distance curve at the lubricated aluminum-steel interface for the step-change pressure test.

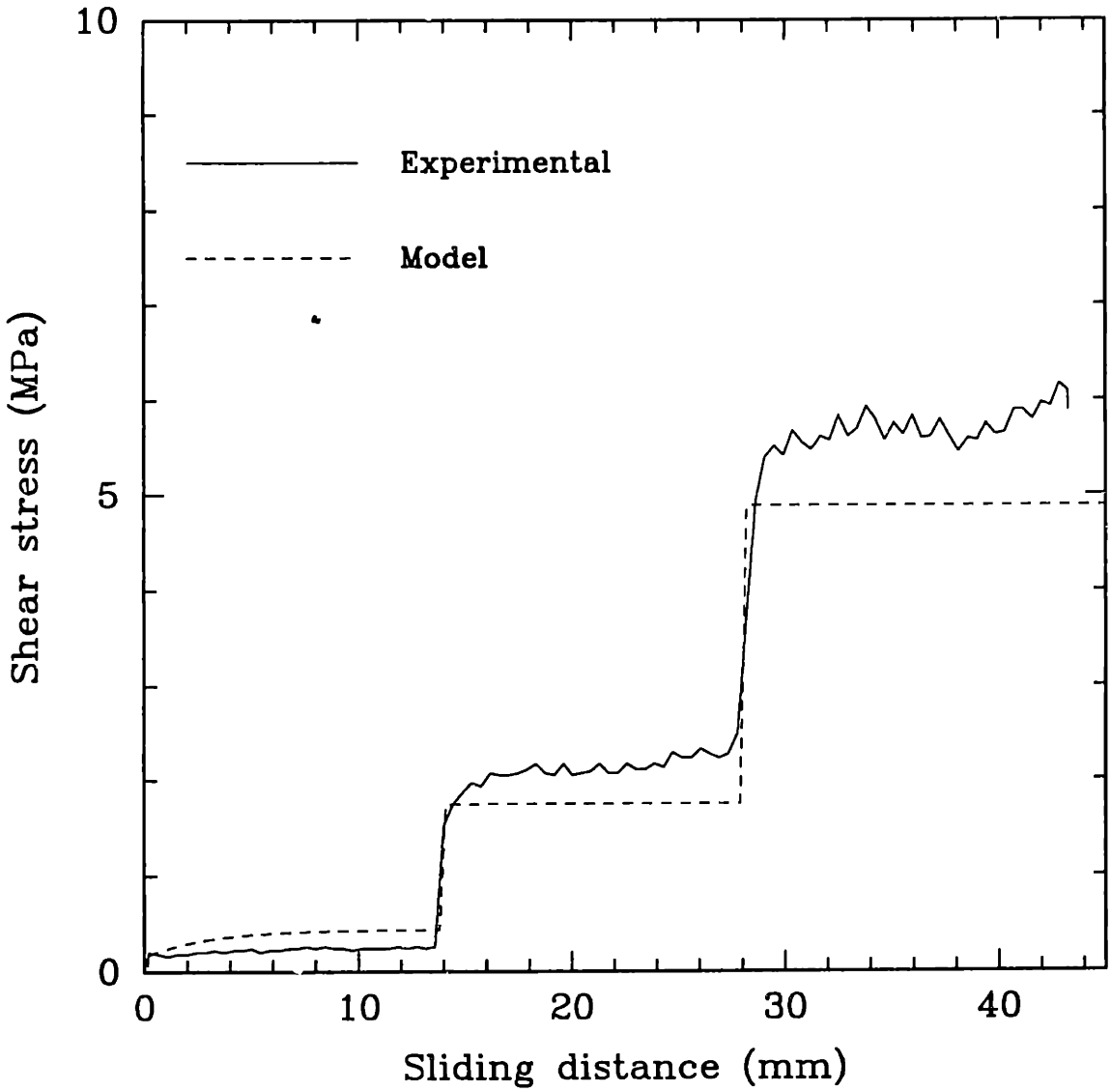

Figure B.3: Comparison of model prediction and experiment for the step-change pressure test, lubricated aluminum-steel interface.

Appendix C

Listing of the FRIC Subroutine

```
c     ************************************************************
c
c           This subroutine models dry friction between metals,
c           at low sliding speed, employing a penalty method.
c           The shear frictional resistance evolves with sliding.
c           The subroutine can be used for both 2D and 3D problems.
c           The following parameters must be provided:
c             initial friction coefficient.....................xmui
c             saturation value for the friction coefficient...xmus
c             hardening constant for the fr. coeff.............h10
c             initial shear cap................................sstari
c             satuaration value for the shear cap..............sstars
c             hardening constant for the shear cap.............h20
c             stiffness in stick...............................sis
c
c                      Attilio C. Pisoni
c                         June 1992
c
c     ************************************************************
      SUBROUTINE FRIC(LM,TAU,DDTDDG,DDTDDP,DSLIP,SED,SPD,
     1 DDTDDT,PNEWDT,STATEV,DGAM,TAULM,PRESS,DPRESS,DDPDDH,SLIP,
     2 KSTEP,KINC,TIME,DTIME,NOEL,ELNAME,NPT,NODES,NPATCH,
     3 COORDS,RCOORD,DROT,TEMP,PREDEF,NFDIR,MCRD,NPRED,NSTATV)
c
c       include 'ABA_PARAM.INC'
c
      implicit real*8(A-H,O-Z)
      character*8 elname
      dimension tau(nfdir),ddtddg(nfdir,nfdir),ddtddp(nfdir),
     1 dslip(nfdir),ddtddt(nfdir,nfdir),statev(nstatv),dgam(nfdir),
     2 taulm(nfdir),slip(nfdir),nodes(3),coords(mcrd),rcoord(mcrd),
     3 drot(2,2),temp(2),predef(2,npred)
c
      external slres,dslrdx,dslrds,dslrdp,hf,dhf
c
```

```
c     ********************************
c        Set parameters
c     ********************************
c      INITIAL COEFFICIENT OF FRICTION
       xmui=.09d+00
c      SATURATION VALUE FOR THE COEFFICIENT OF FRICTION
       xmus=.25d+00
c      HARDENING CONSTANT FOR THE COEFF. OF FRIC.
       h10=.0833d+00
c      INITIAL SHEAR CAP
       sstari=40.d+00
c      SATURATION VALUE FOR THE SHEAR CAP
       sstars=80.d+00
c      HARDENING CONSTANT FOR THE SHEAR CAP
       h20=40.d+00
c      STIFFNESS IN STICK
       sis=10000.d+00
c      TOLERANCES
       tolx=.00001
       tols=.001
c
       lm=0
c
c     ********************************
c        Set initial conditions
c     ********************************
       if(statev(1).lt.xmui)then
       statev(1)=xmui
       statev(2)=sstari
       endif
c
c     ****************************************************************
c        Calculate the trial shear and check adhering or slipping
c     ****************************************************************
       taut1=tau(1)+sis*dgam(1)
c       taut2=tau(2)+sis*dgam(2)
       if(nfdir.eq.1)taut2=0.d+00
       taut=sqrt(taut1**2 + taut2**2)
       p=press-dpress
       s=slres(statev(1),statev(2),p)
       if(dabs(taut).lt.s)then
c
c     ************************
c        Process is adhering
c     ************************
            in=1
            tau(1)=taut1
c            tau(2)=taut2
c
c     *****Calculate jacobian*****
            ddtddg(1,1)=sis
c            ddtddg(1,2)=zero
```

```
c          ddtddg(2,1)=zero
c          ddtddg(2,2)=sis
          ddtddp(1)=zero
c          ddtddp(2)=zero
      else
c
c     ************************
c        Process is slipping
c     ************************
          in=2
c
c     *****Calculate radial return factor*****
          call rfactor(rf,statev,nstatv,tolx,tols,
     &              xmus,sstars,sis,press,taut,h10,h20)
c
c     *****Update shear stress and slip resistance*****
          tau(1)=rf*taut1
c          tau(2)=rf*taut2
          s=slres(statev(1),statev(2),press)
c
c     *****Calculate frictional dissipation in the increment*****
          dsled=(dabs(taut)-s)/sis
          spd=rf*taut*dsled
          dslip(1)=dsled
c
c     *****Calculate jacobian*****
          c1=tau(1)/s
c          c2=tau(2)/s
          call git(sis,rf,statev(1),statev(2),press,dsled,
     &              xmus,sstars,ginvt,h10,h20)
          call gin(sis,statev(1),statev(2),press,dsled,
     &              xmus,sstars,ginvn,h10,h20)
          ddtddg(1,1)=rf*sis-ginvt*(c1*sis)**2
c          ddtddg(1,2)=-ginvt*c1*c2*sis**2
c          ddtddg(2,1)=-ginvt*c1*c2*sis**2
c          ddtddg(2,2)=sis-ginvt*(c2*sis)**2
          ddtddp(1)=ginvn*sis*c1
c          ddtddp(2)=ginvn*sis*c2
       endif
c
c     ****************************************
c        Print information every n1 increments
c     ****************************************
       n1=20
       iflag1=kinc/n1
       iflag=iflag1*n1
       if (iflag.eq.kinc) then
       open (unit=20,file='/home/sparky/attilio/porosity/porf.dit',
     &      status='unknown')
       write (20,5) kinc,in,dgam(1),statev(1),statev(2),press,
     &              tau(1),temp(1),temp(2),nodes(1)
       endif
```

```
    5 format(I5,I3,F8.4,F7.3,F8.2,F11.4,F11.4,F9.2,F9.2,I4)
c
      return
      end
c
c     ********************************************************
c     *  Subroutine rfactor                                  *
c     ********************************************************
          subroutine rfactor(rf,statev,nstatv,tolx,tols,
     &              xmus,sstars,sis,press,taut,h10,h20)
          implicit real*8(a-h, o-z)
          dimension statev(nstatv)
c
c
c     *****Solve nonlinear system of eqns using N-R*****
          call mnewt(statev,nstatv,tolx,tols,
     &              xmus,sstars,sis,press,taut,h10,h20)
c
          s=slres(statev(1),statev(2),press)
          rf=s/taut
c
          return
          end
c
c     ********************************************************
c     *  Newton-Raphson                                      *
c     ********************************************************
      subroutine mnewt(x, n, tolx,tols,bs,sss,
     &          sis,press,taut,h10,h20)
      implicit real*8(a-h, o-z)
      parameter (np=2)
      dimension x(np), alpha(np, np), beta(np), dx(np)
      bn=x(1)
      ssn=x(2)
      do 13 k=1, 20
         call usrfun(x, alpha, beta, bs,sss,
     &          bn,ssn,sis,dtime,press,taut,h10,h20)
         coeff=alpha(2,2)-alpha(2,1)*alpha(1,2)/alpha(1,1)
         dx(2)=(beta(2)-alpha(2,1)*beta(1)/alpha(1,1))/coeff
         dx(1)=(beta(1)-alpha(1,2)*dx2)/alpha(1,1)
         do 12 i=1, n
            x(i)=x(i) + dx(i)
   12 continue
         if(dabs(dx(1)).le.tolx.and.dabs(dx(2)).le.tols)return
   13 continue
      return
      end
c
c     ********************************************************
c     *  Usrfun calculates values of the functions and their *
c     *  derivatives for the N-R subroutine                  *
c     ********************************************************
```

```
      subroutine usrfun(x,alpha,beta,bs,sss,
     &  bn,ssn,sis,dtime,press,taut,h10,h20)
c
      implicit real*8(A-H,O-Z)
      parameter (np=2)
      dimension x(np),alpha(np,np),beta(np)
c
      s=slres(x(1),x(2),press)
      dsdx=dslrdx(x(1),x(2),press)
      dsds=dslrds(x(1),x(2),press)
      h1=hf(h10,x(1),bs)
      h2=hf(h20,x(2),sss)
      h11=dhf(h10,bs)
      h22=dhf(h20,sss)
      dtaut=dabs(taut)
c
      beta(1)=-x(1)+bn+h1*(dtaut-s)/sis
      beta(2)=-x(2)+ssn+h2*(dtaut-s)/sis
c
      alpha(1,1)=1-(h11*(dtaut-s) - h1*dsdx)/sis
      alpha(1,2)=h1*dsds/sis
c
      alpha(2,1)=h2*dsdx/sis
      alpha(2,2)=1-(h22*(dtaut-s) - h2*dsds)/sis
c
      return
      end
c
c     ********************************************************
c     *  Subroutine ginvt                                    *
c     ********************************************************
          subroutine git(sis,rf,x1,x2,press,dsled,
     &                   xmus,sstars,ginvt,h10,h20)
          implicit real*8(a-h, o-z)
          dsds=dslrds(x1,x2,press)
          dsdx=dslrdx(x1,x2,press)
          h1hat=hf(h10,x1,xmus)/(1-dsled*dhf(h10,xmus))
          h2hat=hf(h20,x2,sstars)/(1-dsled*dhf(h20,sstars))
          hhat=dsdx*h1hat+dsds*h2hat
          ginvt=(rf - (hhat/(sis+hhat)))/sis
          return
          end
c
c     ********************************************************
c     *  Subroutine gin                                      *
c     ********************************************************
          subroutine gin(sis,x1,x2,press,dsled,
     &                   xmus,sstars,ginvn,h10,h20)
          implicit real*8(a-h, o-z)
          dsds=dslrds(x1,x2,press)
          dsdx=dslrdx(x1,x2,press)
          dsdp=dslrdp(x1,x2,press)
```

```
      h1hat=hf(h10,x1,xmus)/(1-dsled*dhf(h10,xmus))
      h2hat=hf(h20,x2,sstars)/(1-dsled*dhf(h20,sstars))
      hhat=dsdx*h1hat+dsds*h2hat
      ginvn=dsdp/(sis+hhat)
      return
      end
c
c     ***************************
c     *  Functions statements   *
c     ***************************
c
c     *****Slip resistance function*****
      function slres(x1,x2,p)
      implicit real*8(A-H,O-Z)
      slres=x2*dtanh(x1*p/x2)
      return
      end
c
c     *****Derivative of slip resistance function*****
c     *****       with respect to xmu             *****
      function dslrdx(x1,x2,p)
      implicit real*8(A-H,O-Z)
      arg=x1*p/x2
      dslrdx=p/(dcosh(arg))**2
      return
      end
c
c     *****Derivative of slip resistance function*****
c     *****       with respect to sstar           *****
      function dslrds(x1,x2,p)
      implicit real*8(A-H,O-Z)
      arg=x1*p/x2
      dslrds=dtanh(arg)-x1*p/(x2*(dcosh(arg))**2)
      return
      end
c
c     *****Derivative of slip resistance function*****
c     *****     with respect to the pressure      *****
      function dslrdp(x1,x2,p)
      implicit real*8(A-H,O-Z)
      arg=x1*p/x2
      dslrdp=x1/(dcosh(arg))**2
      return
      end
c
c     *****Hardening function hf*****
      function hf(h0,x,sat)
      implicit real*8(A-H,O-Z)
      hf=h0*(1-x/sat)
      return
      end
c
```

```
c      *****Derivative of hf*****
           function dhf(h0,sat)
           implicit real*8(A-H,O-Z)
           dhf=-h0/sac
           return
           end
```

Appendix D

Listing of ABAQUS Input Decks

```
**************************************************************
**   INPUT DECK FOR SIMPLE COMPRESSION WITH
**     SUPERPOSED RIGID ROTATION PROBLEM
**************************************************************
*HEADING,UNSYMM
Simple compression with superposed rigid rotation
** The UNSYMM parameter indicates that the full jacobian
** matrix will be used in the solution procedure. In this
** case this is needed since the presence of
** friction makes the jacobian matrix non-symmetric
**************************************************************
**   Nodal Data
**************************************************************
*NODE
1,-1.,0.
2,1.,0.
3,1.,1.
4,-1.,1.
1000,0.,0.
*NSET,NSET=ELSE
1,2,3,4
**************************************************************
**   Element Data
**************************************************************
*ELEMENT,TYPE=CPE4,ELSET=all
1,1,2,3,4
*ELEMENT,TYPE=IRS21
100,1,2,1000
** Element IRS21 is a 2 node contact element. It is to be used
** in conjunction with a rigid surface. In this case 100 is the
** element number, 1 and 2 the node numbers which define the element
** and 1000 is the node which the rigid surface is associated to
*ELSET,ELSET=contact1
100
*RIGID SURFACE,ELSET=contact1,TYPE=SEGMENTS
```

```
START,-2.5,0.
LINE,2.5,0.
**********************************************************
**   Interface Properties Definition
**********************************************************
*INTERFACE, ELSET=contact1
*FRICTION,DEPVAR=2,USER
** This option specifies the frictional properties of
** the interface. In this problem a user defined subroutine,
** which makes use of 2 state variables (DEPVAR=2), is
** invoked. The user needs to specify the name of the
** subroutine (with no extension) at the ABAQUS prompt
** when starting the job
*SURFACE CONTACT, SOFTENED
1.,10.
** This option makes the rigid surface compliant. See
** ABAQUS manuals for details.
**********************************************************
**   Initial Boundary Conditions
**********************************************************
*BOUNDARY
1000,ENCASTRE
ELSE,1,2
**********************************************************
**   Material Properties Definition
**********************************************************
*SOLID SECTION, ELSET = all, MATERIAL = METAL
*MATERIAL,NAME=METAL
*ELASTIC
72000.,.33
**********************************************************
**   History Data
**********************************************************
*STEP,INC=10000,NLGEOM,AMPLITUDE=RAMP
*STATIC
.1,1.,.1,.1
*CONTROLS,PARAMETERS=FIELD,FIELD=DISPLACEMENT
.0005,1.
*CONTROLS,PARAMETERS=TIME INCREMENTATION
,,,100,,,30
*CONTROLS,PARAMETERS=CONSTRAINTS
,,,.00005
** The CONTROLS option is needed to specify non-default
** parameters used in the solution procedure. See
** ABAQUS manuals for details
*BOUNDARY,USER SUB
1000,1
1000,6
ELSE,1,2
** This option specifies the displacement boundary
** conditions during the analysis. In this case, since
** the required displacement is not trivial, a user
```

```
** defined subroutine is invoked. The user needs to specify
** the name of the subroutine (with no extension)
** at the ABAQUS prompt when starting the job
**********************************************************
**   Plot and Print Requests
**********************************************************
*PLOT,FREQUENCY=1
*DISPLACED
U,1
*EL PRINT,ELSET=contact1,FREQUENCY=1,POSITION=AVERAGED AT NODES
*EL PRINT,ELSET=all,FREQUENCY=1
S
*EL FILE,ELSET=all,FREQUENCY=1
S
*END STEP
```

```
c*************************************************************
c     This soubroutine calculates the displacements
c     to be imposed to the ''tool'' and the ''workpiece''
c     in the simple compression with superposed rigid
c     rotation problem
c*************************************************************
c
      subroutine disp(u,kstep,kinc,time,node,jdof)
c
      implicit real*8(a-h,o-z)
c
      pi=dacos(-1.d+00)
      tdot=2.d0*pi
      sldot=1.d0
      tdot=0.d0
c
      theta=tdot*time
      slide=sldot*time
c
      c=dcos(theta)
      s=dsin(theta)
c
      if(jdof.eq.1)then
c
          if(node.eq.1)then
          u=(c-1)*(-1)+slide*c
          else if(node.eq.2)then
          u=(c-1)+slide*c
          else if(node.eq.3)then
          u=(c-1)+s+slide*c
          else if(node.eq.4)then
          u=(c-1)*(-1)+s+slide*c
c          else if(node.eq.1000)then
c          u=slide
          end if
c
      else if(jdof.eq.2)then
c
          if(node.eq.1)then
          u=s-slide*s
          else if(node.eq.2)then
          u=-s-slide*s
          else if(node.eq.3)then
          u=c-1-s-slide*s
          else if(node.eq.4)then
          u=c-1+s-slide*s
          end if
c
      else if(jdof.eq.6)then
c
          u=-theta
c
```

```
      end if
c
      return
      end
```

```
*****************************************************
**   INPUT DECK FOR THE RING COMPRESSION PROBLEM
*****************************************************
*HEADING,UNSYMM
Ring Compression Problem - Hardening Model -
xmui=.33, xmus=.626, h10=.418 1/mm,
sstari=108 MPa, sstars=220 MPa, h20= 44 MPa/mm
** The UNSYMM parameter indicates that the full jacobian
** matrix will be used in the solution procedure. In this
** case this is needed since the presence of
** friction makes the jacobian matrix non-symmetric
*****************************************************
**   Nodal Data
*****************************************************
*NODE
1,5.715,0.
31,8.5725,0.
61,11.43,0.
1099,5.715,3.81
1129,8.5725,3.81
1159,11.43,3.81
10000,0.,0.
*NSET,NSET=UNO
1,1099
*NSET,NSET=DUE
31,1129
*NSET,NSET=TRE
61,1159
*NFILL,TWO STEP,BIAS=.9
UNO,DUE,30,1
*NFILL,TWO STEP,BIAS=1.111
DUE,TRE,30,1
*NSET,NSET=BOT,GENERATE
1,61,1
*NSET,NSET=TOP,GENERATE
1099,1159,1
*NFILL,TWO STEP,BIAS=.8
BOT,TOP,18,61
*NSET,NSET=stuck,GENERATE
6,25,1
*NSET,NSET=ok1,GENERATE
1,733,122
61,793,122
*NSET,NSET=ok
ok1,BOT,TOP,10000
*NSET,NSET=rigid
10000
*********************************************
**   Element Data
*********************************************
*ELEMENT,TYPE=CAX4
1,1,3,125,123,2,64,124,62
```

```
*ELGEN,ELSET=all
1,30,2,1,9,122,30
*ELEMENT,TYPE=IRS21A
299,977,855,10000
300,855,733,10000
301,733,611,10000
302,611,489,10000
303,489,367,10000
304,367,245,10000
305,245,123,10000
401,1,3,10000
501,61,183,10000
306,123,1,10000
*ELGEN,ELSET=contact
401,30,2,1
501,7,122,1
299,300,301,302,303,304,305,306
*ELSET,ELSET=cont,GENERATE
301,306,1
401,430,1
501,506,1
*ELSET,ELSET=interest,GENERATE
1,90,1
**********************************************************
**    Interface Properties Definition
**********************************************************
*RIGID SURFACE,ELSET=contact,TYPE=SEGMENTS
START,0.,0.
LINE,18.,0.
*INTERFACE, ELSET=contact
*FRICTION,USER,DEPVAR=2
** This option specifies the frictional properties of
** the interface. In this problem a user defined subroutine,
** which makes use of 2 state variables (DEPVAR=2), is
** invoked. The user needs to specify the name of the
** subroutine (with no extension) at the ABAQUS prompt
** when starting the job
*SURFACE CONTACT, SOFTENED
.0001,5.
**********************************************************
**    Initial Boundary Conditions
**********************************************************
*BOUNDARY
10000,ENCASTRE
TOP,2,2
**********************************************************
**    Material Properties Definition
**********************************************************
*MATERIAL,NAME=OFHCcop
*ELASTIC
123000.,.33
*PLASTIC
```

```
25.,0.
170.,.1
233.,.2
275.,.3
305.,.4
322.,.5
352.,.7
382.,1.
420.,1.5
450.,2.
*SOLID SECTION, MATERIAL=OFHCcop, ELSET=all
*ELSET,ELSET=cont,GENERATE
301,306,1
401,430,1
501,506,1
*ELSET,ELSET=interest,GENERATE
1,90,1
*RESTART,WRITE,FREQUENCY=500
** This option allows to write all the data needed
** to restart the job in the '.res' file
**********************************************************
**   History Data and Postprocessing
**********************************************************
** The analysis is subdivided into 6 steps. Each step
** corresponds to 10 % additional upsetting (relative to
** the initial configuration)
*************
**  STEP 1
*************
*STEP,INC=500,NLGEOM
*STATIC
.005,1.,,.02
*CONTROLS,PARAMETERS=FIELD,FIELD=DISPLACEMENT
.005,1.
**CONTROLS,PARAMETERS=TIME INCREMENTATION
**,,,,,,8
*CONTROLS,PARAMETERS=LINE SEARCH
4
** The CONTROLS option is needed to specify non-default
** parameters used in the solution procedure. See
** ABAQUS manuals for details
*BOUNDARY
10000,2,2,.381
*PLOT,FREQUENCY=200
*DISPLACED
U,1,1
*EL PRINT,ELSET=interest,FREQUENCY=200,POSITION=AVERAGED AT NODES
S
MISES
*EL PRINT,ELSET=cont,FREQUENCY=20,POSITION=AVERAGED AT NODES
*NODE PRINT,NSET=ok,FREQUENCY=200
RF
```

```
COORD
*NODE PRINT,NSET=rigid,FREQUENCY=200
U
*NODE FILE,NSET=ok,FREQUENCY=10
RF
COORD
U
*EL FILE,ELSET=cont,FREQUENCY=20,POSITION=AVERAGED AT NODES
S
*END STEP
*************
**  STEP 2
*************
*STEP,INC=500,NLGEOM
*STATIC
.005,1.,,.02
*CONTROLS,PARAMETERS=FIELD,FIELD=DISPLACEMENT
.005,1.
**CONTROLS,PARAMETERS=TIME INCREMENTATION
**,,,,,,6
*CONTROLS,PARAMETERS=LINE SEARCH
2
*BOUNDARY
10000,2,2,.762
*PLOT,FREQUENCY=200
*DISPLACED
U,1,1
*EL PRINT,ELSET=interest,FREQUENCY=200,POSITION=AVERAGED AT NODES
S
MISES
*EL PRINT,ELSET=cont,FREQUENCY=200,POSITION=AVERAGED AT NODES
*NODE PRINT,NSET=ok,FREQUENCY=200
RF
COORD
*NODE PRINT,NSET=rigid,FREQUENCY=200
U
*NODE FILE,NSET=ok,FREQUENCY=10
RF
COORD
U
*EL FILE,ELSET=cont,FREQUENCY=20,POSITION=AVERAGED AT NODES
S
*END STEP
*************
**  STEP 3
*************
*STEP,INC=500,NLGEOM
*STATIC
.005,1.,,.02
*CONTROLS,PARAMETERS=FIELD,FIELD=DISPLACEMENT
.005,1.
**CONTROLS,PARAMETERS=TIME INCREMENTATION
```

```
**,,,,,,6
*CONTROLS,PARAMETERS=LINE SEARCH
2
*BOUNDARY
10000,2,2,1.143
*PLOT,FREQUENCY=200
*DISPLACED
U,1,1
*EL PRINT,ELSET=interest,FREQUENCY=200,POSITION=AVERAGED AT NODES
S
MISES
*EL PRINT,ELSET=cont,FREQUENCY=200,POSITION=AVERAGED AT NODES
*NODE PRINT,NSET=ok,FREQUENCY=200
RF
COORD
*NODE PRINT,NSET=rigid,FREQUENCY=200
U
*NODE FILE,NSET=ok,FREQUENCY=10
RF
COORD
U
*EL FILE,ELSET=cont,FREQUENCY=20,POSITION=AVERAGED AT NODES
S
*END STEP
*************
**  STEP 4
*************
*STEP,INC=500,NLGEOM
*STATIC
.005,1.,,.02
*CONTROLS,PARAMETERS=FIELD,FIELD=DISPLACEMENT
.005,1.
**CONTROLS,PARAMETERS=TIME INCREMENTATION
**,,,,,,6
*CONTROLS,PARAMETERS=LINE SEARCH
2
*BOUNDARY
10000,2,2,1.524
*PLOT,FREQUENCY=200
*DISPLACED
U,1,1
*ELSET,ELSET=interest,GENERATE
1,90,1
*EL PRINT,ELSET=interest,FREQUENCY=200,POSITION=AVERAGED AT NODES
S
MISES
*EL PRINT,ELSET=cont,FREQUENCY=200,POSITION=AVERAGED AT NODES
*NODE PRINT,NSET=ok,FREQUENCY=200
RF
COORD
*NODE PRINT,NSET=rigid,FREQUENCY=200
U
```

```
*NODE FILE,NSET=ok,FREQUENCY=10
RF
COORD
U
*EL FILE,ELSET=cont,FREQUENCY=20,POSITION=AVERAGED AT NODES
S
*END STEP
*************
**  STEP 5
*************
*STEP,INC=400,NLGEOM
*STATIC
.005,1.,,.02
*CONTROLS,PARAMETERS=FIELD,FIELD=DISPLACEMENT
.005,1.
**CONTROLS,PARAMETERS=TIME INCREMENTATION
**,,,,,,6
*CONTROLS,PARAMETERS=LINE SEARCH
2
*BOUNDARY
10000,2,2,1.905
*PLOT,FREQUENCY=100
*DISPLACED
U,1,1
*EL PRINT,ELSET=interest,FREQUENCY=200,POSITION=AVERAGED AT NODES
S
MISES
*EL PRINT,ELSET=cont,FREQUENCY=200,POSITION=AVERAGED AT NODES
*NODE PRINT,NSET=ok,FREQUENCY=200
RF
COORD
*NODE PRINT,NSET=rigid,FREQUENCY=200
U
*NODE FILE,NSET=ok,FREQUENCY=10
RF
COORD
U
*EL FILE,ELSET=cont,FREQUENCY=20,POSITION=AVERAGED AT NODES
S
*END STEP
*************
**  STEP 6
*************
*STEP,INC=400,NLGEOM
*STATIC
.005,1.,,.02
*CONTROLS,PARAMETERS=FIELD,FIELD=DISPLACEMENT
.005,1.
**CONTROLS,PARAMETERS=TIME INCREMENTATION
**,,,,,,6
*CONTROLS,PARAMETERS=LINE SEARCH
2
```

```
*BOUNDARY
10000,2,2,2.286
*PLOT,FREQUENCY=200
*DISPLACED
U,1,1
*EL PRINT,ELSET=interest,FREQUENCY=200,POSITION=AVERAGED AT NODES
S
MISES
*EL PRINT,ELSET=cont,FREQUENCY=200,POSITION=AVERAGED AT NODES
*NODE PRINT,NSET=ok,FREQUENCY=200
RF
COORD
*NODE PRINT,NSET=rigid,FREQUENCY=200
U
*NODE FILE,NSET=ok,FREQUENCY=10
RF
COORD
U
*EL FILE,ELSET=cont,FREQUENCY=20,POSITION=AVERAGED AT NODES
S
*END STEP
```

```
**********************************************************
** INPUT DECK FOR THE EXTRUSION PROBLEM
**********************************************************
*HEADING,UNSYMM
Extrusion problem - Hardening Model -
xmui=.33, xmus=.626, h10=.418 1/mm,
stari=108 MPa, sstars=220 MPa, h20= 44 MPa/mm
** The UNSYMM parameter indicates that the full jacobian
** matrix will be used in the solution procedure. In this
** case this is needed since the presence of
** friction makes the jacobian matrix non-symmetric
**********************************************************
**   Nodal Data
**********************************************************
*NODE
1,5.045,0.
65,5.045,20.32
81,4.63556,25.4
1201,1.d-10,0.
1265,1.d-10,20.32
1281,1.d-10,25.4
9999,9.,15.7
*NGEN,NSET=uno
1,65,1
*NGEN,NSET=due
1201,1265,1
*NGEN,NSET=tre
65,81,1
*NGEN,NSET=quattro
1265,1281,1
*NFILL,BIAS=.65,TWO STEP
uno,due,12,100
*NFILL,BIAS=.65,TWO STEP
tre,quattro,12,100
*NSET,NSET=begin,GENERATE
1,1201,100
*NSET,NSET=end,GENERATE
81,1281,100
*NSET,NSET=rigid
9999
*NSET,NSET=radius
uno,tre
**********************************************************
**   Element Data
**********************************************************
*ELEMENT,TYPE=CAX4
1,1,3,203,201,2,103,202,101
*ELEMENT,TYPE=IRS21A
1001,1,3,9999
*ELGEN,ELSET=all
1,40,2,1,6,200,40
*ELGEN,ELSET=contact
```

```
1001,40,2,1
*ELSET,ELSET=interest,GENERATE
1,40,1
**************************************************************
**     Interface Properties Definition
**************************************************************
*RIGID SURFACE,ELSET=contact,TYPE=SEGMENTS,SMOOTH=.8
START,5.08,0.
LINE,5.08,20.32
LINE,4.63556,25.4
LINE,4.63556,30.48
LINE,10.,30.48
*INTERFACE, ELSET=contact
*FRICTION, USER, DEPVAR=2
** This option specifies the frictional properties of
** the interface. In this problem a user defined subroutine,
** which makes use of 2 state variables (DEPVAR=2), is
** invoked. The user needs to specify the name of the
** subroutine (with no extension) at the ABAQUS prompt
*SURFACE CONTACT, SOFTENED
.0001,5.
**************************************************************
**     Initial Boundary Conditions
**************************************************************
*BOUNDARY
9999,ENCASTRE
due,1,1
quattro,1,1
**************************************************************
**     Material Properties Definition
**************************************************************
*MATERIAL,NAME=OFHCcop
*ELASTIC
123000.,.33
*PLASTIC
25.,0.
170.,.1
233.,.2
275.,.3
305.,.4
322.,.5
352.,.7
382.,1.
420.,1.5
450.,2.
*SOLID SECTION, MATERIAL=OFHCcop, ELSET=all
*ELSET,ELSET=interest,GENERATE
1,40,1
************************************
** Plotting of the Undeformed Mesh
************************************
*PLOT
```

```
*DRAW
*RESTART,WRITE,FREQUENCY=200
** This option allows to write all the data needed
** to restart the job in the '.res'
**************************************************
**  History Data
**************************************************
*STEP,INC=2000,NLGEOM
*STATIC
.0001,1.,,.002
*CONTROLS,PARAMETERS=FIELD,FIELD=DISPLACEMENT
.005,1.
**CONTROLS,PARAMETERS=TIME INCREMENTATION
**,,,,,,10
**CONTROLS,PARAMETERS=CONSTRAINTS
**.00002
*CONTROLS,PARAMETERS=LINE SEARCH
4
** The CONTROLS option is needed to specify non-default
** parameters used in the solution procedure. See
** ABAQUS manuals for details
**************************************************
**   Boundary Conditions
**************************************************
*BOUNDARY
begin,2,2,15.
**************************************************
**  Plot and Print Requests
**************************************************
*PLOT,FREQUENCY=200
*DISPLACED
U,1,1
*EL PRINT,ELSET=interest,FREQUENCY=100,POSITION=AVERAGED AT NODES
S
MISES
*EL PRINT,ELSET=contact,FREQUENCY=10,POSITION=AVERAGED AT NODES
*NODE PRINT,NSET=radius,FREQUENCY=100
COORD
*NODE PRINT,NSET=rigid,FREQUENCY=50
RF
*EL FILE,ELSET=interest,FREQUENCY=20,POSITION=AVERAGED AT NODES
S
*EL FILE,ELSET=contact,FREQUENCY=20,POSITION=AVERAGED AT NODES
S
*NODE FILE,NSET=begin,FREQUENCY=5
U
*NODE FILE,NSET=rigid,FREQUENCY=5
RF
*END STEP
```

```
**********************************************************************
**   INPUT DECK FOR THE ROD DRAWING PROBLEM
**********************************************************************
*HEADING,UNSYMM
Drawing Problem - Hardening Model -
xmui=.09, xmus=.25, h10=.0833 1/mm,
sstari=40 MPa, sstars=80 MPa, h20= 44 MPa/mm
** The UNSYMM parameter indicates that the full jacobian
** matrix will be used in the solution procedure. In this
** case this is needed since the presence of
** friction makes the jacobian matrix non-symmetric
**********************************************************
**   Nodal Data
**********************************************************
*NODE
  1,      1.0E-10,    -1.E-10
289,      1.0E-10, -400.0
  9,   99.8,    0.0
297,   99.8, -400.0
307,     1.E-10, -430.
315,    85., -430.
325,     1.E-10, -480.
333,    85., -480.
*NGEN,NSET=ONY
1,289, 9
289,307,9
307,325,9
*NGEN,NSET=ONDIE
  9,297, 9
297,315, 9
315,333, 9
*NGEN,NSET=PULL
315,333, 9
*NFILL, NSET=NALL, BIAS=1.15
ONY,ONDIE, 8, 1
*BOUNDARY
ONY,1,,0.0
PULL,1,,0.0
*NODE
1001,100.0001, -300.
1007,100.0001, -400.
1010,91.50, -433.
1012,91.50,-460.
1301,200.,-300.
1307,200.,-400.
1310,200.,-433.
1312,200.,-460.
*NGEN,NSET=inner
1001,1007,1
1007,1010,1
1010,1012,1
*NGEN,NSET=outer
```

```
1301,1307,1
1307,1310,1
1310,1312,1
*NFILL,BIAS=.7,NSET=die
inner,outer,3,100
*NSET,NSET=constr,GENERATE
1012,1312,100
*NODE,NSET=RIGID
1000 ,0.,400.0
**********************************************************
**   Element Data
**********************************************************
*ELEMENT, TYPE=CAX4T
1,1,10,11,2
*ELGEN, ELSET=BODY1
1,8,1,1,36, 9,9
*ELEMENT,TYPE=CAX4T
1001,1001,1002,1102,1101
*ELGEN,ELSET=body2
1001,11,1,1,3,100,11
*ELSET,ELSET=body
BODY1,body2
*ELEMENT,TYPE=ISL21AT
501,9,18,1000
500,8,9,1000
** Element ISL21AT is a 2 node coupled contact element. It is
** to be used in association with a slide line in temperature
** displacement coupled problems when there is heat generation and
** transfer across the interface of two deformable bodies
*ELGEN, ELSET=INTRF
501, 32, 9,1
*ELSET,ELSET=INTRF1
500,INTRF
**********************************************************
**   Material Properties Definition
**********************************************************
** In this case user defined subroutine is used
** to specify the constitutive model for the workpiece
** bulk material while the die is defined to be elastic
*MATERIAL, NAME=MATER1
*USER MATERIAL, CONSTANTS=22
2.,2.,69.1826D3,0.33,1.14909D25,150.,0.008314,0.007
30.5,5250.00, 133.4,2.0,0.024,1.E-02,300.,933.
0.5,0.3,22.E-6,1.0,2.42375,0.9
*DEPVAR
46
*DENSITY
1.00
*CONDUCTIVITY, TYPE=ISO
160.,298.
*SPECIFIC HEAT
2.42375,298.
```

```
*MATERIAL, NAME=MATER2
*ELASTIC
205000.,0.3
*DENSITY
1.
*SPECIFIC HEAT
4.88,298.
*CONDUCTIVITY, TYPE=ISO
49.,298.
*EXPANSION
1.2E-05
*INITIAL CONDITIONS, TYPE=TEMPERATURE
NALL, 298.
die,298.01
*SOLID SECTION, ELSET=BODY1, MATERIAL=MATER1
*SOLID SECTION, ELSET=body2, MATERIAL=MATER2
**********************************************************
**    Interface Properties Definition
**********************************************************
*SLIDE LINE, TYPE=LINEAR,ELSET=INTRF1,SMOOTH=.49
1112,1012,1011,1010,1009,1008,1007,1006,1005,1004,1003,1002,1001
** This option specifies the line of contact between two deformable
** bodies. The entries are the sequence of nodes at the interface
** of one of the two bodies. The parameter ELSET is used to specify
** the other body.
*INTERFACE,ELSET=INTRF1
*FRICTION,USER,DEPVAR=2
** This option specifies the frictional properties of
** the interface. In this problem a user defined subroutine,
** which makes use of 2 state variables (DEPVAR=2), is
** invoked. The user needs to specify the name of the
** subroutine (with no extension) at the ABAQUS prompt
** when starting the job
*SURFACE CONTACT, SOFTENED
.05,1.
*GAP CONDUCTANCE
1000.
** This option specifies the conductance across the interface
*GAP HEAT GENERATION
1.
** This option specifies what fraction of the frictional
** work is dissipated into heat
**********************************************
**  Initial Boundary Conditions
**********************************************
*NSET,NSET=fixed
1012
*EQUATION
2
1312,2,1.,1012,2,-1
2
1212,2,1.,1012,2,-1
```

```
2
1112,2,1.,1012,2,-1.
*BOUNDARY
1012,2,2,0.
constr,1,1,0.
**********************************************************
**   Plotting of the undeformed mesh
**********************************************************
*PLOT
*DRAW
*RESTART, WRITE, FREQ=150
**********************************************************
**   History Data
**********************************************************
*STEP, INC=1000, NLGEOM, AMP=RAMP
*COUPLED TEMPERATURE-DISPLACEMENT, DELTMX=10., CETOL=1.
0.000005,.03,0.00000000001,.0004
*CONTROLS, PARAMETERS=FIELD,FIELD=DISPLACEMENT
.001,1.
*CONTROLS, PARAMETERS=FIELD,FIELD=TEMPERATURE
.001,1.
*CONTROLS,PARAMETERS=TIME INCREMENTATION,ANALYSIS=DISCONTINUOUS
** The CONTROLS option is needed to specify non-default
** parameters used in the solution procedure. See
** ABAQUS manuals for details
**********************************************************
**   Boundary Conditions
**********************************************************
*BOUNDARY
PULL,2,,-300.
************ **************************************
**    Print and Plot Requests
**********************************************************
*NODE PRINT, FREQ=500
U
RF
*EL PRINT, FREQ=500,ELSET=BODY1
S
SDV
*EL PRINT, ELSET=INTRF1,FREQ=100
*EL FILE, FREQ=200
S
SDV
*NODE FILE, FREQ=200
U
RF
*NODE FILE, FREQ=1, NSET=fixed
RF
*NODE FILE, FREQ=1, NSET=PULL
U
*PLOT, FREQ=50
*DISPLACED
```

```
U,1.0,1
*DETAIL,ELSET=body
*CONTOUR
TEMP,8
*PLOT, FREQ=200
Deformation resistance
0.,0.,90.
*DETAIL,ELSET=BODY1
*CONTOUR
SDV1,10
*PLOT, FREQ=50
Porosity
*DETAIL,ELSET=BODY1
*CONTOUR
SDV2,10
*PLOT, FREQ=50
PRESSURE
*DETAIL,ELSET=BODY1
*CONTOUR
SDV12,10
*END STEP
```